RS3

Stress Analysis

Verification Manual

Table of Contents

1. Boussinesq Problem

1.1. Problem Description

In the Boussinesq problem we subject a half space to a point load, as shown in Figure 1.1. The medium has some Young's modulus, *E,* and Poisson's ratio, ν. The magnitude of the point load is *P*. The associated material has the following properties:

Young's modulus (*E*) = 20,000 MPa

Poisson's ratio (*v*) = 0.3

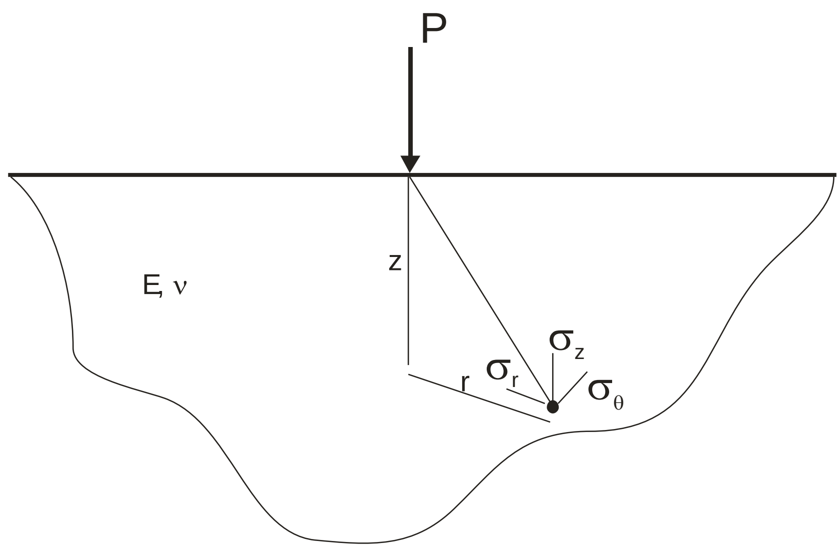

Figure 1.1: Boussinesq problem

1.2. Closed Form Solution

The analytical solution (Craig, 1997) for the problem of a point load on a half space gives the vertical displacement as:

$$w = \frac{P}{2\pi E}\left[\frac{(1+\nu)z^2}{(r^2+z^2)^{3/2}} + \frac{2(1-\nu^2)}{(r^2+z^2)^{1/2}}\right] \tag{1.1}$$

where r and z are radial and vertical distances from the point load, respectively. This equation clearly shows the $1/r$ singularity at the point of application of the load ($r = 0$).

The stress components at a point are given by:

$$\sigma_z = \frac{3P}{2\pi}\left[\frac{z^3}{(r^2+z^2)^{5/2}}\right] \tag{1.2}$$

$$\sigma_r = \frac{P}{2\pi}\left[\frac{3r^2 z}{(r^2+z^2)^{5/2}} - \frac{1-2\nu}{(r^2+z^2)+z(r^2+z^2)^{1/2}}\right] \tag{1.3}$$

$$\sigma_\theta = -\frac{P}{2\pi}(1-2\nu)\left[\frac{z}{(r^2+z^2)^{3/2}} - \frac{1}{(r^2+z^2)+z(r^2+z^2)^{1/2}}\right] \tag{1.4}$$

$$\tau_{rz} = \frac{3P}{2\pi}\left[\frac{rz^2}{(r^2+z^2)^{5/2}}\right] \tag{1.5}$$

1.3. Model Information

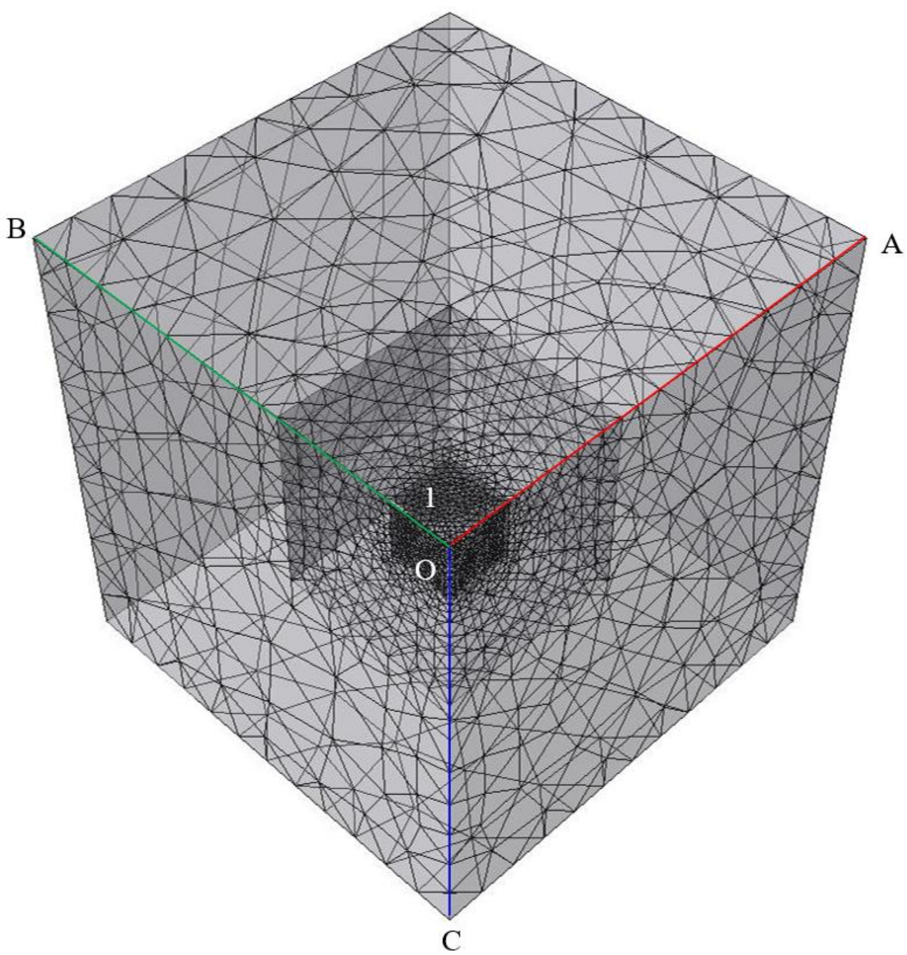

Figure 1.2: *RS3* model with mesh and query line segments

Exploiting symmetry, we analyze only a quarter of the half space close to the action point. The *RS3* model for this problem has the following specifications:

- Dimensions of 2m × 2m × 2m
- 10-noded tetrahedral elements
- Boundary conditions and discretization density as depicted in Figure 1.2

1.4. Results and Discussions

The Boussinesq problem is a true 3D problem because we can have different results in all 3 directions. Vertical displacement, stress in the x direction and stress in the y direction are analyzed along line segments OA and OB. They are presented in Figure 1.3 through Figure 1.8. See Figure 1.2 for visualization of line segments. Figure 1.10 through Figure 1.11 present the vertical displacement and stresses along line segment OC.

Note: For all the graphs presented here, the initial few points from *RS3* results are omitted. The problem is ill-posed because the point load induces an asymptotic stress.

For all of these graphs, the *RS3* results are very similar or identical in both the x-direction and y-direction. The vertical displacement and stress results are very close to the analytical solution.

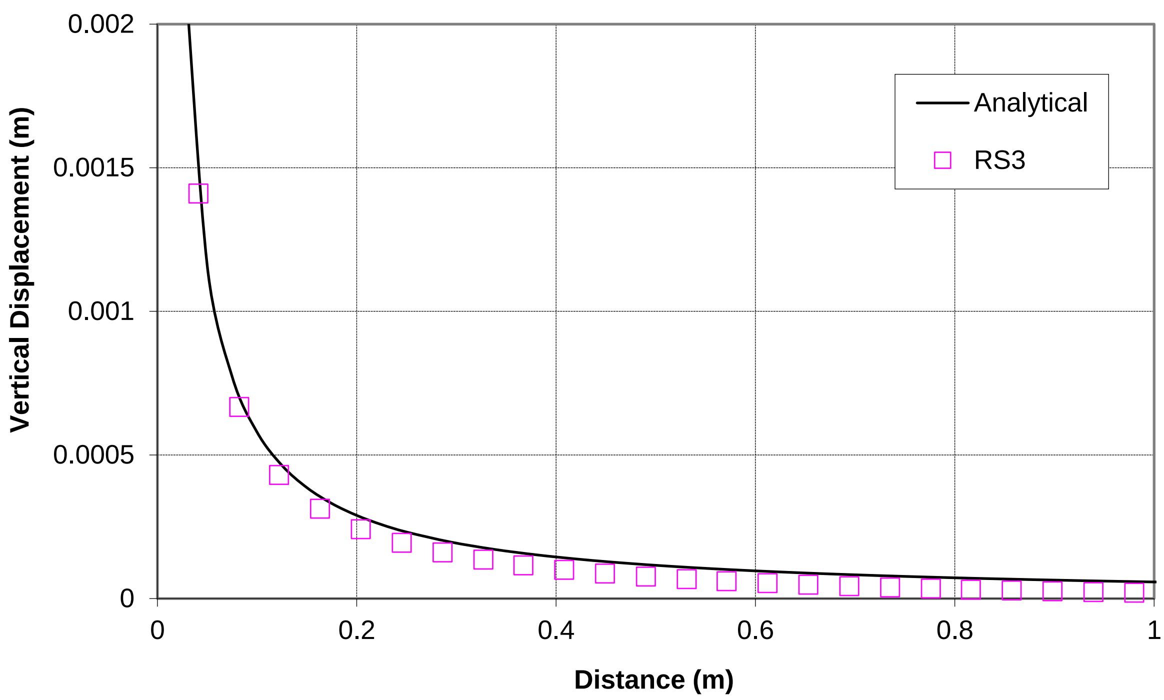

Figure 1.3: Comparison of vertical displacement along line segment OA

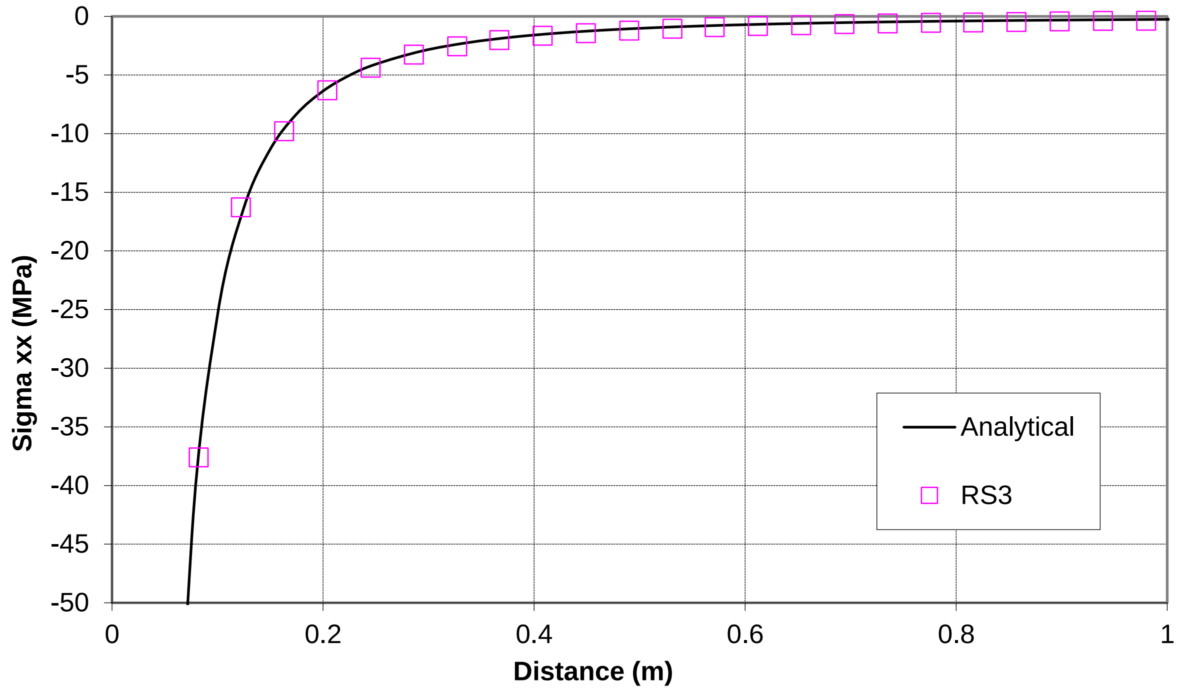

Figure 1.4: Comparison of stress in the x direction along line segment OA

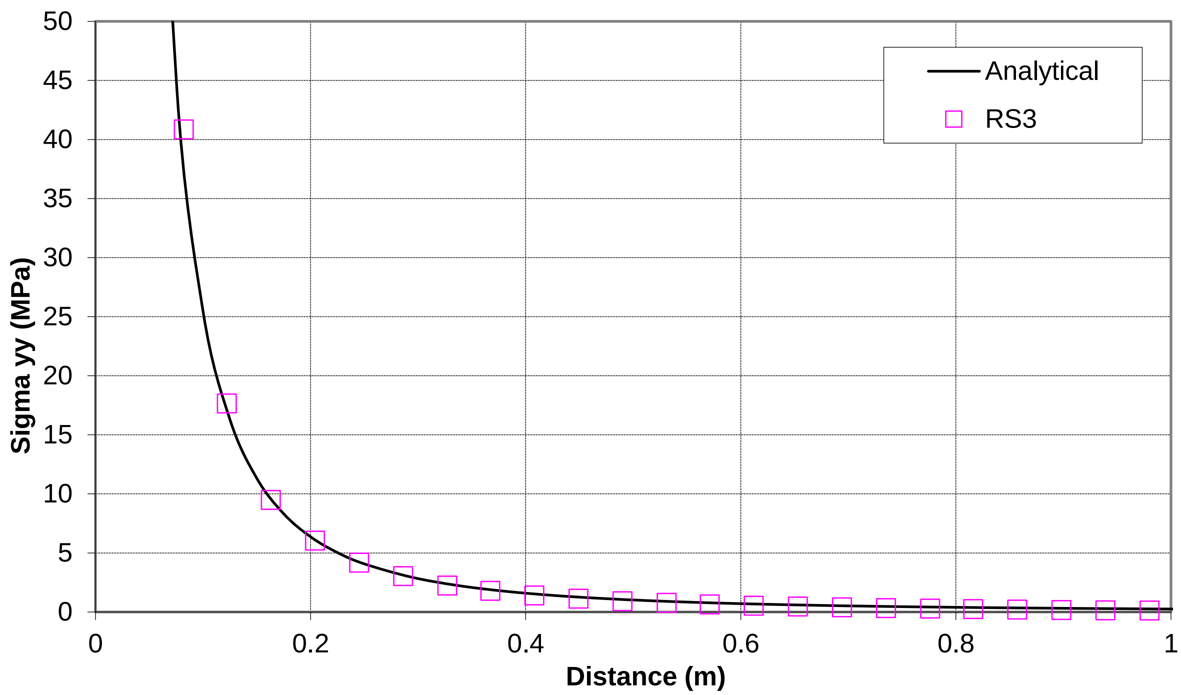

Figure 1.5: Comparison of stress in the y direction along line segment OA

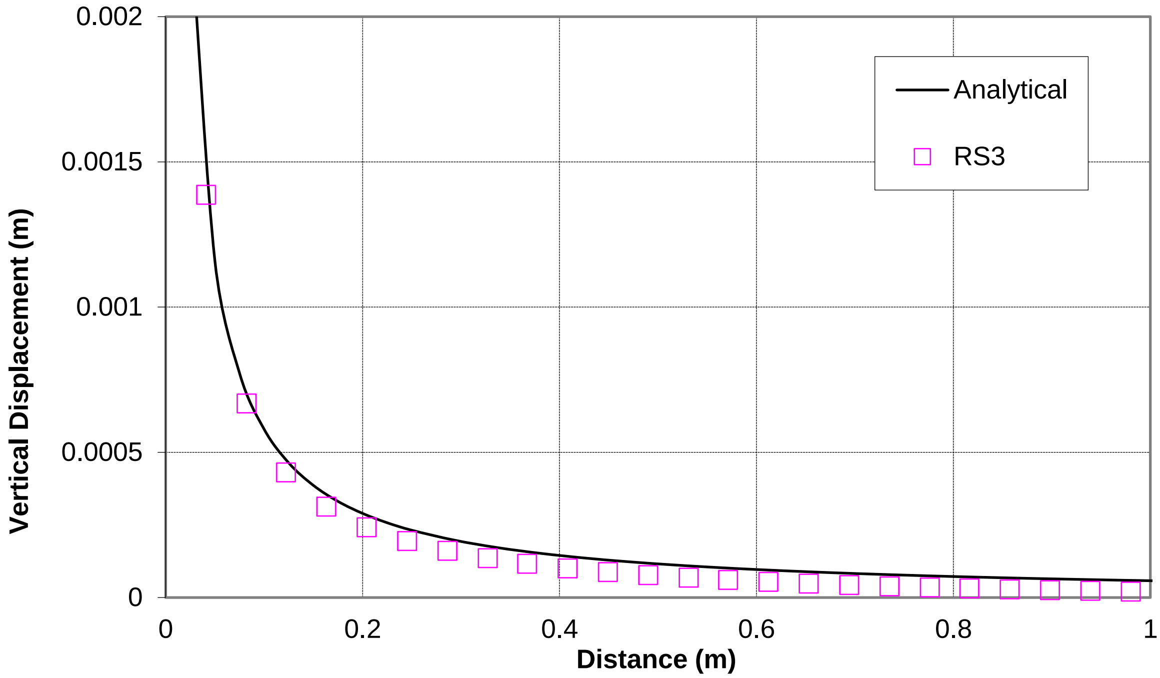

Figure 1.6: Comparison of vertical displacement along line segment OB

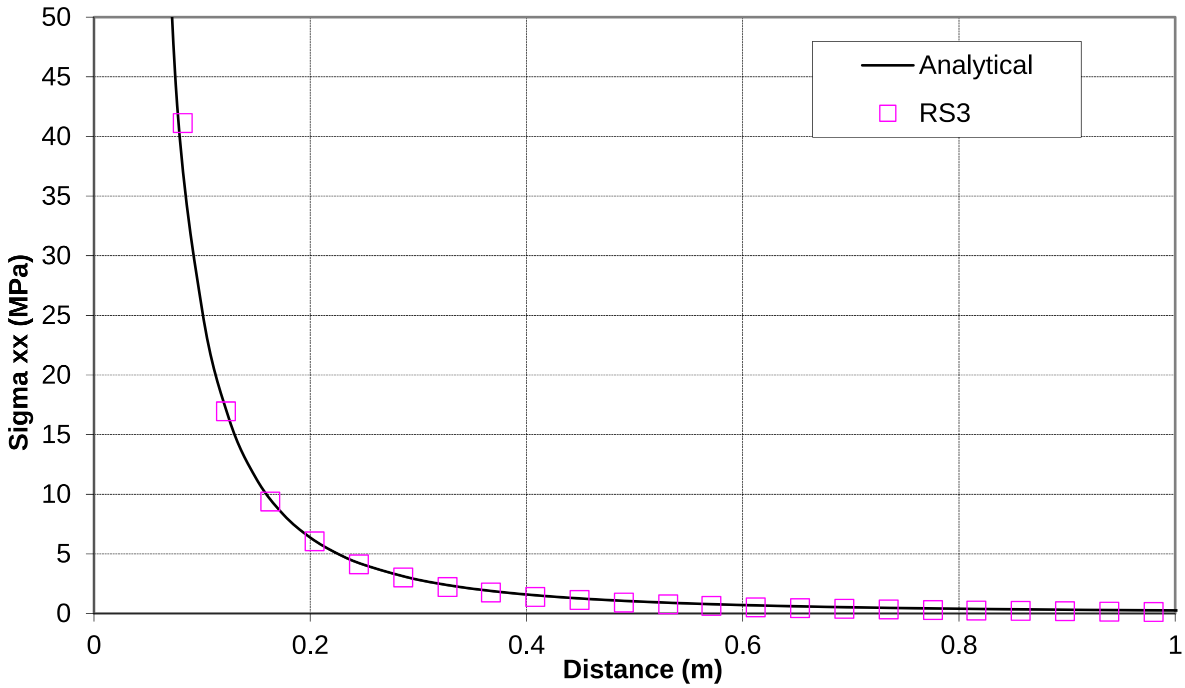

Figure 1.7: Comparison of stress in the x direction along line segment OB

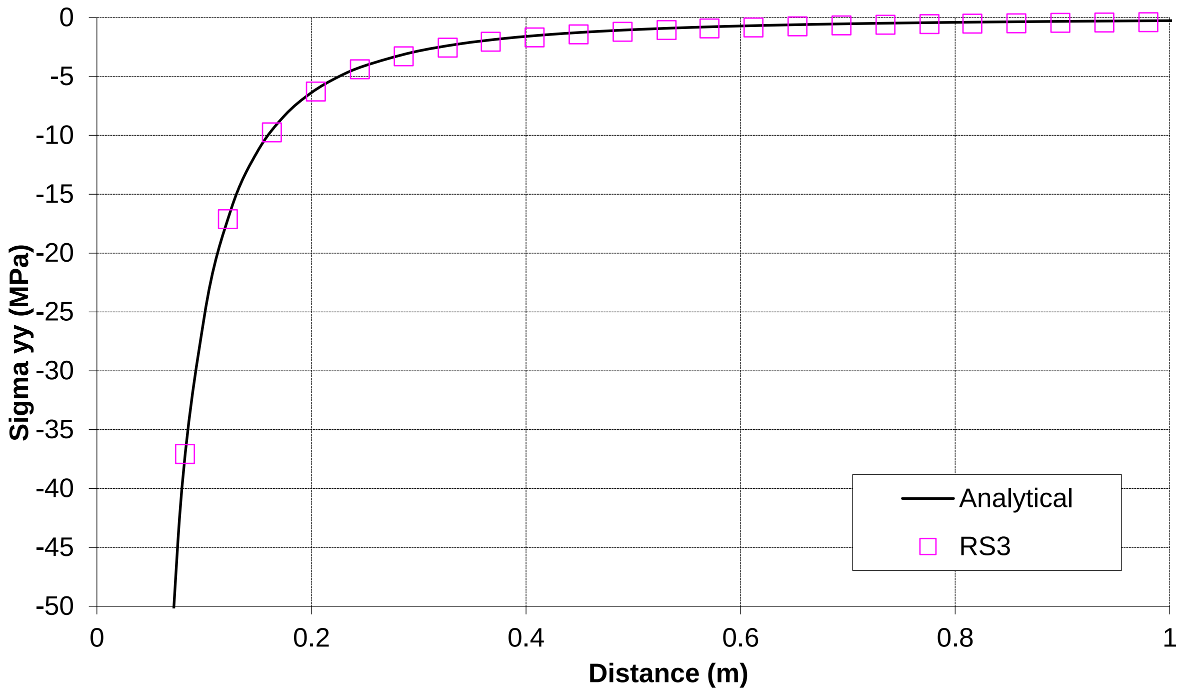

Figure 1.8: Comparison of stress in the y direction along line segment OB

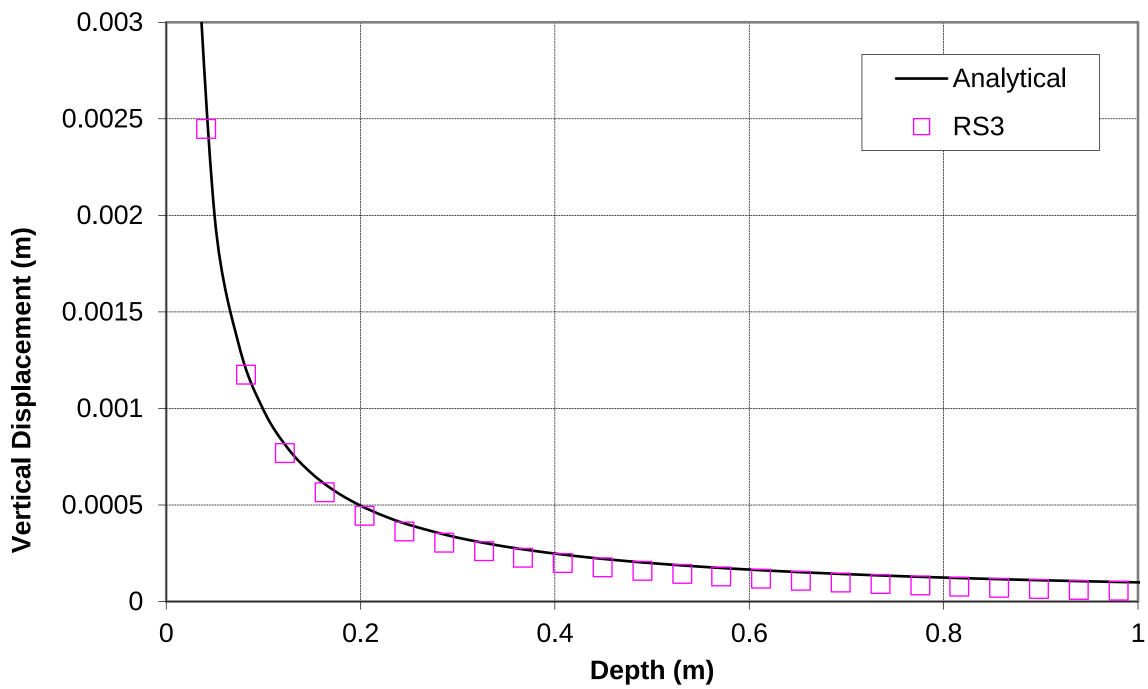

Figure 1.9: Comparison of vertical displacement along line segment OC

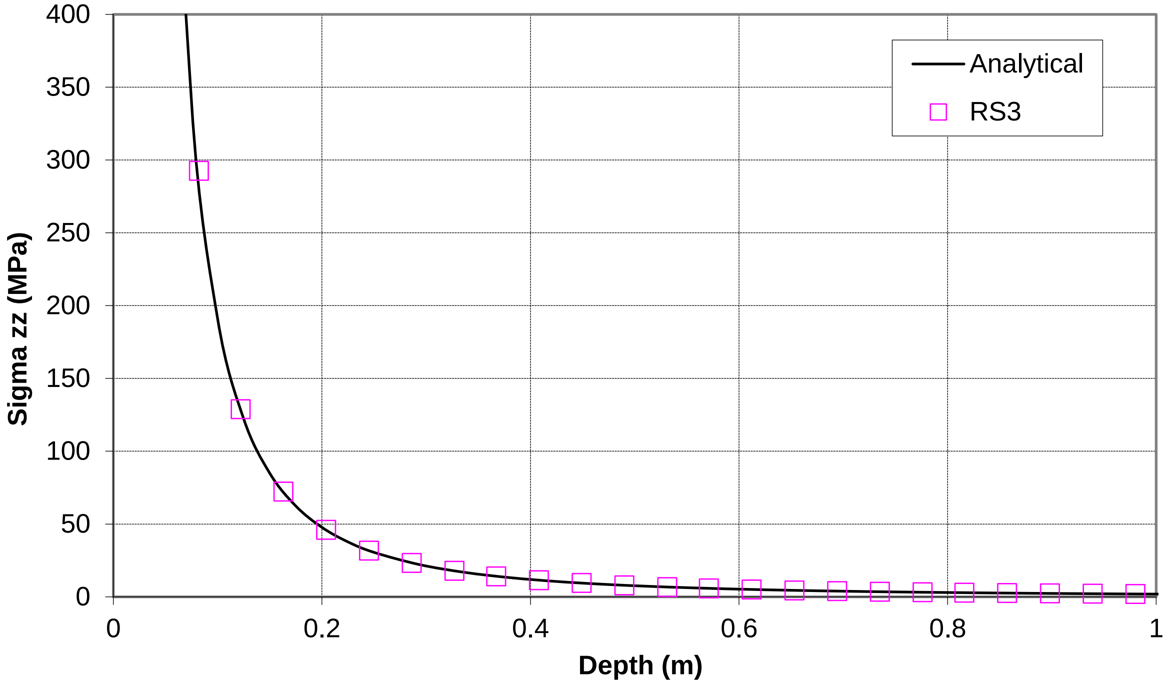

Figure 1.10: Comparison of vertical stress along line segment OC

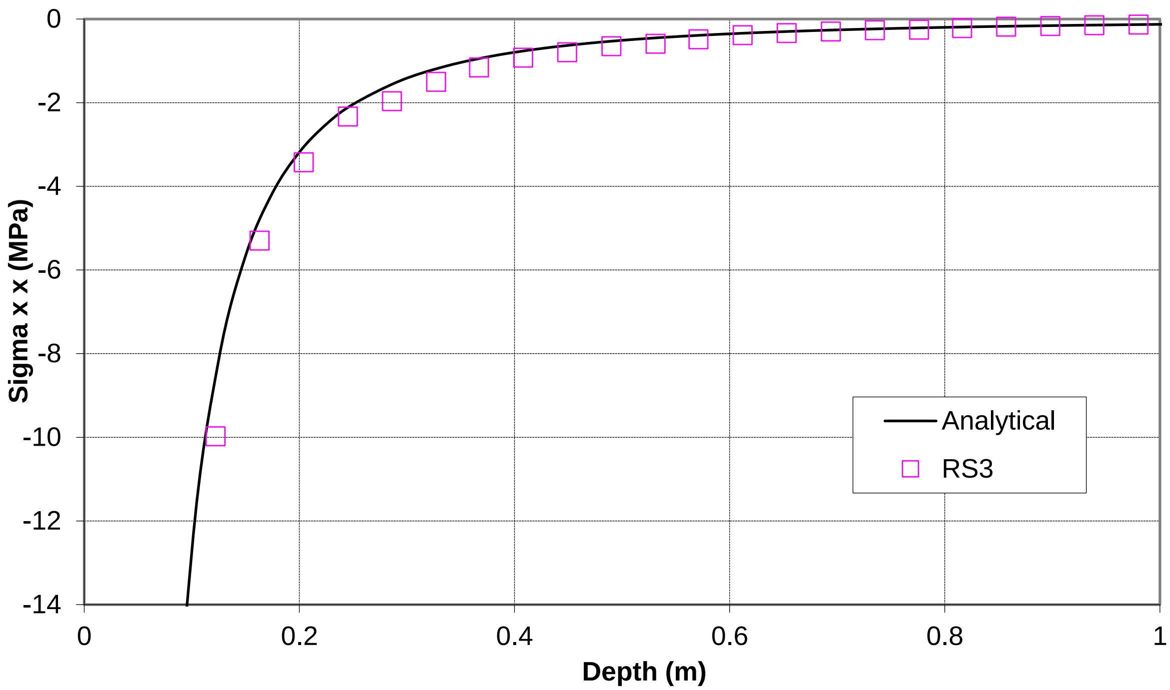

Figure 1.11: Comparison of stress in the x direction along line segment OC

1.5. References

1. Craig, R.F. (1997). *Soil Mechanics 6th Edition.* New York: Spon Press.

1.6. Data Files

The input data file **StressVerification-01.rs3v3** can be downloaded from the RS3 Online Help page for Verification Manuals

2. Cylindrical Hole in an Infinite Elastic Medium

2.1. Problem Description

This problem verifies stresses and displacements for the case of a cylindrical hole in an infinite elastic medium subjected to a constant in-situ (compression +) stress field of:

P_0 = 30 MPa

The material is isotropic and elastic with the following properties:

Young's modulus = 10,000 MPa

Poisson's ratio = 0.2

The model was built in *RS3*. The results can be directly compared to the 2D analytical solution as well as a *RS2* model. The radius of the hole is 1 m and is assumed to be small compared to the length of the cylinder.

2.2. Closed Form Solution

The classical Kirsch solution can be used to find the radial and tangential displacement fields and stress distributions, for a cylindrical hole in an infinite isotropic elastic medium under plane strain conditions (Jaeger and Cook, 1976).

The stresses σ_r, σ_θ and $\tau_{r\theta}$ for a point at polar coordinate (r, θ) near the cylindrical opening of radius *a* (Figure 2.1) are given by:

$$\sigma_r = \frac{p_1 + p_2}{2}\left(1 - \frac{a^2}{r^2}\right) + \frac{p_1 - p_2}{2}\left(1 - \frac{4a^2}{r^2} + \frac{3a^4}{r^4}\right) cos\,2\theta \tag{2.1}$$

$$\sigma_\theta = \frac{p_1 + p_2}{2}\left(1 + \frac{a^2}{r^2}\right) - \frac{p_1 - p_2}{2}\left(1 + \frac{3a^4}{r^4}\right) cos\,2\theta \tag{2.2}$$

$$\tau_{r\theta} = -\frac{p_1 - p_2}{2}\left(1 + \frac{2a^2}{r^2} - \frac{3a^4}{r^4}\right) sin\,2\theta \tag{2.3}$$

The radial (outward) and tangential displacements (see Figure 2.1), assuming conditions of plane strain, are given by:

$$u_r = \frac{p_1 + p_2}{4G}\frac{a^2}{r} + \frac{p_1 - p_2}{4G}\frac{a^2}{r}\left[4(1 - \nu) - \frac{a^2}{r^2}\right] cos\,2\theta \tag{2.4}$$

$$u_\theta = -\frac{p_1 - p_2}{4G}\frac{a^2}{r}\left[2(1 - 2\nu) + \frac{a^2}{r^2}\right] sin\,2\theta \tag{2.5}$$

where G is the shear modulus and ν is Poisson's ratio.

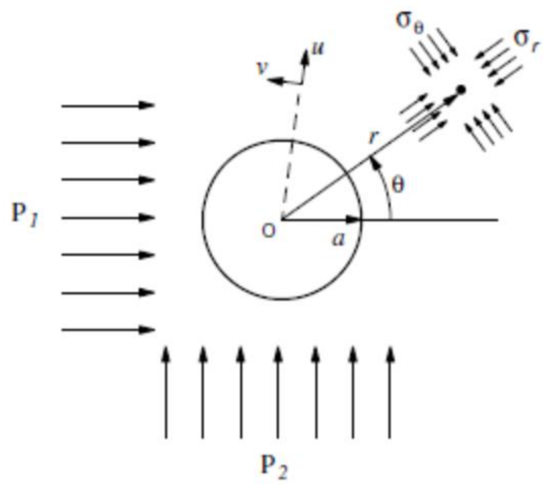

Figure 2.1: Cylindrical hole in an infinite elastic medium

2.3. Model Information

The model for this problem is built in *RS3* with a graded mesh of 10-noded tetrahedron elements as shown in Figure 2.2. The model uses the following parameters.

- excavation radius *a* = 1 m
- extrusion length = 1 m
- fixed external boundary, located 21 m from the center
- y-restrained boundary conditions on front and back face

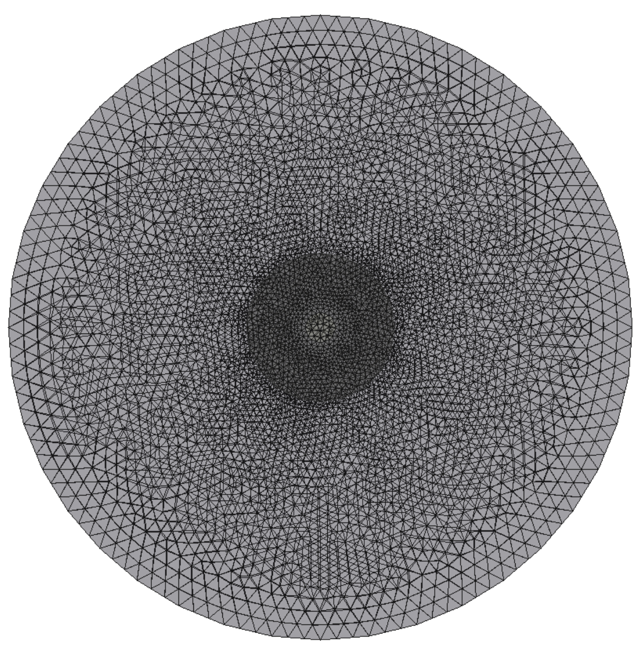

Figure 2.2: Model of cylindrical hole in an infinite elastic medium in *RS3*

2.4. Results and Discussions

Figure 2.3, Figure 2.4 and Figure 2.5 show the radial stress, tangential stress, and radial displacement along a line (either the x- or z-axis) through the center of the models. The *RS3* results are in very close agreement with the analytical solutions and *RS2* results.

Contour plots of the stresses and displacement are rendered in *RS3*. The tangential stress (σ_1), radial stress (σ_3), and radial displacement distribution are presented in Figure 2.6, Figure 2.7, and Figure 2.8 respectively.

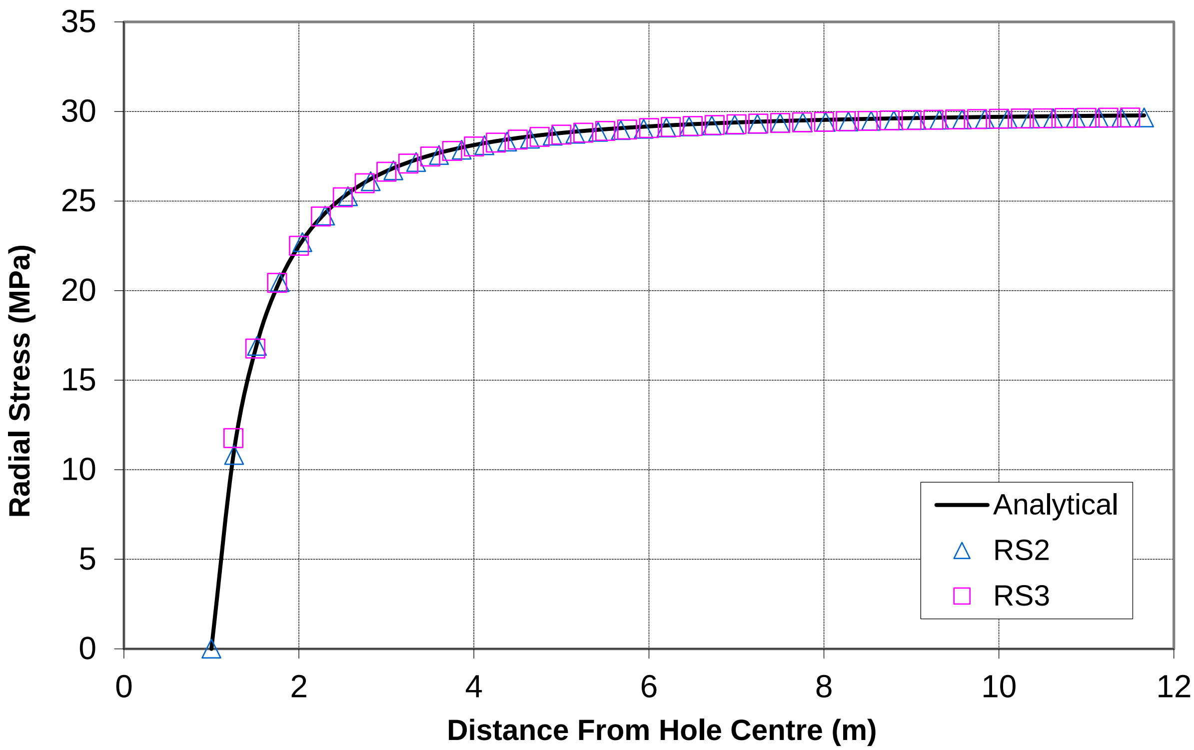

Figure 2.3: Comparison of radial stresses for all solutions

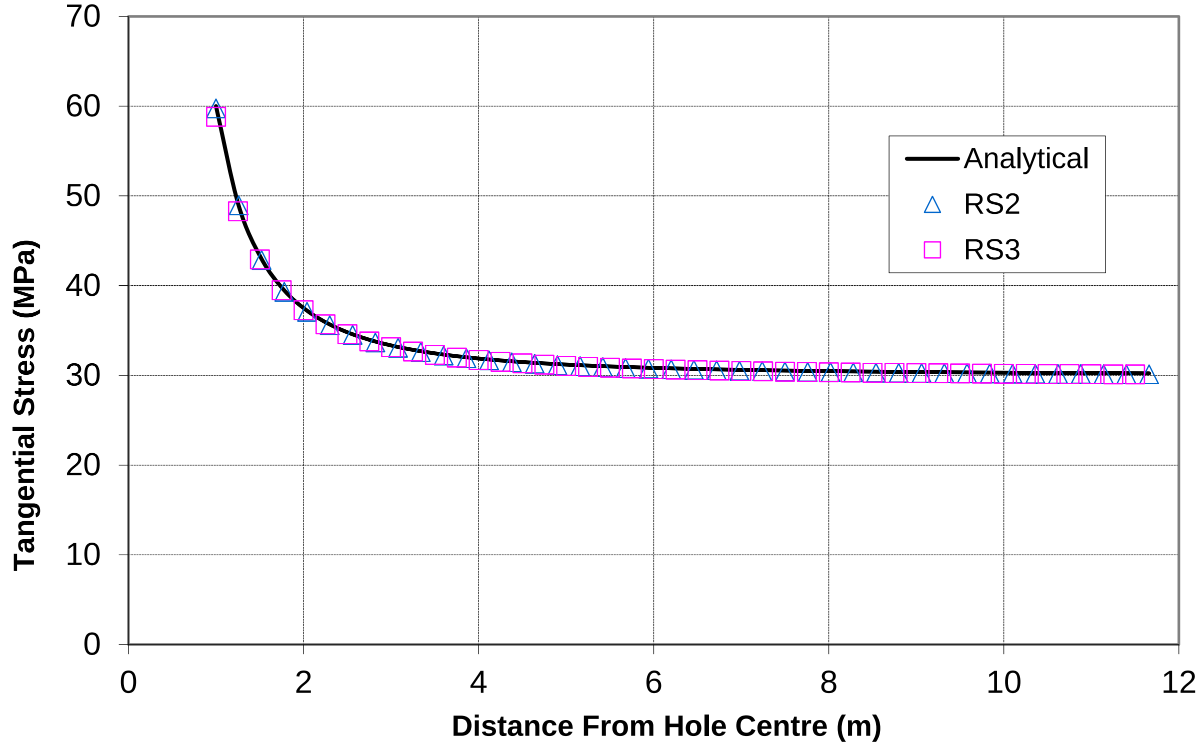

Figure 2.4: Comparison of tangential stresses for all solutions

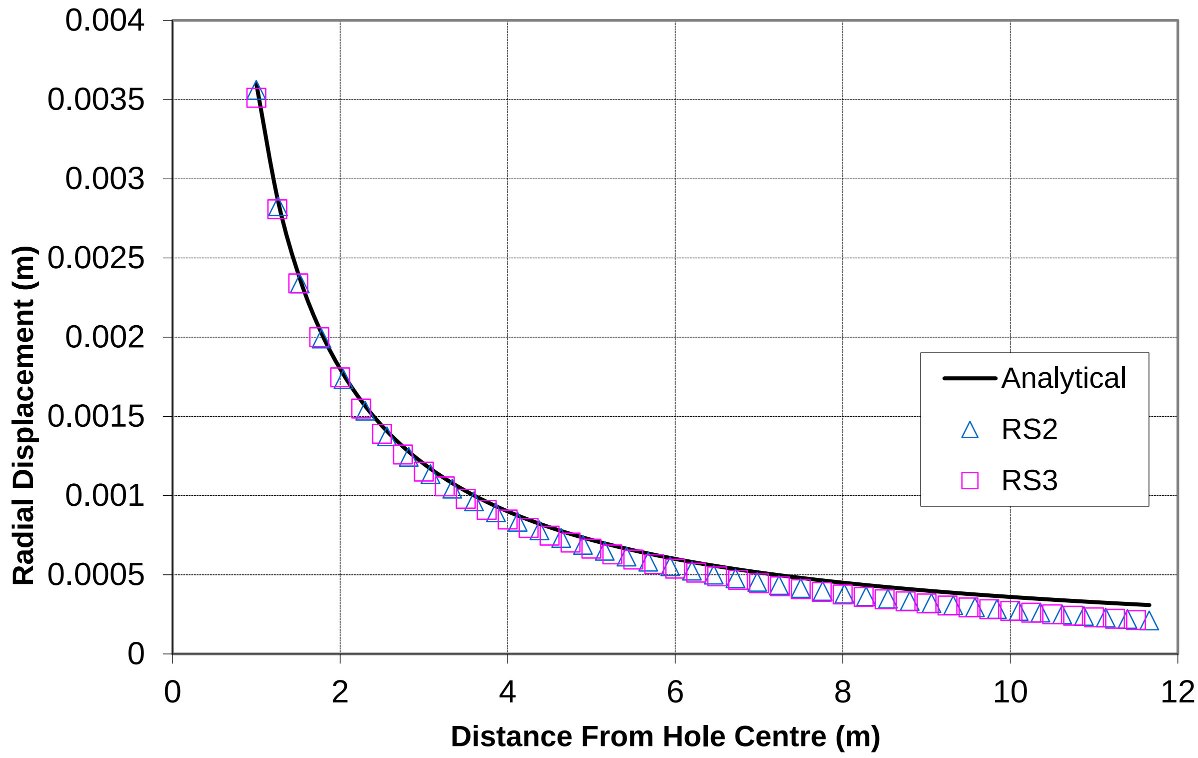

Figure 2.5: Comparison of radial displacement for all solutions

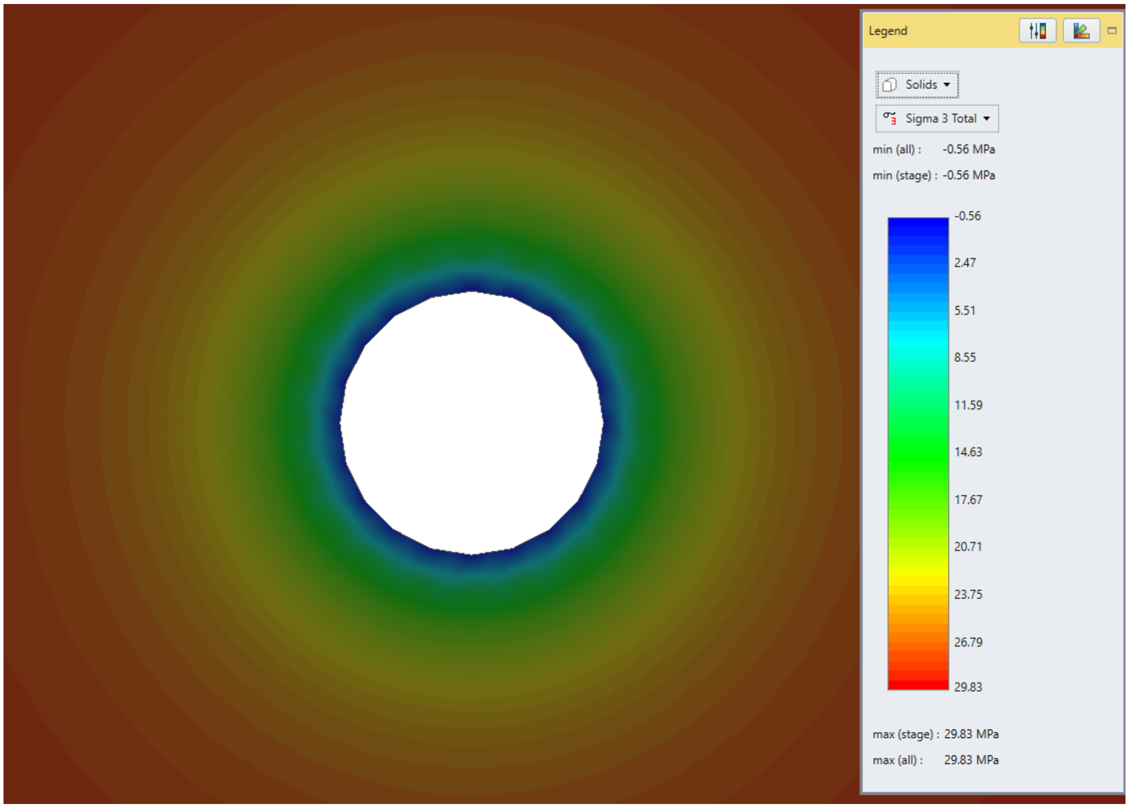

Figure 2.6: Radial stress distribution for *RS3* results

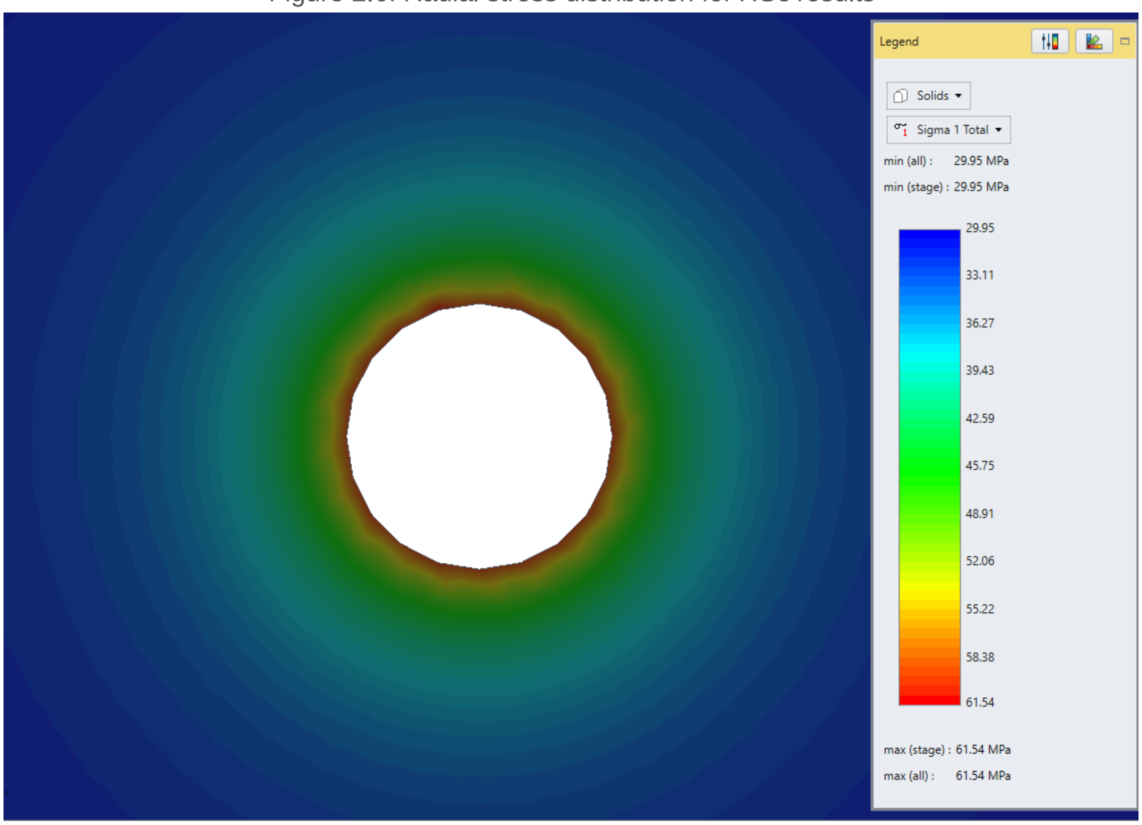

Figure 2.7: Tangential stress distribution for *RS3* results

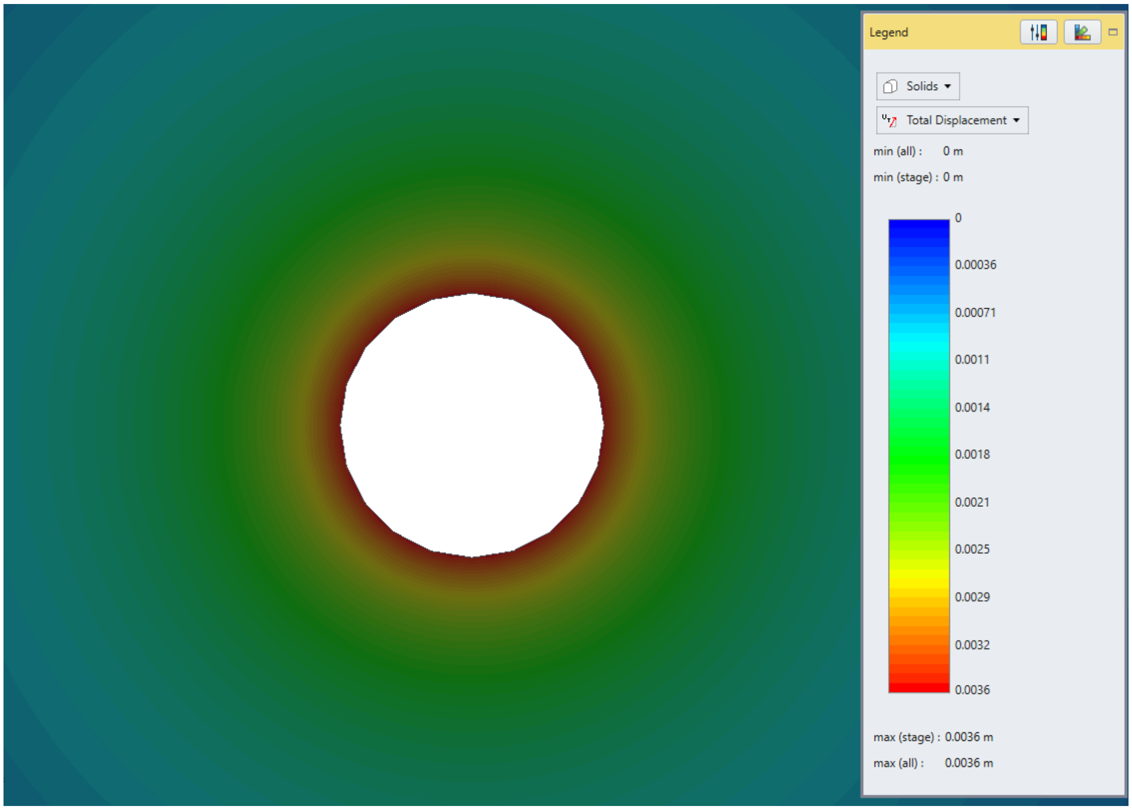

Figure 2.8: Total displacement distribution for *RS3* results

2.5. References

1. Jaeger, J.C. and N.G.W. Cook. (1976) *Fundamentals of Rock Mechanics*, 3rd Ed. London, Chapman and Hall.

2. O.C. Zienkiewicz. *The Finite Element Method in Engineering Science*, New York: McGraw Hill, 1971.

2.6. Data Files

The input data file **StressVerification-02.rs3v3** can be downloaded from the RS3 Online Help page for Verification Manuals.

3. Cylindrical Hole in an Infinite Mohr-Coulomb Medium

3.1. Problem Description

This problem verifies stresses and displacements for the case of a cylindrical hole in an infinite elastic-plastic medium subjected to a constant in-situ (compression +) stress field of:

P_0 = 30 MPa

The material is assumed to be linearly elastic and perfectly plastic with a failure surface defined by the Mohr-Coulomb criterion. Both the associated (dilatancy = friction angle) and non-associated (dilatancy = 0) flow rules are used. The following material properties are assumed:

Young's modulus (E) = 6778 *MPa*

Poisson's ratio (v) = 0.21

Cohesion (*c*) = 3.45 *MPa*

Friction angle (φ) = 30°

Dilation angle (ψ) = 0° and 30°

The results can be directly compared to the 2D analytical solution. The radius of the hole is 1 m and is assumed to be small compared to the length of the cylinder; 2D plane strain conditions are in effect.

3.2. Closed Form Solution

The yield zone radius R_0 is given analytically by a theoretical model based on the solution of Salencon (Salencon, 1969):

$$R_0 = a\left(\frac{2}{K_p+1}\frac{P_0+\frac{q}{K_p-1}}{P_i+\frac{q}{K_p-1}}\right)^{1/(K_p-1)} \qquad (3.1)$$

where

$K_p = \frac{1+\sin\phi}{1-\sin\phi}$

$q = 2 \cdot c \cdot \tan(45+\phi/2)$

P_0 = initial in-situ stress

P_i = internal pressure

The radial stress at the elastic-plastic interface is

$$\sigma_{re} = \frac{1}{K_p + 1}(2P_0 - q) \tag{3.2}$$

The stresses and radial displacement in the elastic zone are

$$\sigma_r = P_0 - (P_0 - \sigma_{re})\left(\frac{R_0}{r}\right)^2 \tag{3.3}$$

$$\sigma_\theta = P_0 + (P_0 - \sigma_{re})\left(\frac{R_0}{r}\right)^2 \tag{3.4}$$

$$u_r = \frac{{R_0}^2}{2G}\left(P_0 - \frac{2P_0 - q}{K_p + 1}\right)\frac{1}{r} \tag{3.5}$$

where r is the distance from the field point (*x*,*y*) to the center of the hole. The stresses and radial displacement in the plastic zone are

$$\sigma_r = -\frac{q}{K_p - 1} + \left(P_i + \frac{q}{K_p - 1}\right)\left(\frac{r}{a}\right)^{(K_p-1)} \tag{3.6}$$

$$\sigma_\theta = -\frac{q}{K_p - 1} + K_p\left(P_i + \frac{q}{K_p - 1}\right)\left(\frac{r}{a}\right)^{(K_p-1)} \tag{3.7}$$

$$\begin{aligned} u_r = \frac{r}{2G}\Bigg[&(2\nu - 1)\left(P_0 + \frac{q}{K_p - 1}\right) \\ &+ \frac{(1-\nu)\left({K_p}^2 - 1\right)}{K_p + K_{ps}}\left(P_i + \frac{q}{K_p - 1}\right)\left(\frac{R_0}{a}\right)^{(K_p-1)}\left(\frac{R_0}{r}\right)^{(K_{ps}+1)} \\ &+ \left(\frac{(1-\nu)\left(K_pK_{ps} + 1\right)}{K_p + K_{ps}} - \nu\right)\left(P_i + \frac{q}{K_p - 1}\right)\left(\frac{r}{a}\right)^{(K_p-1)}\Bigg] \end{aligned} \tag{3.8}$$

where

$K_{ps} = \frac{1+\sin\Psi}{1-\sin\Psi}$

$\Psi =$ Dilation angle

$\nu =$ Poisson's Ratio

$G =$ Shear modulus

3.3. Model Information

The *RS3* model for this problem is built with 10-noded tetrahedron elements. As seen in Figure 3.1, the model uses:

- a graded mesh
- excavation radius *a* = 1 m
- 1 m extrusion
- 40 segments (discretizations) around the circular opening
- fixed external boundary, located 21 m from the hole center

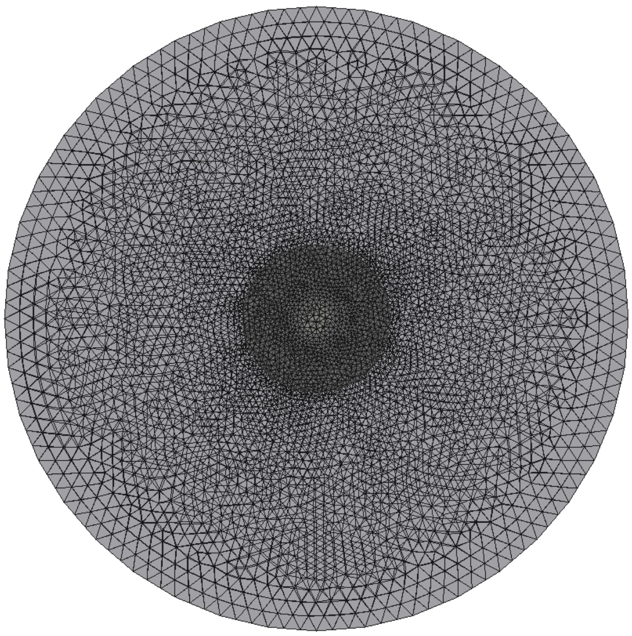

Figure 3.1: Cylindrical hole in Mohr-Coulomb medium

3.4. Results and Discussions

For associated flow (dilation angle $\Psi = 30°$), Figure 3.2 and Figure 3.3 show a direct comparison between *RS3* results and the analytical solution along the x-axis. Tangential stress (σ_θ) is plotted against radial distance in Figure 3.2, while radial displacement (u_r) is plotted against radial distance in Figure 3.3. The comparable results of stresses and displacement for non-associated flow with dilation angle $\Psi = 0°$are shown in Figure 3.4 and Figure 3.5. These plots indicate a close agreement between *RS3* results and the analytical solution.

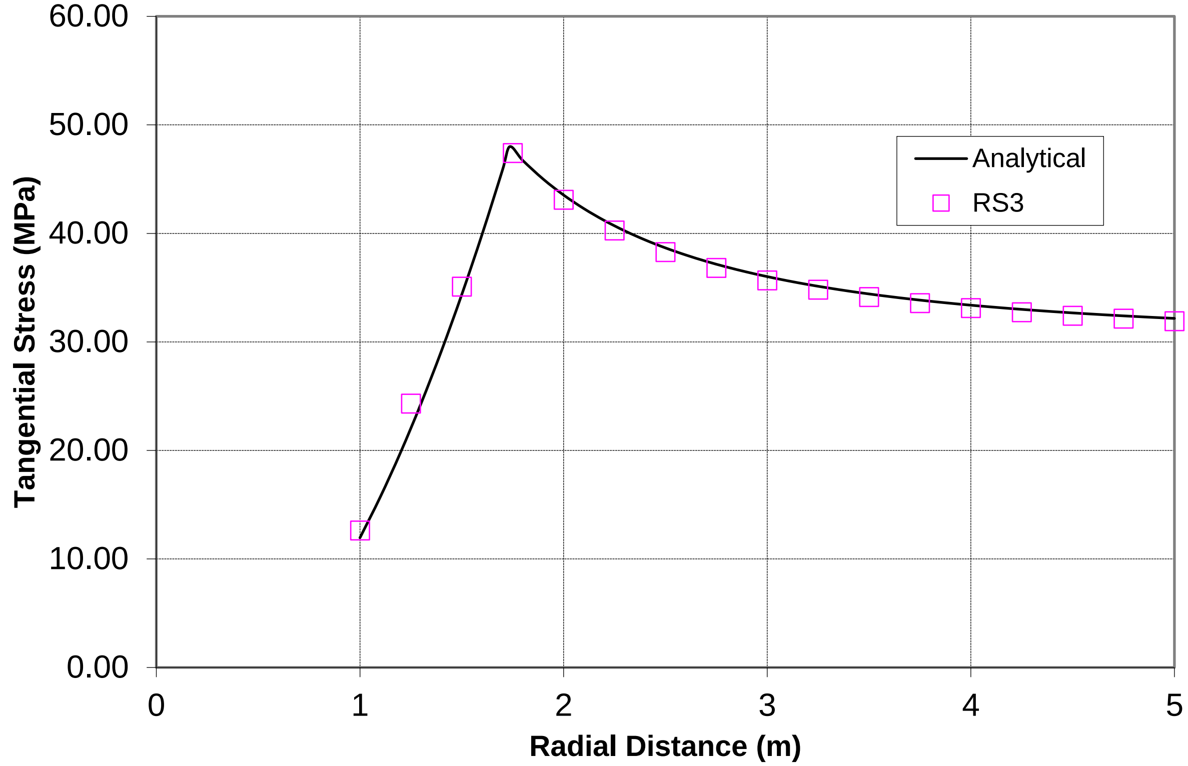

Figure 3.2: Comparison of tangential stress for associated flow

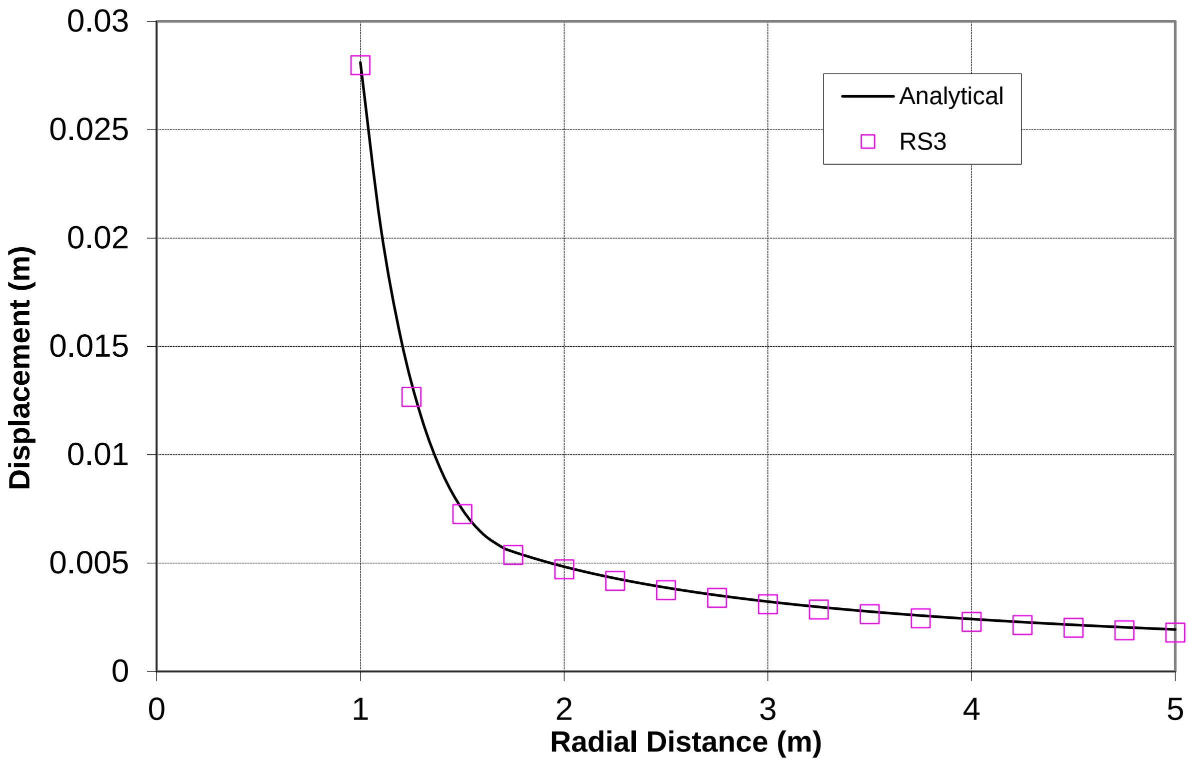

Figure 3.3: Comparison of radial displacement for associated flow

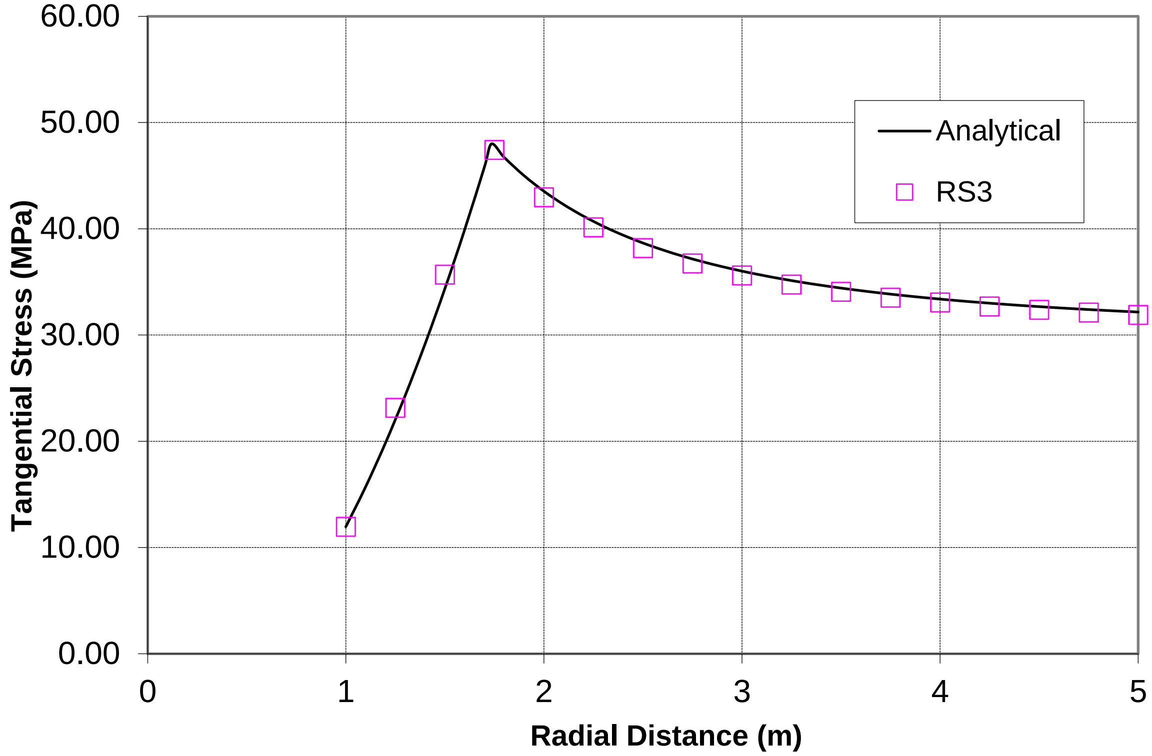

Figure 3.4: Comparison of tangential stress for non-associated flow

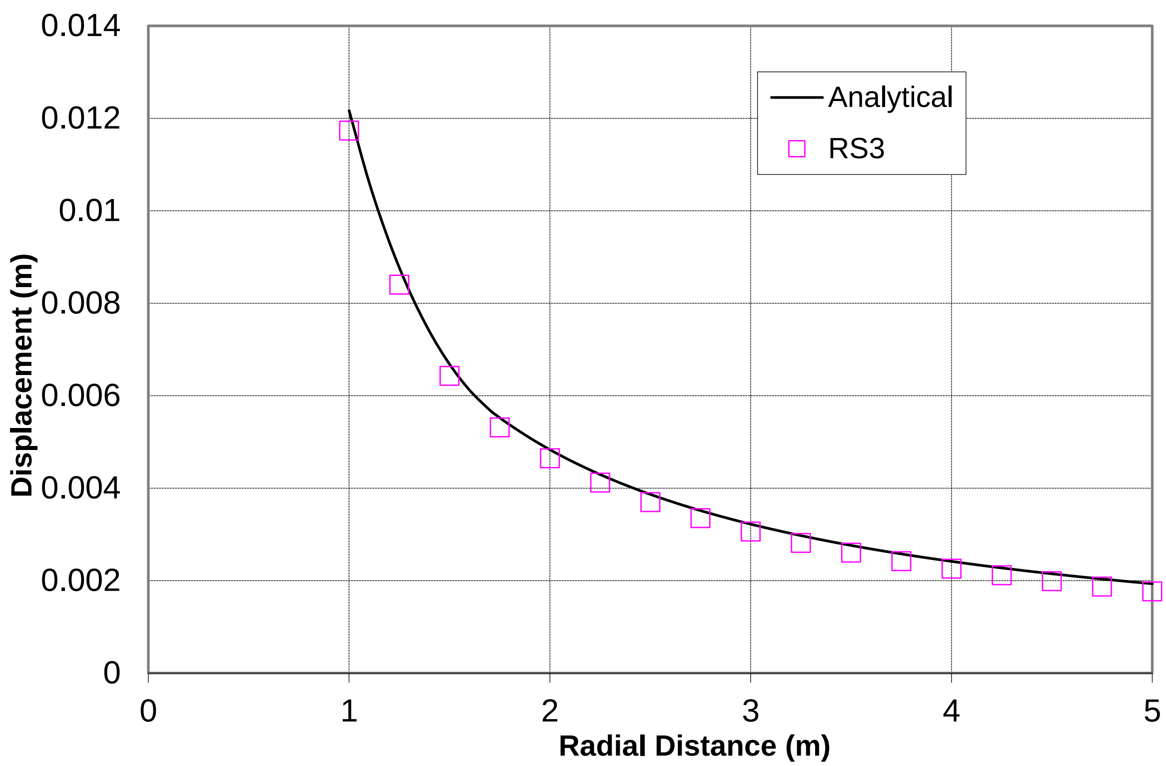

Figure 3.5: Comparison of radial displacement for non-associated flow

3.5. References

1. Salencon, J. (1969), « Contraction Quasi-Statique D'une Cavite a Symetrie Spherique Ou Cylindrique Dans Un Milieu Elasto-Plastique », *Annales Des Ports Et Chaussees*, Vol. 4, pp. 231-236.

3.6. Data Files

The input data files can be downloaded from the RS3 Online Help page:

- **StressVerification-03-Associated.rs3v3**
- **StressVerification-03-NonAssociated.rs3v3**

4. Strip Footing on Surface of Mohr-Coulomb Material

4.1. Problem Description

The prediction of collapse loads under steady plastic-flow conditions is one that can be difficult model to simulate accurately (Sloan and Randolph, 1982). A classic problem involving steady flow is the determination of the bearing capacity of a strip footing on a rigid-plastic half space. The bearing capacity is dependent on the steady plastic flow beneath the footing and is practically significant for footing type problems in foundation engineering. The classic solution for the collapse load derived by Prandtl is a worthy problem for comparison purposes.

The strip footing with a half-width 3 m is located on an elasto-plastic Mohr-Coulomb material with the following properties:

Young's modulus = 250 *MPa*

Poisson's ratio = 0.2

Cohesion (c) = 0.1 *MPa*

Friction angle (ϕ) = 0

4.2. Closed Form Solution

The collapse load from Prandtl's Wedge solution can be found in Terzaghi and Peck (1967):

$$q = (2 + \pi)c \cong 5.14c \qquad (4.1)$$

where c is the cohesion of the material and q is the collapse load. The plastic flow region is shown in Figure 4.1.

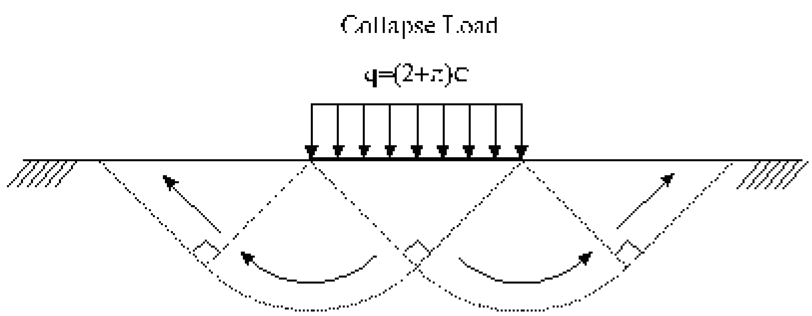

Figure 4.1: Prandtl's wedge problem of a strip load on a frictionless soil

4.3. Model Information

The model for this problem is built with 10-noded tetrahedral elements in *RS3* as shown in Figure 4.2. Half-symmetry is used and the strip load is increased with each stage. This model is extruded 1 m to create a prismatic shape. The boundary conditions are set according to Figure 4.3.

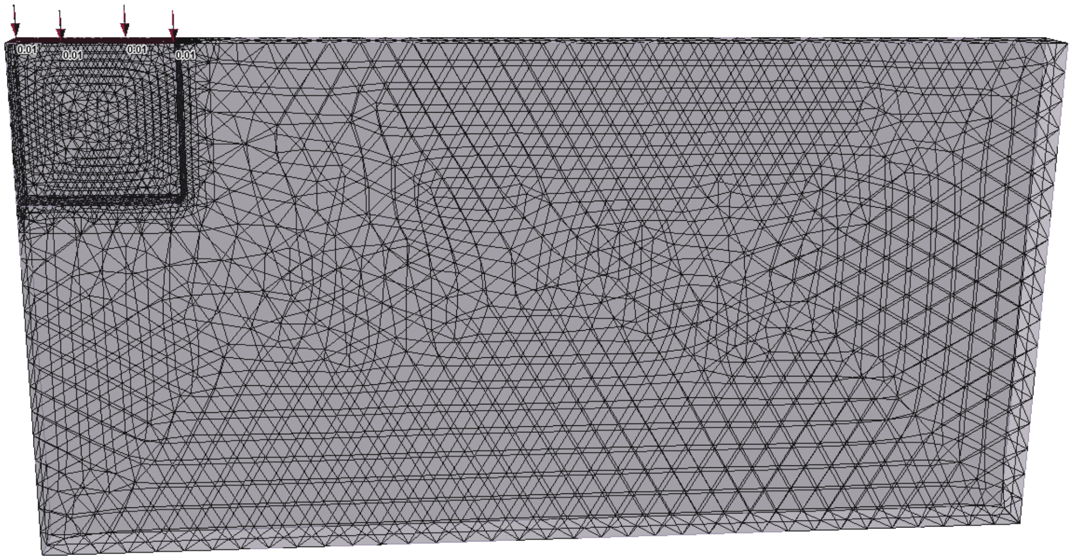

Figure 4.2: *RS3* model of strip load on frictionless soil at stage 15

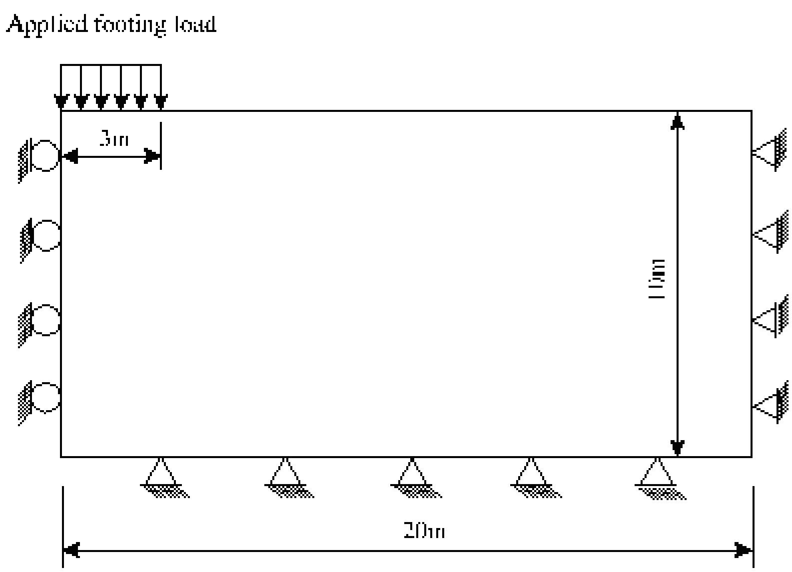

Figure 4.3: Model for *RS3* analysis

4.4. Results and Discussions

Figure 4.4 shows a history of bearing capacity versus applied footing load results from *RS3* were compared with *RS2* and the analytical solution. The pressure-displacement curve for *RS3* and *RS2* models accurately predicted the limit load of 514 kPa.

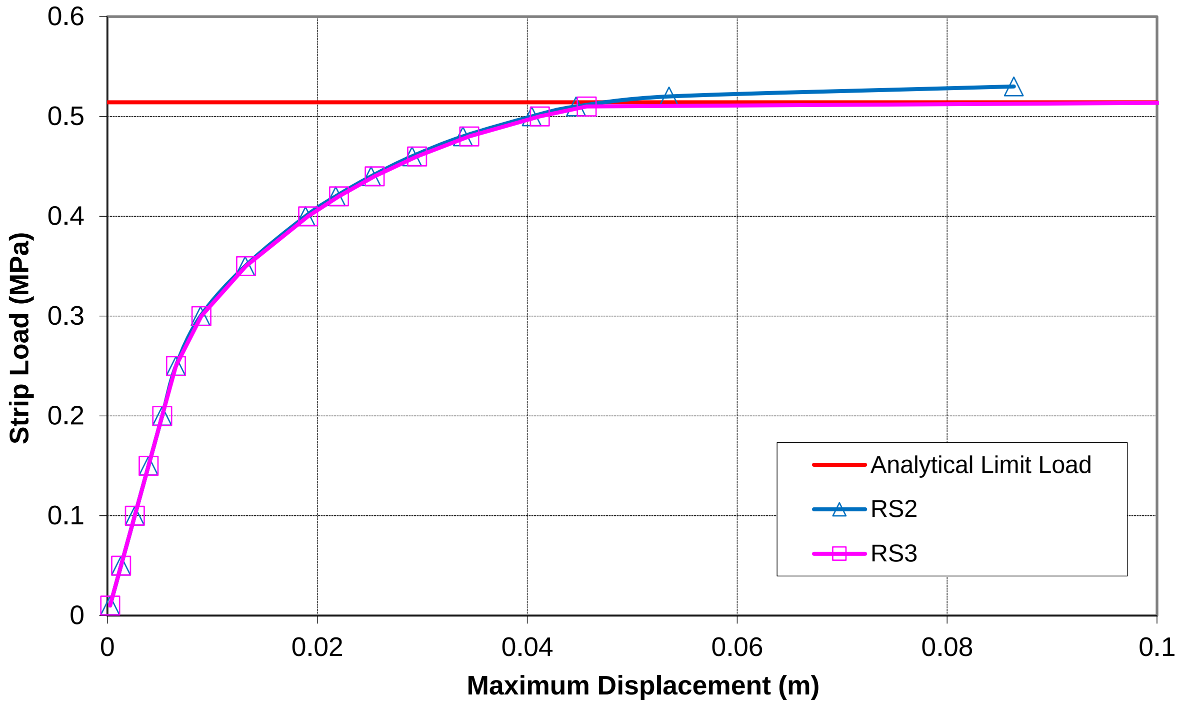

Figure 4.4: Pressure-displacement history of the bearing capacity

4.5. References

1. S. W. Sloan and M. F. Randolph (1982), Numerical Prediction of Collapse Loads Using Finite Element Methods, *Int. J. Num. & Anal. Methods in Geomech.*, Vol. 6, 47-76.

2. K. Terzaghi and R. B. Peck (1967), *Soil Mechanics in Engineering Practice*, 2nd Ed. New York, John Wiley and sons.

4.6. Data Files

The input data file **StressVerification-04.rs3v3** can be downloaded from the RS3 Online Help page for Verification Manuals.

5. Circular Footing on an Associated Mohr-Coulomb Material

5.1. Problem Description

The bearing capacity of a circular footing on a Mohr-Coulomb medium is determined numerically in this section. The footing, represented by a circle of radius *a*, is located on an associated material with the following properties.

Young's modulus = 250 *MPa*

Poisson's ratio = 0.2

Cohesion (c) = 0.1 *MPa*

Friction angle (ϕ) = 20°

Dilation angle (ψ) = 20°

5.2. Semi-Analytical Solution

Cox et al. (1961) have solved numerically the slip-line equations for this axisymmetric-footing problem. The semi-analytical value of the average pressure over the footing at failure for a friction angle of 20° is found to be:

$$q = 20.1c \tag{5.1}$$

where q is the bearing capacity and c is the cohesion of the material.

5.3. Model Information

The model for this problem is built in *RS3* (Figure 5.1). A system of coordinate axes is selected with the x- and y-axes in the plane of the cylinder and the z-axis pointing downward along the cylinder axis. The slab is represented by a disk segment with radius *a*=3m. The radius of the domain is 15 m and its height is 30 m. The parameters are:

- Graded mesh
- 10 noded-tetrahedral element
- 40 segments (discretizations) around the circular opening
- Fixed external boundary, located 15 m from the center

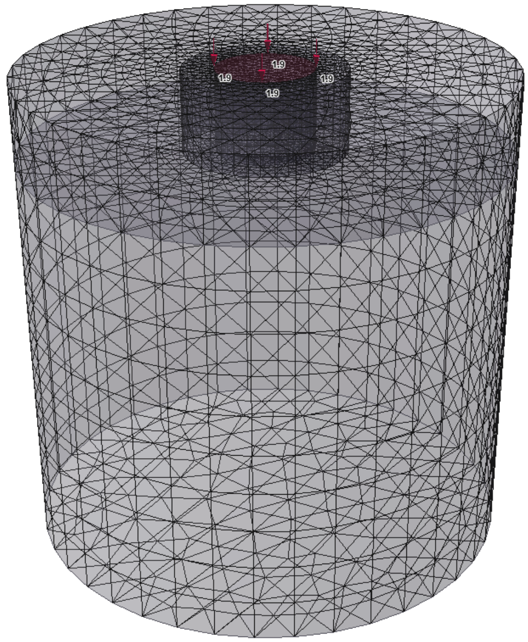

Figure 5.1: Model of circular footing on an associated Mohr-Coulomb material

The displacement of the circular boundary and that of the cylinder base is restricted in all directions. Downward loads are applied in successive stages to represent the footing in the positive z-direction. The magnitudes of the staged loads are summarized in Table 5-1.

Table 5-1: Loads at different stages

Stage Number	***Load [kPa]***
1	50
2	100
3	200
4	300
5	400
6	500
7	600
8	700
9	900
10	1100
11	1300
12	1500

13	1700
14	1900
15	1950
16	2000
17	2025

5.4. Results and Discussions

The load-displacement curve produced by the *RS3* numerical simulation is presented in Figure 5.2. The analytical value of the bearing capacity, *q*, is 2010 kPa. *RS3* results begin to plateau at about 2000 kPa as this was the point of non-convergence. The graph shows that *RS3* results are in close agreement with the analytical solution.

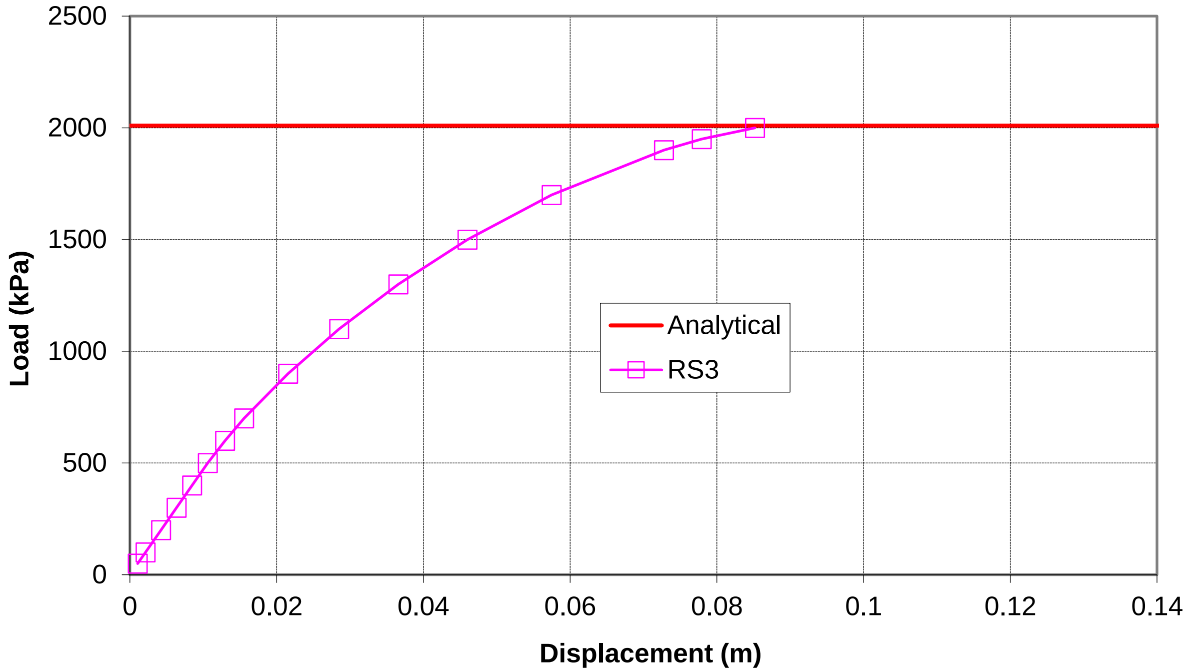

Figure 5.2: Load-displacement curve for a circular footing on a Mohr-Coulomb material

5.5. References

1. Cox, A. D., G. Eason and H. G. Hopkins. (1961) “Axially Symmetric Plastic Deformation in Soils,” Phys. Trans. Royal Soc. London, Series A, 254(1036), 1-45.

5.6. Data Files

The input data file **StressVerification-05.rs3v3** can be downloaded from the RS3 Online Help page.

6. Cylindrical Hole in an Infinite Hoek-Brown Medium

6.1. Problem Description

This problem addresses the case of a cylindrical tunnel in an infinite Hoek-Brown medium subjected to a uniform compressive in-situ stress field. Materials with failure surfaces defined according to the Hoek-Brown criterion have non-linear and stress-dependent shear strength. Plane strain condition is enforced by restricting the displacement of all the surfaces parallel to the face of the cylinder. Figure 6.1 shows the configuration and the finite element mesh of the model. Table 6-1 summarizes the model parameters.

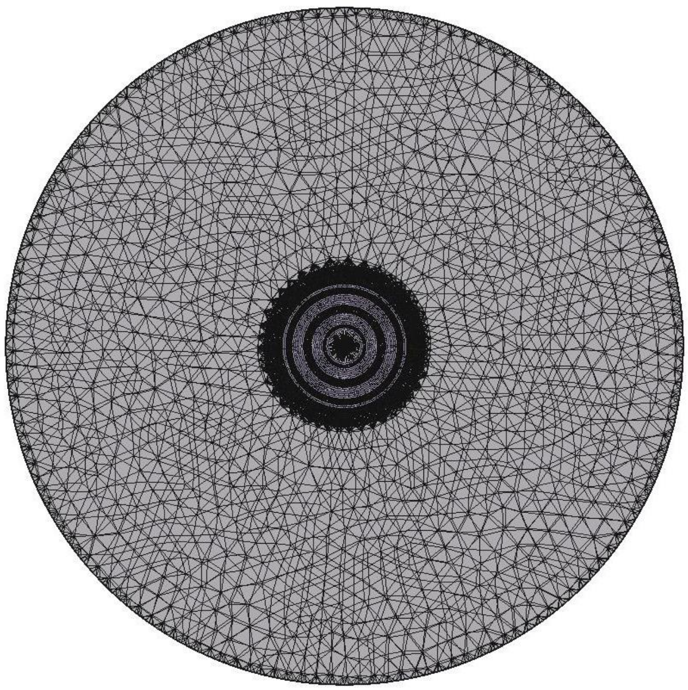

Figure 6.1: Circular tunnel in Hoek-Brown medium as constructed in RS3

Table 6-1: Model parameters

Parameter	***Value***
In-situ stress field (P_0)	30 MPa
Hole radius (*a*)	1 m
Young's modulus (E)	10000 MPa
Poisson's ratio (*v*)	0.25

Uniaxial compressive strength of intact rock (σ_c)	100 MPa
Dilation parameter	0º
m	2.515
s	0.003865
m_r	0.5
s_r	1e-5

The *RS3* model constructed uses a graded mesh with 4-noded tetrahedral elements and an in-situ hydrostatic stress field of 30 MPa.

6.2. Analytical Solution

According to both sources, the radius of the yield zone r_e is given by (Hoek & Brown, 1982) (Itasca, 1993):

$$r_e = ae^{\left[N - \frac{2}{m_r \sigma_c}(m_r \sigma_c P_i + s_r \sigma_c^2)^{\frac{1}{2}}\right]} \qquad (6.1)$$

Where

$$N = \frac{2}{m_r \sigma_c}(m_r \sigma_c P_0 + s_r \sigma_c^2 - m_r \sigma_c^2 M)^{\frac{1}{2}} \qquad (6.2)$$

$$M = \frac{1}{2}\left[\left(\frac{m}{4}\right)^2 + \frac{mP_0}{\sigma_c} + s\right]^{\frac{1}{2}} - \frac{m}{8} \qquad (6.3)$$

The radial stress at $r = r_e$ is given by:

$$\sigma_{re} = P_0 - M\sigma_c \qquad (6.4)$$

In the elastic region, the radial and tangential stresses are given by:

$$\sigma_r = P_0 - (P_0 - \sigma_{re})\left(\frac{r_e}{r}\right)^2 \qquad (6.5)$$

$$\sigma_\theta = P_0 + (P_0 - \sigma_{re})\left(\frac{r_e}{r}\right)^2 \qquad (6.6)$$

In the plastic (yielded) region, the radial and tangential stresses are given by:

$$\sigma_r = \frac{m_r \sigma_r}{4}\left[\ln\left(\frac{r}{a}\right)\right]^2 + \ln\left(\frac{r}{a}\right)(m_r \sigma_c P_i + s_r \sigma_c^2)^{\frac{1}{2}} + P_i \quad (6.7)$$

$$\sigma_\theta = \sigma_r + (m_r \sigma_c \sigma_r + s_r \sigma_c^2)^{\frac{1}{2}} \quad (6.8)$$

where P_i is the internal pressure (in this example, 0 MPa). Figure 6.2 shows the distinction between the plastic and the elastic zone.

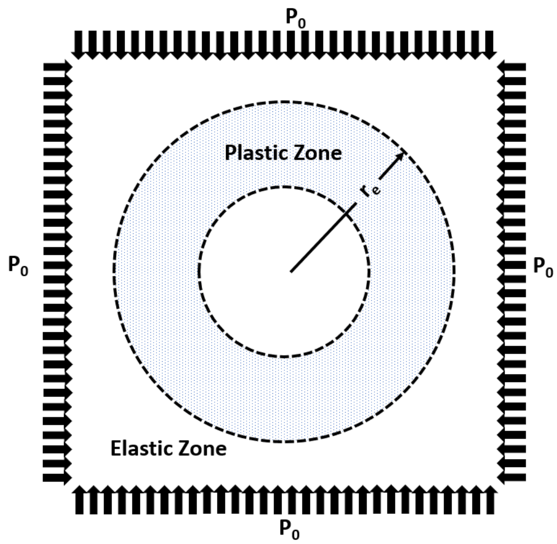

Figure 6.2: Tunnel Elastic and Plastic Zones (Hoek & Brown, 1982)

6.3. Results

Figure 6.3 and Figure 6.4 compare the stress distributions calculated by *RS3* with the *RS2* results and analytical solution. *RS3* results are in very close agreement with the other two in both graphs. See Figure 6.5 and Figure 6.6 for contour plots of the radial and tangential stress distribution produced in *RS3*.

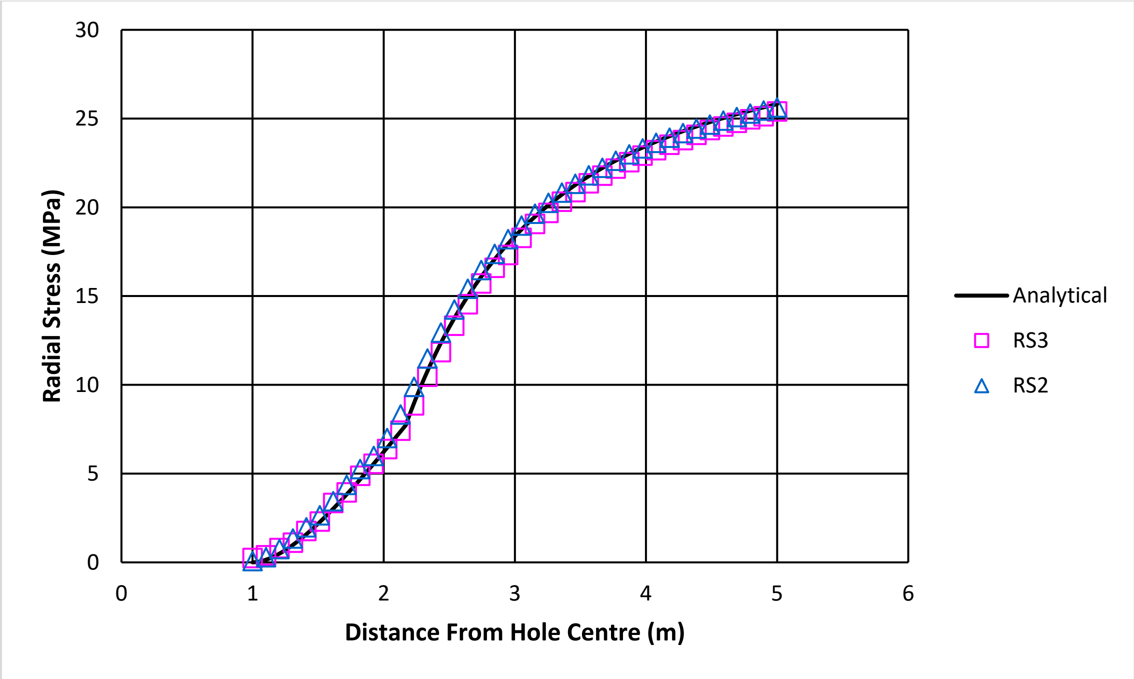

Figure 6.3: Comparison of radial stresses for all solutions

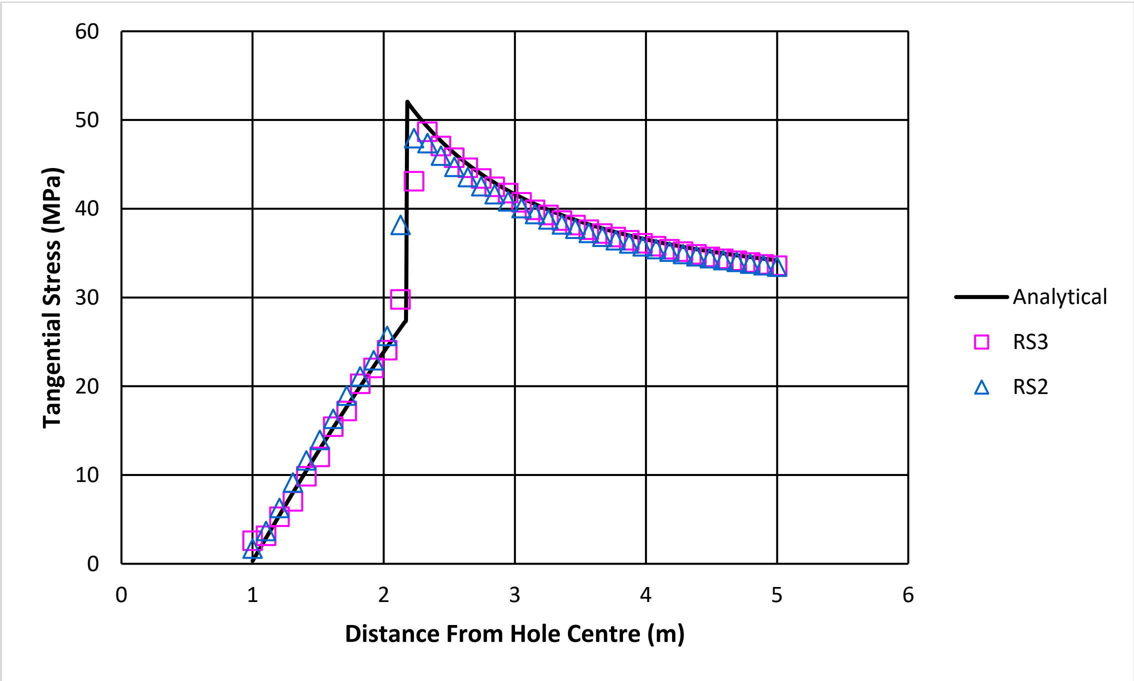

Figure 6.4: Comparison of tangential stresses for all solutions

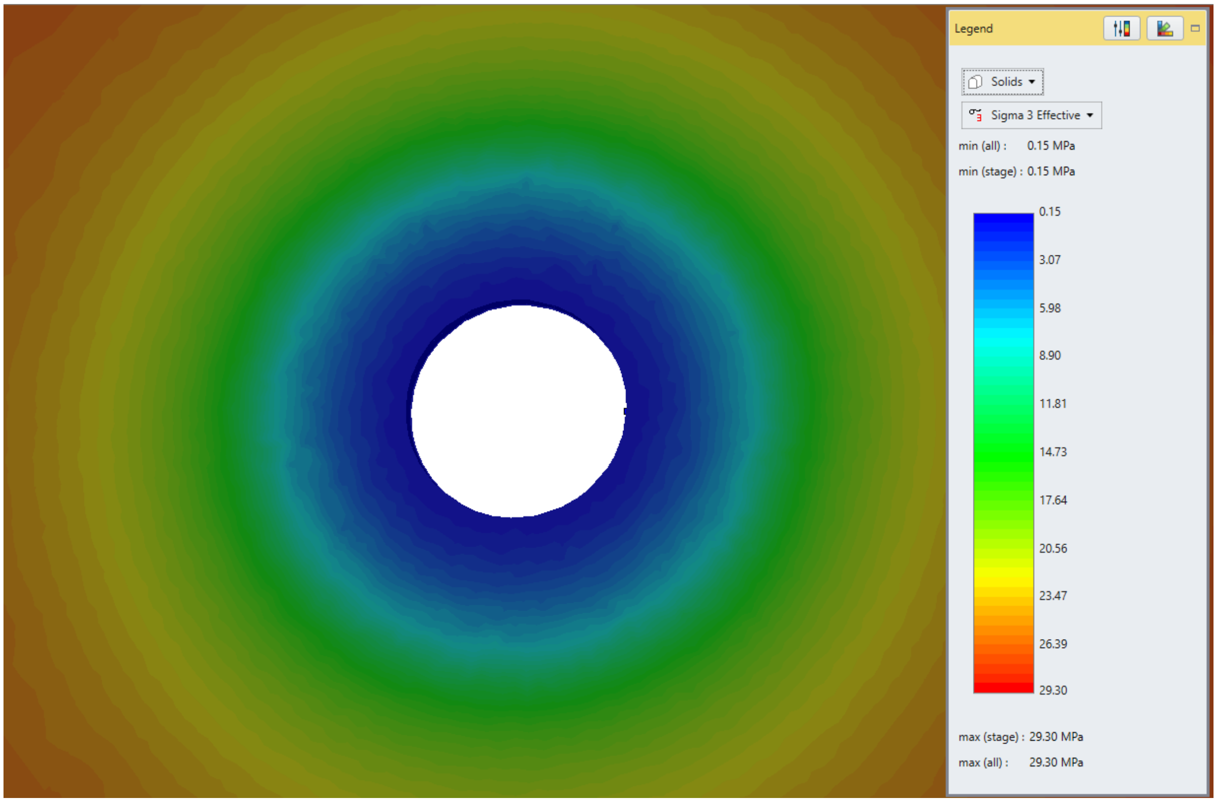

Figure 6.5: Radial stress contour plot in RS3

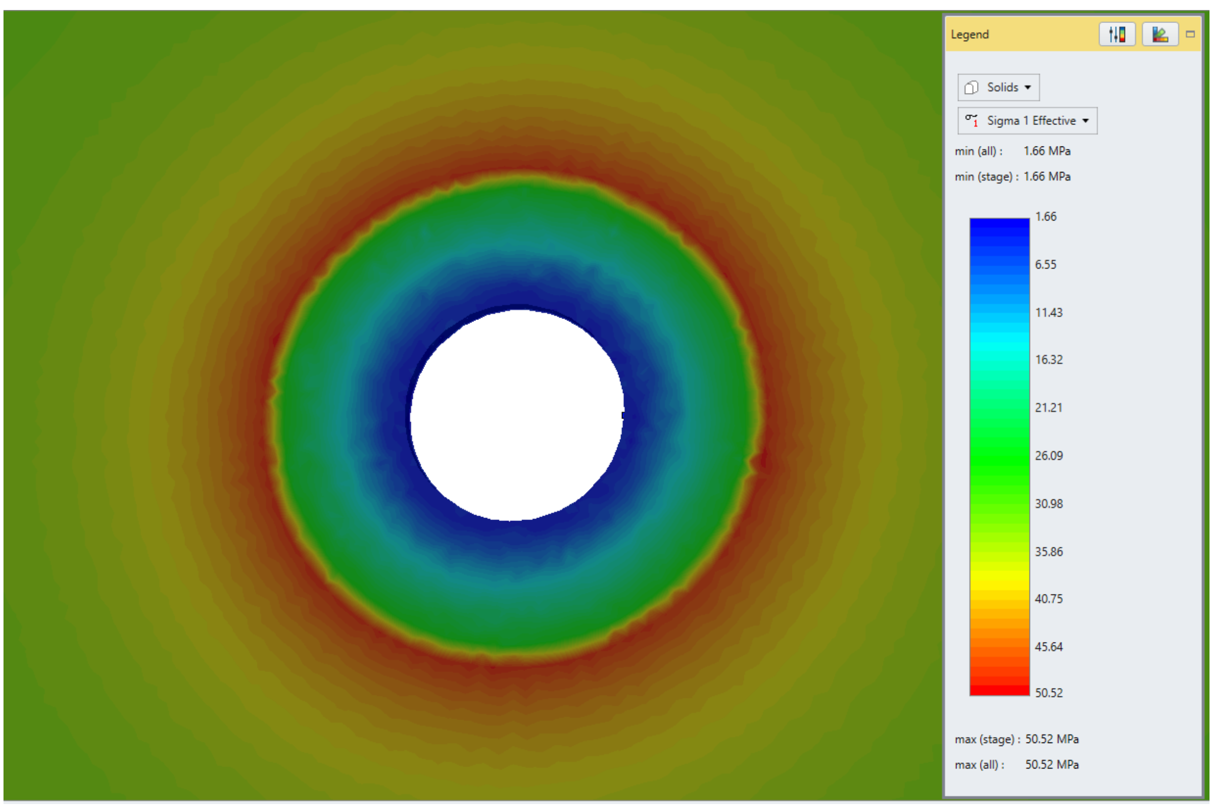

Figure 6.6: Tangential stress contour in RS3

6.4. References

1. Hoek, E. and Brown, E. T., (1982) Underground Excavations in Rock, London: IMM, PP. 249-253

2. Itasca Consulting Group, INC (1993), “Cylindrical hole in an Infinite Hoek-Brown Medium”, Fast Lagrangian analysis of Continua (Version 3.2), Verification Manual.

6.5. Data Files

The input data file **StressVerification-06.rs3v3** can be downloaded from the RS3 Online Help page.

7. Drained Triaxial Compressive Test of Modified Cam Clay Material

7.1. Problem Description

The Modified Cam Clay (MCC) constitutive relationship is one of the earliest critical state models for realistically describing the behaviour of soft soils. As a result, it is one of the most widely applied stress-strain relationship in the non-linear finite element modeling of practical geotechnical problems. The state at a point in an MCC soil is characterized by three parameters: effective mean stress p', deviatoric (shear stress) q, and specific volume v.

Due to the complexity of the MCC model, very few MCC problems have closed-form solutions, which can be used to verify the accuracy, stability, and convergence of MCC finite element algorithms. One of the problems with an analytical solution is the consolidated-drained triaxial test on a MCC sample. In this test, the sample is first consolidated under a hydrostatic pressure, and then sheared by applying additional axial load (see Figure 7.1). The drainage condition is such that there is no buildup of excess pore water pressures (i.e. excess pore pressures are allowed to fully dissipate).

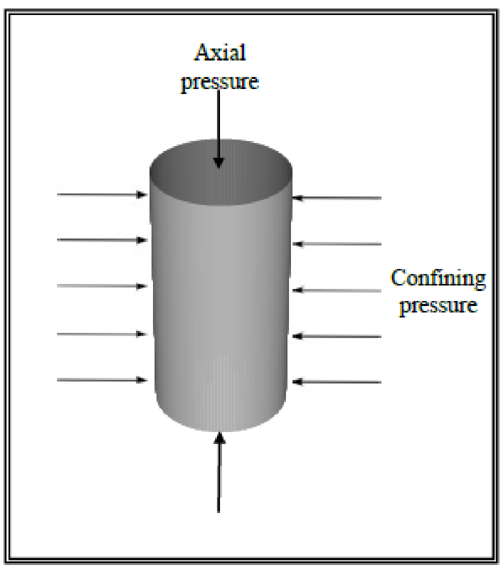

Figure 7.1: Triaxial compressive test of cylindrical soil sample

In *RS3*, the MCC constitutive model is integrated implicitly over a finite strain increment using the approach presented by Borja (Borja, 1991). Major advantages of this approach are its accuracy, robustness, and efficiency. The performance of this algorithm in *RS3* will be tested in three examples of drained triaxial test. The first test on a normally consolidated clay sample involves only post-yield (elasto-plastic) loading; a behavior that is associated with hardening of the material. The second test is on a lightly over consolidated clay sample where the initial behavior is elastic and it is followed by a transition to elasto-plastic response. The last example demonstrates the behavior of a highly over consolidated clay sample that includes an initial elastic behavior followed by failure and a softening branch in its stress path. The stress paths, initial and final yield surfaces of these tests are shown in Figure 7.2 to Figure 7.4.

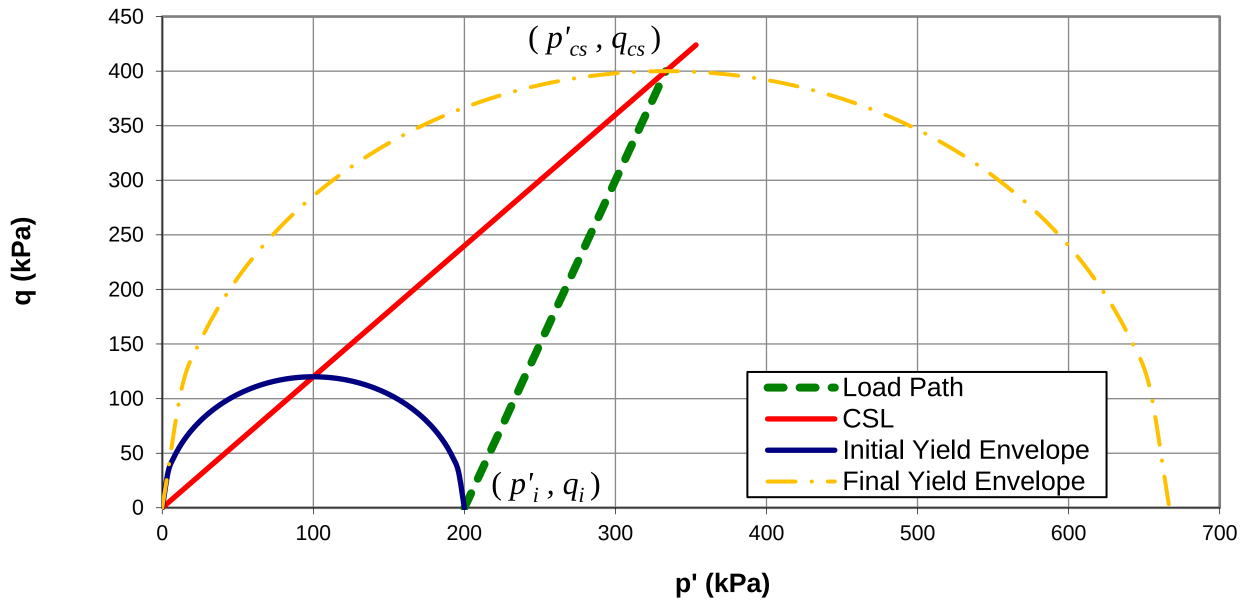

Figure 7.2 : Example 1, drained triaxial compressive test on a normally consolidated clay sample, stress path, initial and final yield surfaces in *p'-q* space

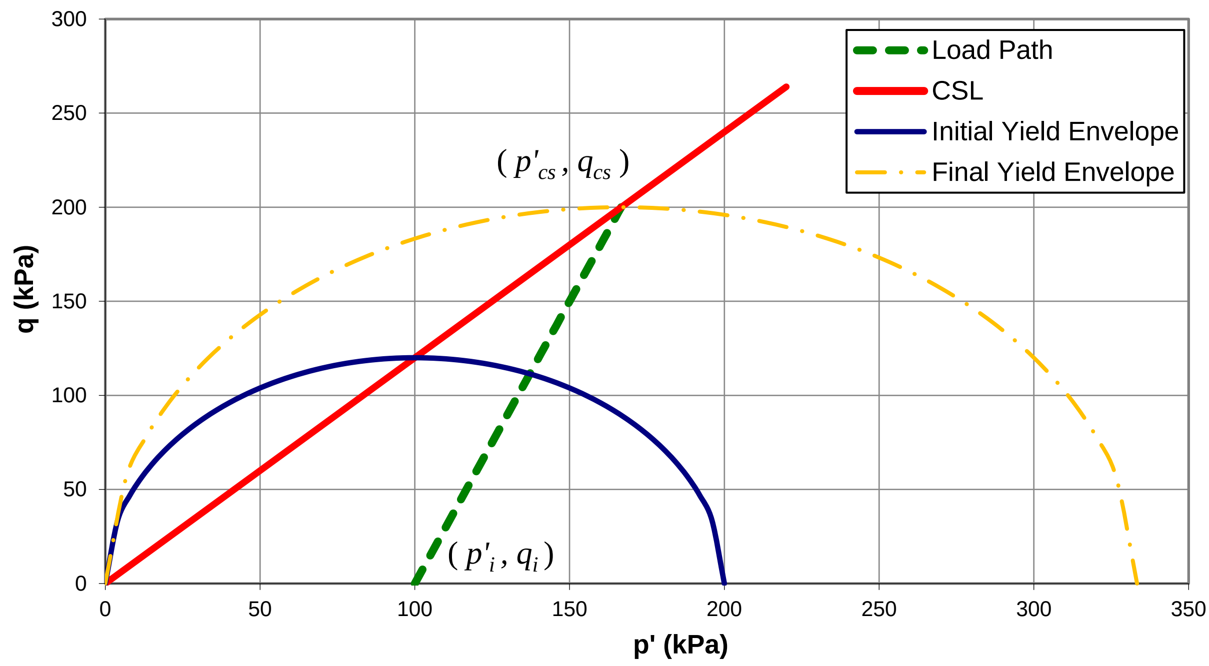

Figure 7.3 : Example 2, drained triaxial compressive test on a lighttly over consolidated caly sample(OCR=2), stress pth, initial and fimnaly yield surfaces in *p'-q'* space

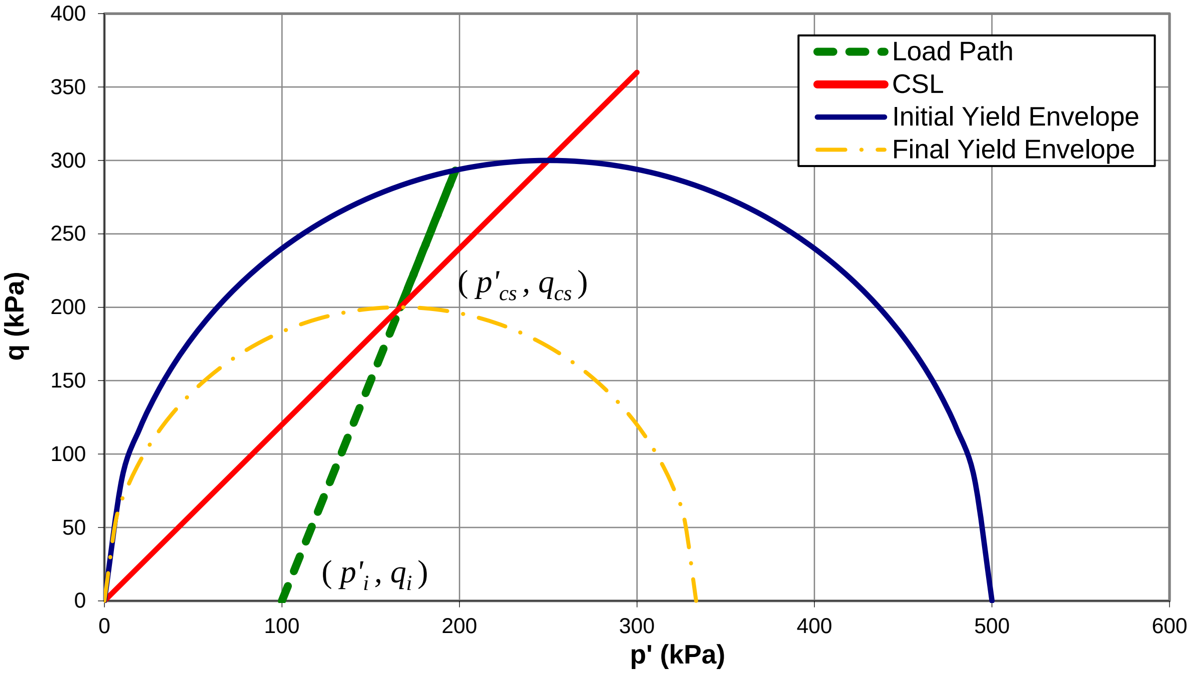

Figure 7.4: Example 3, drained triaxial compressive test on a highly over consolidated clay sample (OCR=5), stress pth, initial and final yield surfaces in *p'=q'* space

For each triaxial test, two plots will be generated to compare the performance of the MCC implementation in RS3 in relation to the drained triaxial test benchmark solution. The first plot examines the relationship between deviatoric (shear stress), q, and axial strain, ε_a, of the test sample, while the second compares volumetric strains, ε_v, to axial strains.

Five material parameters are required to specify the behaviour of the MCC sample. These are:

1. λ – the slope of the normal compression (virgin consolidation) line and critical state line (CSL) in $v - \ln p'$ space

2. κ – the slope of a swelling (loading-unloading) line in $v - \ln p'$ space

3. M – the slope of the CSL in $q - p'$ space

4. $\begin{cases} N - \text{the specific volume of the normal compression line at unit pressure} \\ or \\ \Gamma \ - \text{the specific volume of the CSL at unit pressure} \end{cases}$

5. $\begin{cases} \nu - \text{Poisson's ratio} \\ or \\ G - \text{shear modulus} \end{cases}$

As can be seen from the description of input parameters, the MCC formulation requires specification of either a constant shear modulus G or a constant Poisson's ratio μ, but not both. The verification example will examine the performance of RS3 using both of these options.

The initial state of consolidation of the MCC soil is specified in terms of a pre-consolidation pressure, p_o. (RS3 also allows users to specify the initial state of consolidation through the over-consolidation ratio.)

For the test, the following material properties and conditions are assumed:

Table 7-1 : Model parameters

Parameter	Value
N	1.788
M	1.2
λ	0.066
κ	0.0077
G (for the case of constant elasticity)	20000 kPa
μ (for the case of variable elasticity)	0.3
Initial State of the Normally Consolidated Clay	
Preconsolidation pressure, po	200 kPa
Initial mean volumetric stress, p'	200 kPa
Initial shear stress, q	0 kPa
Initial State of the Lightly Over Consolidated Clay	
Preconsolidation pressure, po	200 kPa
Initial mean volumetric stress, 'p	100 kPa
Initial shear stress, q	0 kPa
Initial State of Highly Over Consolidated Clay	
Preconsolidation pressure, po	500 kPa
Initial mean volumetric stress, p'	100 kPa
Initial shear stress, q	0 kPa

7.2. Analytical Solution

The analytical solution presented here is adopted from an article by Peric (Peric, 2006). The solution distinguishes between the volumetric, (p', ε_v), and the deviatoric, (q, ε_q), behaviour of the material.

7.2.1. The volumetric behaviour

Decomposing to its elastic and plastic parts, the rate of the volumetric strain can be obtained from its nonlinear elastic behavior and the hardening rule.

$$\dot{\varepsilon}_v^e = k\dot{p}' = \left(\frac{\kappa}{v_n}\right)\frac{\dot{p}'}{p'} \quad (7.1)$$

$$\dot{\varepsilon}_v^p = \left(\frac{\lambda - \kappa}{v_n}\right)\frac{\dot{p}_0}{(p_0)_n} \quad (7.2)$$

Considering a general rate of stress, using the definition of the yield surface, the rate of plastic volumetric strain can be rewritten as

$$\dot{\varepsilon}_v^p = \left(\frac{\lambda - \kappa}{v_n}\right)\left(\frac{\dot{p}'}{p'} + \frac{2\eta\dot{\eta}}{M^2 + \eta^2}\right) \quad (7.3)$$

$$\eta = \frac{q}{p'} \quad (7.4)$$

$$\dot{\eta} = \frac{\dot{q}}{\dot{p}'} \quad (7.5)$$

Integrating above equations (7.1) and (7.3) over a finite time increment (step *n* to step $n + 1$), assuming that the change in specific volume is insignificant, results in the following incremental equations

$$\Delta\varepsilon_v^e = \frac{1}{v_n}\ln\left(\frac{p'_{n+1}}{p'_n}\right)^{\kappa} \quad (7.6)$$

$$\Delta\varepsilon_v^p = \frac{1}{v_n}\ln\left(\left(\frac{p'_{n+1}}{p'_n}\right)\left(\frac{M^2 + \eta_{n+1}^2}{M^2 + \eta_n^2}\right)\right)^{\lambda-\kappa} \quad (7.7)$$

Thus, the total increment of volumetric strain is

$$\Delta\varepsilon_v = \frac{1}{v_n}\ln\left(\left(\frac{p'_{n+1}}{p'_n}\right)^{\lambda}\left(\frac{M^2 + \eta_{n+1}^2}{M^2 + \eta_n^2}\right)^{\lambda-\kappa}\right) \quad (7.8)$$

Considering a straight stress path in $(p' - q)$ space, with a slope of $(\Delta q/\Delta p') = k$, the above equation (7.8) can be rewritten as

$$\Delta\varepsilon_v = \frac{1}{v_n}\ln\left(\left(\frac{k - \eta_n}{k - \eta_{n+1}}\right)^{\lambda}\left(\frac{M^2 + \eta_{n+1}^2}{M^2 + \eta_n^2}\right)^{\lambda-\kappa}\right) \quad (7.9)$$

Note that in the case of a drained triaxial test $k = 3$.

The change in the specific volume can also be calculated from the

$$\Delta v = \frac{\Delta\varepsilon_v}{v_n} \quad (7.10)$$

7.2.2. The deviatoric behavior

According to the flow rule the rate of plastic strains are calculated as

$$\dot{\varepsilon}_v^p = \dot{\lambda}\frac{\partial F}{\partial p'} \tag{7.11}$$

$$\dot{\varepsilon}_q^p = \dot{\lambda}\frac{\partial F}{\partial q} \tag{7.12}$$

So the relation between the rate of volumetric strain and the deviatoric one is

$$\dot{\varepsilon}_q^p \frac{\partial F}{\partial p'} = \dot{\varepsilon}_v^p \frac{\partial F}{\partial q} \tag{7.13}$$

Thus, the rate of deviatoric plastic strain is

$$\dot{\varepsilon}_q^p = \frac{2\eta}{M^2 - \eta^2}\dot{\varepsilon}_v^p = \left(\frac{\lambda - \kappa}{v_n}\right)\left(\frac{2\eta}{M^2 - \eta^2}\right)\left(\frac{\dot{p}'}{p'} + \frac{2\eta\dot{\eta}}{M^2 + \eta^2}\right) \tag{7.14}$$

Once again by considering a straight stress path, with a slope of $(\Delta q/\Delta p') = k$, the plastic deviatoric strain can be calculated as

$$\dot{\varepsilon}_q^p = \left(\frac{\lambda - \kappa}{v_n}\right)\left(\frac{2\eta}{(M^2 - \eta^2)(k - \eta)} + \frac{4\eta^2}{M^4 + \eta^4}\right)\eta^{\cdot} \tag{7.15}$$

The elastic portion of the deviatoric strain can be calculated from Hooke's law:

$$\dot{\varepsilon}_q^p = \frac{\dot{q}}{3G} \tag{7.16}$$

In case the model uses a constant Poisson's ratio, the shear modulus should be calculated as

$$G = \alpha K = \frac{\alpha v_n p'}{\kappa} \tag{7.17}$$

$$\alpha = \frac{3(1 - 2\nu)}{2(1 + \nu)} \tag{7.18}$$

Integrating the rate of deviatoric strain over a finite time increment (step *n* to step *n* +1), results in the following incremental equation for the plastic and elastic portion of deviatoric strain

$$\begin{aligned}\Delta\varepsilon_q^p = \frac{1}{v_n}\ln\left[\left(\frac{M - \eta_{n+1}}{M - \eta_n}\right)^{\frac{(\lambda-\kappa)k}{M(M+k)}}\left(\frac{M + \eta_{n+1}}{M + \eta_n}\right)^{\frac{(\lambda-\kappa)k}{M(M+k)}}\left(\frac{M + \eta_{n+1}}{M + \eta_n}\right)^{\frac{2(\lambda-\kappa)k}{k^2-M^2}}\right] \\ - \frac{2(\lambda - \kappa)}{Mv_n}\left[\arctan\left(\frac{\eta_{n+1}}{M}\right) - \arctan\left(\frac{\eta_n}{M}\right)\right]\end{aligned} \tag{7.19}$$

In the case of constant shear modulus, the elastic part of the increment of deviatoric strain is

$$\Delta\varepsilon_q^e = \frac{q_{n+1} - q_n}{3G} \tag{7.20}$$

Otherwise,

$$\Delta\varepsilon_q^e = \frac{1}{v_n}\ln\left(\frac{k - \eta_{n+1}}{k - \eta_n}\right)^{-\frac{\kappa k}{3\alpha}} \tag{7.21}$$

The volumetric and shear strains calculated in a triaxial test can be related to the axial and radial strains, ε_a and ε_r, respectively, of the test sample. The relationships are as follows

$$\varepsilon_\mathrm{a} = \frac{1}{3}\varepsilon_v + \varepsilon_q \tag{7.22}$$

$$\varepsilon_\mathrm{r} = \frac{1}{3}\varepsilon_v - \frac{1}{2}\varepsilon_q \tag{7.23}$$

The formulations presented above have been implemented in Excel spreadsheets included with this document.

7.3. RS3 Model

The drained compressive triaxial tests of the MCC sample were modeled in RS3 using 4-noded tetrahedral elements. The deviatoric stress is generated in the sample in two different ways using load-control and displacement-control processes. In the load–control method the axial load is increased in a number of stages that match the load steps used in the analytical solution. In the displacement-control simulations axial displacement is imposed on the sample, once again in a number of stages that match the displacement history of analytical solutions. The boundary conditions and an example of the applied loads used are shown on Figure 7.5 and Figure 7.6 for load-control and displacement-control simulations.

As mentioned before, for each example the stage factors for the axial loads or axial deformation were calculated (from the attached spreadsheet) such that the resulting effective mean and deviatoric stresses conformed to the selected triaxial loading path. In the first test, which starts with stresses on the initial yield envelope, the load path (shown on Figure 7.2) was applied in 31 stages. In Examples 2 and 3 (Figure 7.3 and Figure 7.4), the load path was applied in 35 stages.

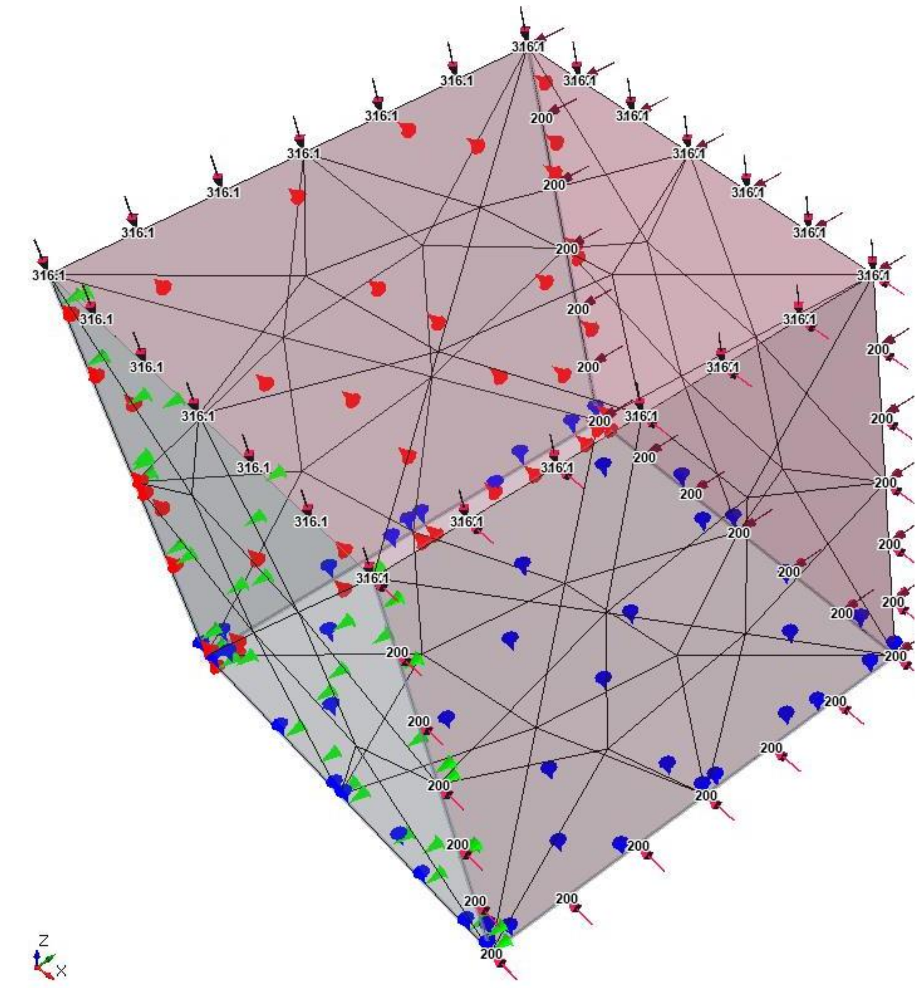

Figure 7.5: Boundary conditions and loads for axisymmetric *RS3* analysis; load-control control simulation

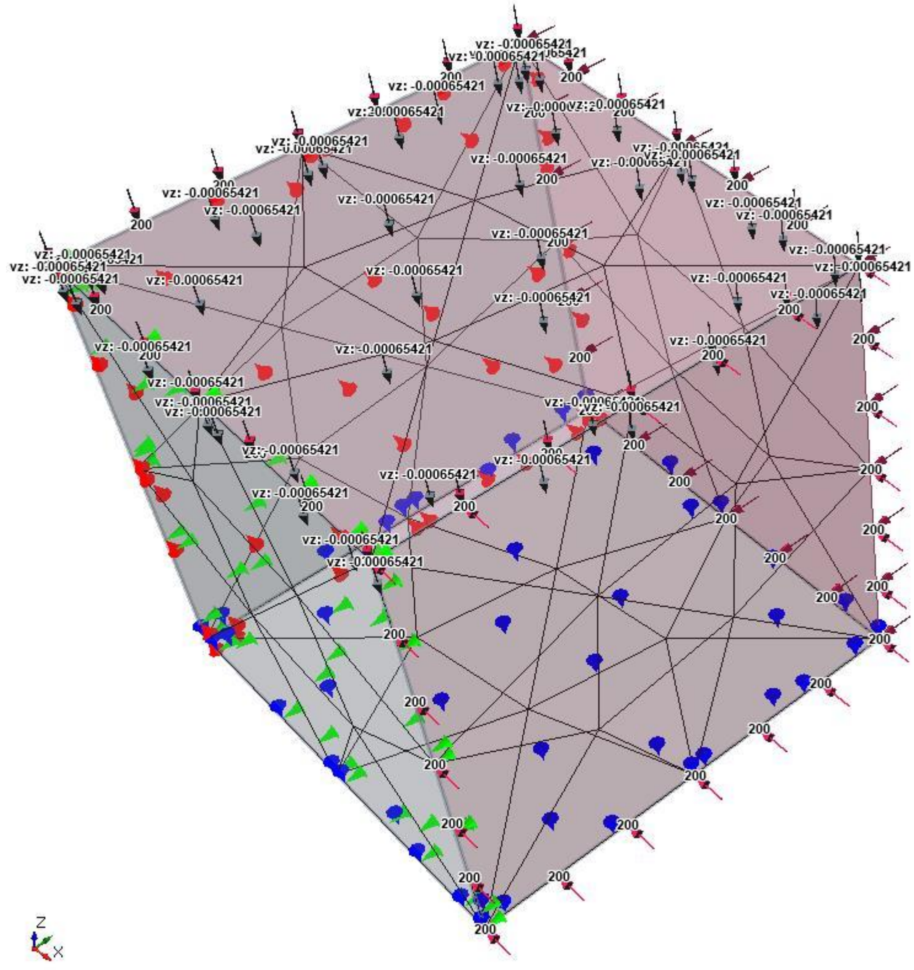

Figure 7.6: Boundary conditions and loads for axisymmetric *RS3* analysis; displacement-control control simulation

7.4. Results

Table 7-2 and Table 7-3 present the variation of the deviatoric stress, axial and volumetric strains calculated from the analytical solution and from RS3 for the first triaxial test example (Example 1). Table 7-2 represents the case of constant shear modulus, while in Table 7-3 the Poisson's ratio is constant.

Figure 7.7 and Figure 7.8 show the plots of $\varepsilon_a - q$ and $\varepsilon_a - \varepsilon_v$ obtained from the analytical and numerical solutions for the case of constant shear modulus. Figure 7.9 and Figure 7.10 show the same results but for the case of constant Poisson's ratio.

Accordingly, the results for the second and third examples are summarized in Table 7-4 to Table 7-6 and Figure 7.11 to Figure 7.16.

For all the cases analyzed below, there is a good agreement between the analytical results and the numerical results obtained from RS3.

Table 7-2: Example 1, Triaxial test on a normally consolidated clay sample; results for case of constant shear modulus

	***RS3* Load-Control**			***RS3* Displacement-Control**			**Analytical Solution**		
No.	**q (kPa)**	**Axial strain, εa**	**Volumetric strain, εv**	**q (kPa)**	**Axial strain, εa**	**Volumetric strain, εv**	**q (kPa)**	**Axial strain, εa**	**Volumetric strain, εv**
1	0.00	0.00000	0.00000	0.00	0.00000	0.00000	0.00	0.00000	0.00000
2	12.90	0.00063	0.00109	12.70	0.00062	0.00107	12.90	0.00062	0.00109
3	25.81	0.00144	0.00237	25.44	0.00142	0.00233	25.81	0.00142	0.00236
4	38.71	0.00243	0.00381	38.21	0.00239	0.00375	38.71	0.00239	0.00379
5	51.61	0.00362	0.00538	51.01	0.00357	0.00530	51.61	0.00357	0.00535
6	64.52	0.00502	0.00705	63.83	0.00494	0.00696	64.52	0.00494	0.00702
7	77.42	0.00662	0.00882	76.68	0.00653	0.00871	77.42	0.00653	0.00877
8	90.32	0.00843	0.01065	89.55	0.00832	0.01054	90.32	0.00832	0.01059
9	103.23	0.01044	0.01253	102.45	0.01032	0.01241	103.23	0.01032	0.01246
10	116.13	0.01267	0.01444	115.37	0.01254	0.01433	116.13	0.01254	0.01436
11	129.03	0.01510	0.01638	128.33	0.01498	0.01628	129.03	0.01498	0.01628
12	141.93	0.01775	0.01833	141.32	0.01763	0.01824	141.94	0.01763	0.01822
13	154.84	0.02062	0.02028	154.34	0.02052	0.02021	154.84	0.02052	0.02016
14	167.74	0.02372	0.02223	167.40	0.02365	0.02218	167.74	0.02365	0.02209
15	180.64	0.02704	0.02417	180.51	0.02702	0.02415	180.65	0.02702	0.02402
16	193.55	0.03062	0.02609	193.64	0.03067	0.02611	193.55	0.03067	0.02593
17	206.45	0.03447	0.02799	206.82	0.03460	0.02805	206.45	0.03460	0.02782
18	219.35	0.03860	0.02987	220.02	0.03884	0.02998	219.35	0.03884	0.02968
19	232.26	0.04305	0.03173	233.30	0.04344	0.03188	232.26	0.04344	0.03153
20	245.16	0.04785	0.03356	246.63	0.04843	0.03377	245.16	0.04843	0.03334
21	258.06	0.05305	0.03536	260.04	0.05387	0.03563	258.06	0.05387	0.03513
22	270.97	0.05872	0.03713	273.48	0.05984	0.03747	270.97	0.05984	0.03689
23	283.87	0.06493	0.03887	287.00	0.06644	0.03929	283.87	0.06644	0.03862
24	296.77	0.07179	0.04058	300.60	0.07380	0.04108	296.77	0.07380	0.04032
25	309.68	0.07945	0.04226	314.26	0.08212	0.04285	309.68	0.08212	0.04199
26	322.58	0.08814	0.04391	328.04	0.09170	0.04460	322.58	0.09170	0.04363
27	335.48	0.09817	0.04553	341.78	0.10297	0.04631	335.48	0.10297	0.04524

28	348.39	0.11009	0.04712	355.66	0.11669	0.04800	348.39	0.11669	0.04682
29	361.29	0.12484	0.04868	369.66	0.13426	0.04967	361.29	0.13426	0.04838
30	374.19	0.14440	0.05021	383.41	0.15887	0.05128	374.19	0.15887	0.04990
31	387.10	0.17448	0.05171	396.88	0.20061	0.05281	387.10	0.20061	0.05139

Table 7-3: Example 1, Triaxial test on a normally consolidated clay sample; results for case of constant Poisson's ratio

	***RS3* Load-Control**			***RS3* Displacement-Control**			**Analytical Solution**		
No.	**q (kPa)**	**Axial strain, εa**	**Volumetric strain, εv**	**q (kPa)**	**Axial strain, εa**	**Volumetric strain, εv**	**q (kPa)**	**Axial strain, εa**	**Volumetric strain, εv**
1	0.00	0.00000	0.00000	0.00	0.00000	0.00000	0.00	0.00000	0.00000
2	12.90	0.00066	0.00109	12.71	0.00065	0.00107	12.90	0.00065	0.00109
3	25.81	0.00150	0.00237	25.46	0.00147	0.00233	25.81	0.00147	0.00236
4	38.71	0.00251	0.00381	38.26	0.00247	0.00375	38.71	0.00247	0.00379
5	51.61	0.00372	0.00538	51.08	0.00367	0.00531	51.61	0.00367	0.00535
6	64.52	0.00512	0.00705	63.93	0.00506	0.00698	64.52	0.00506	0.00702
7	77.42	0.00673	0.00882	76.80	0.00665	0.00873	77.42	0.00665	0.00877
8	90.32	0.00854	0.01065	89.68	0.00845	0.01056	90.32	0.00845	0.01059
9	103.23	0.01055	0.01253	102.58	0.01045	0.01243	103.23	0.01045	0.01246
10	116.13	0.01278	0.01444	115.49	0.01267	0.01435	116.13	0.01267	0.01436
11	129.03	0.01521	0.01638	128.41	0.01510	0.01629	129.03	0.01510	0.01628
12	141.93	0.01786	0.01833	141.35	0.01775	0.01824	141.94	0.01775	0.01822
13	154.84	0.02074	0.02028	154.30	0.02063	0.02020	154.84	0.02063	0.02016
14	167.74	0.02384	0.02223	167.26	0.02374	0.02216	167.74	0.02374	0.02209
15	180.64	0.02719	0.02417	180.23	0.02710	0.02411	180.65	0.02710	0.02402
16	193.55	0.03079	0.02609	193.22	0.03072	0.02604	193.55	0.03072	0.02593
17	206.45	0.03468	0.02799	206.21	0.03463	0.02796	206.45	0.03463	0.02782
18	219.35	0.03886	0.02987	219.23	0.03885	0.02986	219.35	0.03885	0.02968
19	232.26	0.04339	0.03173	232.28	0.04342	0.03173	232.26	0.04342	0.03153
20	245.16	0.04828	0.03356	245.37	0.04838	0.03359	245.16	0.04838	0.03334
21	258.06	0.05362	0.03536	258.45	0.05379	0.03541	258.06	0.05379	0.03513

22	270.97	0.05945	0.03713	271.57	0.05972	0.03721	270.97	0.05972	0.03689
23	283.87	0.06588	0.03887	284.70	0.06628	0.03898	283.87	0.06628	0.03862
24	296.77	0.07304	0.04058	297.87	0.07360	0.04072	296.77	0.07360	0.04032
25	309.68	0.08111	0.04226	311.09	0.08188	0.04244	309.68	0.08188	0.04199
26	322.58	0.09035	0.04391	324.23	0.09141	0.04412	322.58	0.09141	0.04363
27	335.48	0.10117	0.04553	337.44	0.10264	0.04577	335.48	0.10264	0.04524
28	348.39	0.11425	0.04712	350.78	0.11631	0.04740	348.39	0.11631	0.04682
29	361.29	0.13086	0.04868	364.03	0.13383	0.04900	361.29	0.13383	0.04838
30	374.19	0.15379	0.05021	377.61	0.15838	0.05059	374.19	0.15838	0.04990
31	387.10	0.19184	0.05171	391.54	0.20007	0.05219	387.10	0.20007	0.05139

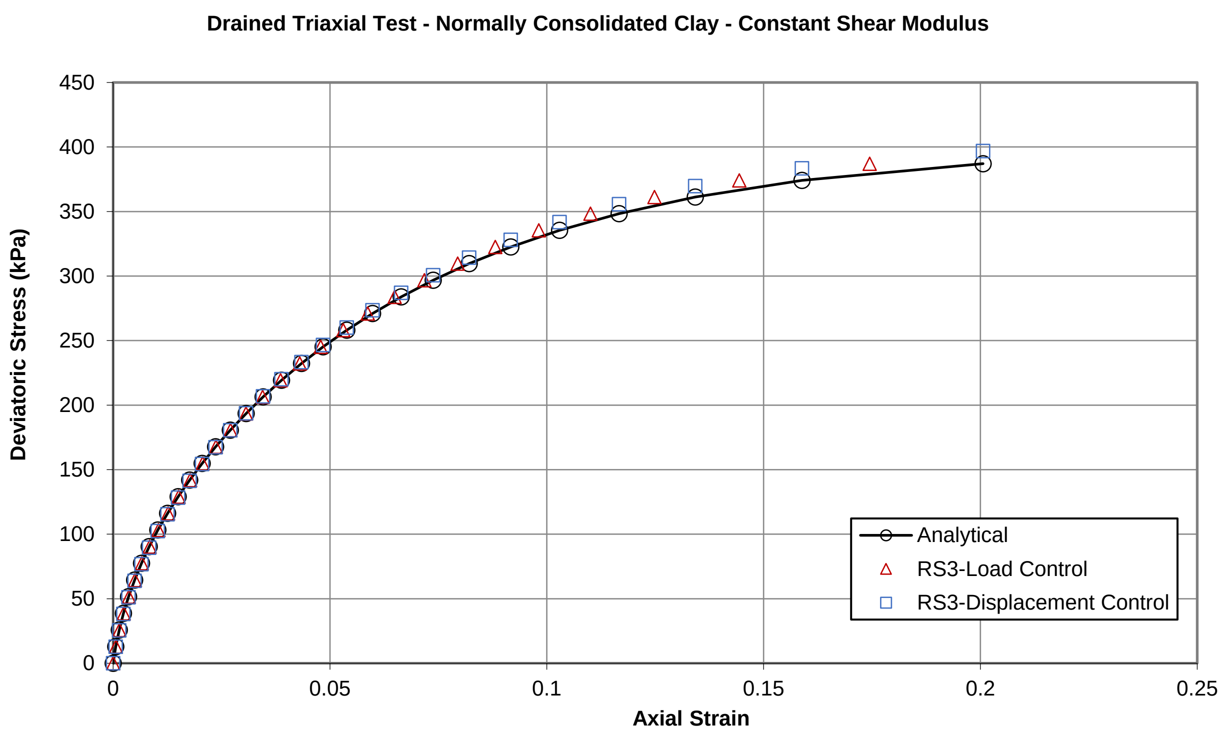

Figure 7.7: Variation of deviatoric stress with axial strain for Example 1 case of constant shear modulus

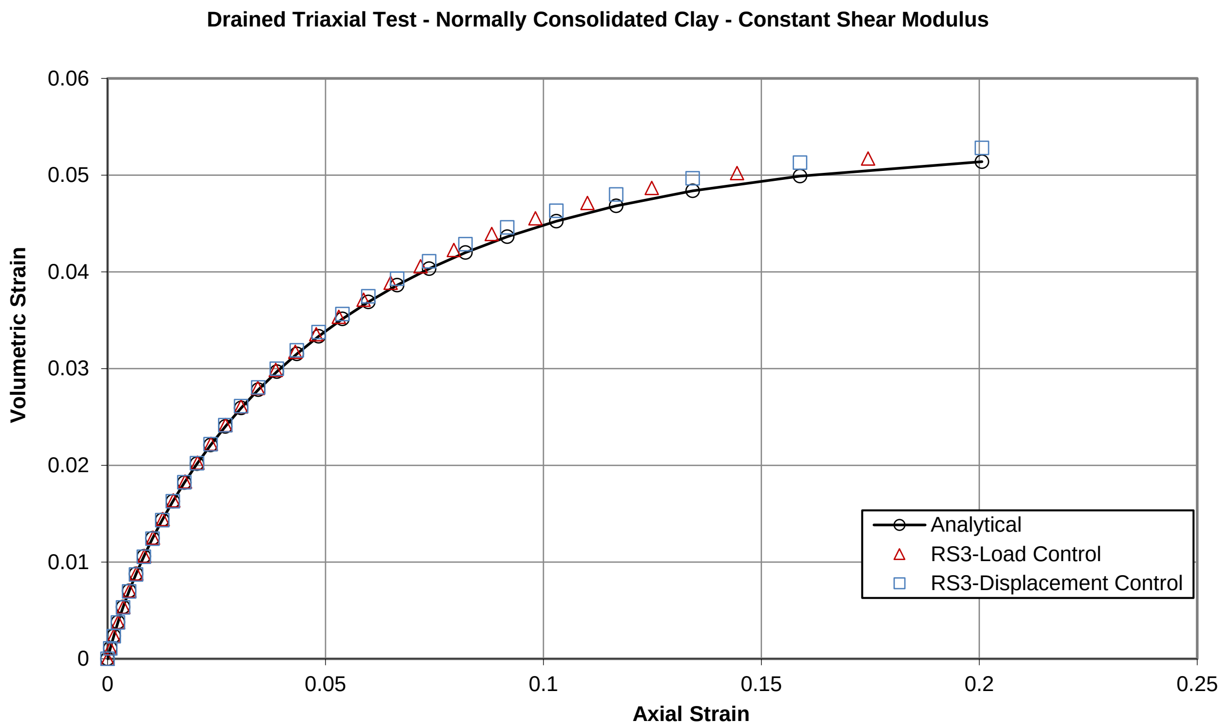

Figure 7.8: Variation of volumetric strain with axial strain for Example 1 case of constant shear modulus

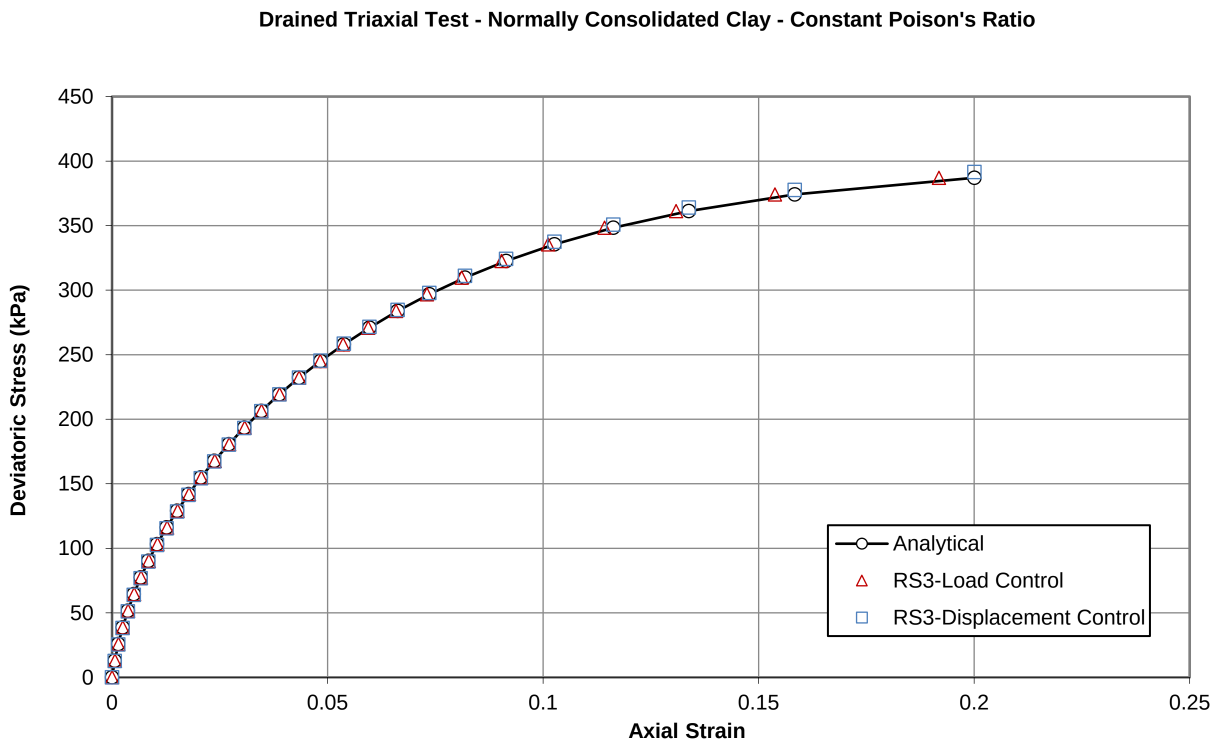

Figure 7.9: Variation of deviatoric stress with axial strain for Example 1 case of constant Poisson's ratio

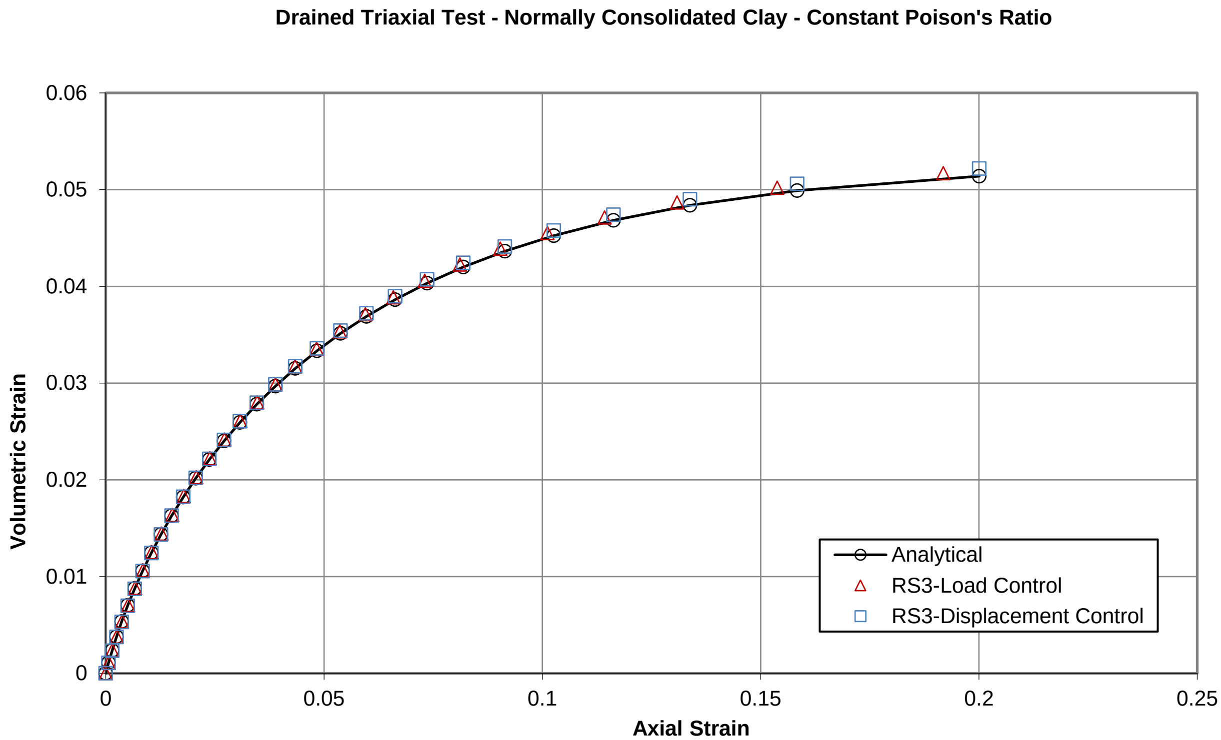

Figure 7.10: Variation of volumetric strain with axial strain for Example 1 case of constant Poisson's ratio

Table 7-4: Example 2, Triaxial test on a lightly over consolidated clay sample; results for case of constant shear modulus

	***RS3* Load-Control**			***RS3* Displacement-Control**			**Analytical Solution**		
No.	**q (kPa)**	**Axial strain, εa**	**Volumetric strain, εv**	**q (kPa)**	**Axial strain, εa**	**Volumetric strain, εv**	**q (kPa)**	**Axial strain, εa**	**Volumetric strain, εv**
1	0.00	0.00000	0.00000	0.00	0.00000	0.00000	0.00	0.00000	0.00000
2	27.85	0.00062	0.00048	27.75	0.00062	0.00048	27.85	0.00062	0.00047
3	55.71	0.00124	0.00092	55.52	0.00123	0.00092	55.71	0.00123	0.00091
4	83.56	0.00184	0.00133	83.31	0.00183	0.00132	83.56	0.00183	0.00131
5	111.42	0.00243	0.00171	111.11	0.00242	0.00170	111.42	0.00242	0.00169
6	114.27	0.00446	0.00250	114.12	0.00434	0.00246	114.27	0.00434	0.00248
7	117.13	0.00658	0.00329	116.84	0.00634	0.00321	117.13	0.00634	0.00326
8	119.99	0.00877	0.00407	119.57	0.00842	0.00396	119.99	0.00842	0.00405
9	122.85	0.01105	0.00485	122.29	0.01057	0.00470	122.85	0.01057	0.00482

10	125.70	0.01343	0.00562	125.02	0.01281	0.00544	125.70	0.01281	0.00559
11	128.56	0.01590	0.00639	127.76	0.01514	0.00618	128.56	0.01514	0.00636
12	131.42	0.01848	0.00715	130.50	0.01758	0.00691	131.42	0.01758	0.00712
13	134.28	0.02118	0.00791	133.24	0.02011	0.00764	134.28	0.02011	0.00787
14	137.13	0.02400	0.00866	135.99	0.02276	0.00836	137.13	0.02276	0.00862
15	139.99	0.02696	0.00941	138.74	0.02554	0.00908	139.99	0.02554	0.00937
16	142.85	0.03006	0.01015	141.50	0.02845	0.00979	142.85	0.02845	0.01010
17	145.71	0.03333	0.01088	144.24	0.03152	0.01050	145.71	0.03152	0.01084
18	148.56	0.03678	0.01161	147.00	0.03474	0.01121	148.56	0.03474	0.01156
19	151.42	0.04044	0.01233	149.77	0.03815	0.01191	151.42	0.03815	0.01228
20	154.28	0.04431	0.01305	152.55	0.04176	0.01261	154.28	0.04176	0.01300
21	157.14	0.04845	0.01376	155.33	0.04561	0.01331	157.14	0.04561	0.01371
22	159.99	0.05287	0.01446	158.12	0.04971	0.01400	159.99	0.04971	0.01441
23	162.85	0.05763	0.01516	160.91	0.05411	0.01469	162.85	0.05411	0.01511
24	165.71	0.06278	0.01586	163.72	0.05886	0.01537	165.71	0.05886	0.01580
25	168.57	0.06839	0.01654	166.54	0.06401	0.01605	168.57	0.06401	0.01649
26	171.42	0.07455	0.01723	169.36	0.06965	0.01673	171.42	0.06965	0.01717
27	174.28	0.08138	0.01790	172.21	0.07586	0.01741	174.28	0.07586	0.01784
28	177.14	0.08906	0.01857	175.07	0.08280	0.01808	177.14	0.08280	0.01851
29	180.00	0.09781	0.01924	177.95	0.09064	0.01875	180.00	0.09064	0.01917
30	182.85	0.10799	0.01990	180.80	0.09968	0.01942	182.85	0.09968	0.01983
31	185.71	0.12017	0.02055	183.74	0.11034	0.02009	185.71	0.11034	0.02049
32	188.57	0.13531	0.02120	186.72	0.12336	0.02077	188.57	0.12336	0.02113
33	191.43	0.15533	0.02184	189.79	0.14010	0.02146	191.43	0.14010	0.02177
34	194.28	0.18475	0.02248	192.96	0.16363	0.02217	194.28	0.16363	0.02241
35	197.14	0.23966	0.02311	196.71	0.20374	0.02299	197.14	0.20374	0.02304

Table 7-5: Example 2, Triaxial test on a lightly over consolidated clay sample; results for case of constant Poisson's ratio

	***RS3* Load-Control**			***RS3* Displacement-Control**			**Analytical Solution**		
No.	**q (kPa)**	**Axial strain, εa**	**Volumetric strain, εv**	**q (kPa)**	**Axial strain, εa**	**Volumetric strain, εv**	**q (kPa)**	**Axial strain, εa**	**Volumetric strain, εv**
1	0.00	0.00000	0.00000	0.00	0.00000	0.00000	0.00	0.00000	0.00000
2	27.86	0.00120	0.00048	27.85	0.00120	0.00048	27.85	0.00118	0.00047
3	55.71	0.00230	0.00092	54.94	0.00227	0.00091	55.71	0.00227	0.00091
4	83.56	0.00332	0.00133	82.44	0.00328	0.00131	83.56	0.00328	0.00131
5	111.42	0.00427	0.00171	109.96	0.00422	0.00169	111.42	0.00422	0.00169
6	114.27	0.00621	0.00250	114.22	0.00617	0.00248	114.27	0.00617	0.00248
7	117.13	0.00823	0.00329	117.10	0.00820	0.00328	117.13	0.00820	0.00326
8	119.99	0.01032	0.00407	119.98	0.01031	0.00407	119.99	0.01031	0.00405
9	122.85	0.01250	0.00485	122.86	0.01250	0.00485	122.85	0.01250	0.00482
10	125.70	0.01475	0.00563	125.74	0.01477	0.00563	125.70	0.01477	0.00559
11	128.56	0.01710	0.00639	128.62	0.01713	0.00641	128.56	0.01713	0.00636
12	131.42	0.01954	0.00716	131.49	0.01959	0.00717	131.42	0.01959	0.00712
13	134.28	0.02208	0.00791	134.38	0.02216	0.00794	134.28	0.02216	0.00787
14	137.13	0.02474	0.00866	137.26	0.02484	0.00870	137.13	0.02484	0.00862
15	139.99	0.02751	0.00941	140.14	0.02764	0.00945	139.99	0.02764	0.00937
16	142.85	0.03042	0.01015	143.03	0.03058	0.01019	142.85	0.03058	0.01010
17	145.71	0.03347	0.01088	145.92	0.03367	0.01093	145.71	0.03367	0.01084
18	148.56	0.03669	0.01161	148.80	0.03693	0.01167	148.56	0.03693	0.01156
19	151.42	0.04008	0.01233	151.69	0.04036	0.01240	151.42	0.04036	0.01228
20	154.28	0.04366	0.01305	154.58	0.04400	0.01312	154.28	0.04400	0.01300
21	157.14	0.04747	0.01376	157.48	0.04787	0.01384	157.14	0.04787	0.01371
22	159.99	0.05153	0.01447	160.37	0.05200	0.01456	159.99	0.05200	0.01441
23	162.85	0.05588	0.01516	163.27	0.05643	0.01526	162.85	0.05643	0.01511
24	165.71	0.06056	0.01586	166.17	0.06120	0.01596	165.71	0.06120	0.01580
25	168.57	0.06562	0.01655	169.05	0.06638	0.01666	168.57	0.06638	0.01649
26	171.42	0.07115	0.01723	171.95	0.07204	0.01735	171.42	0.07204	0.01717
27	174.28	0.07722	0.01790	174.85	0.07828	0.01804	174.28	0.07828	0.01784

28	177.14	0.08398	0.01858	177.76	0.08524	0.01872	177.14	0.08524	0.01851
29	180.00	0.09160	0.01924	180.68	0.09310	0.01939	180.00	0.09310	0.01917
30	182.85	0.10033	0.01990	183.59	0.10216	0.02006	182.85	0.10216	0.01983
31	185.71	0.11057	0.02056	186.54	0.11285	0.02073	185.71	0.11285	0.02049
32	188.57	0.12298	0.02120	189.44	0.12589	0.02140	188.57	0.12589	0.02113
33	191.43	0.13878	0.02185	192.42	0.14265	0.02206	191.43	0.14265	0.02177
34	194.28	0.16067	0.02249	195.51	0.16620	0.02274	194.28	0.16620	0.02241
35	197.14	0.19714	0.02312	199.00	0.20632	0.02349	197.14	0.20632	0.02304

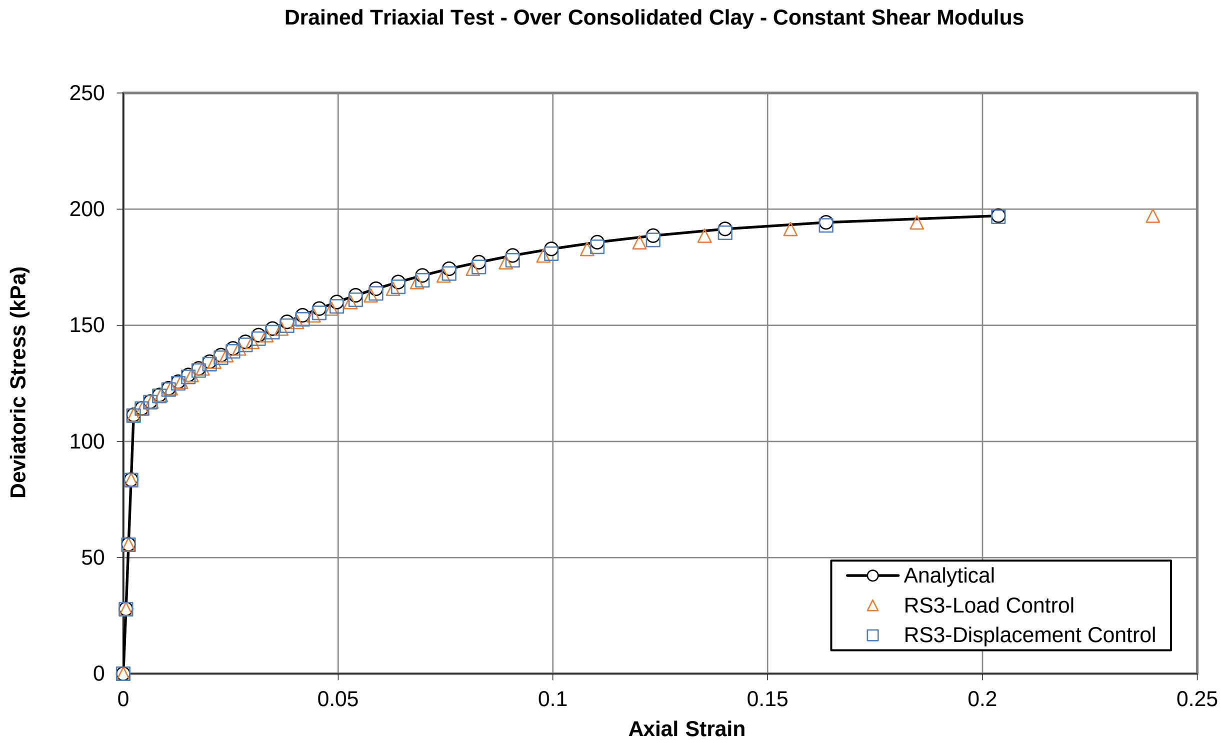

Figure 7.11: Variation of deviatoric stress with axial strain for Example 2 case of constant shear modulus

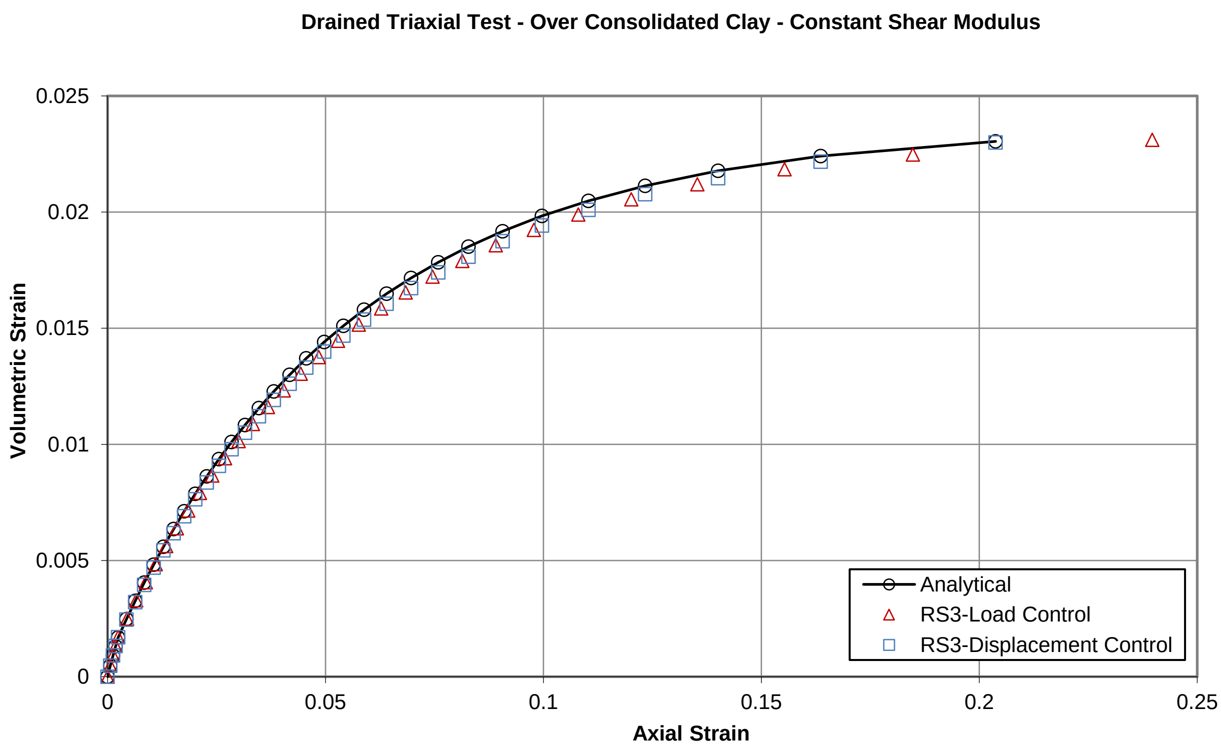

Figure 7.12: Variation of volumetric strain with axial strain for Example 2 case of constant shear modulus

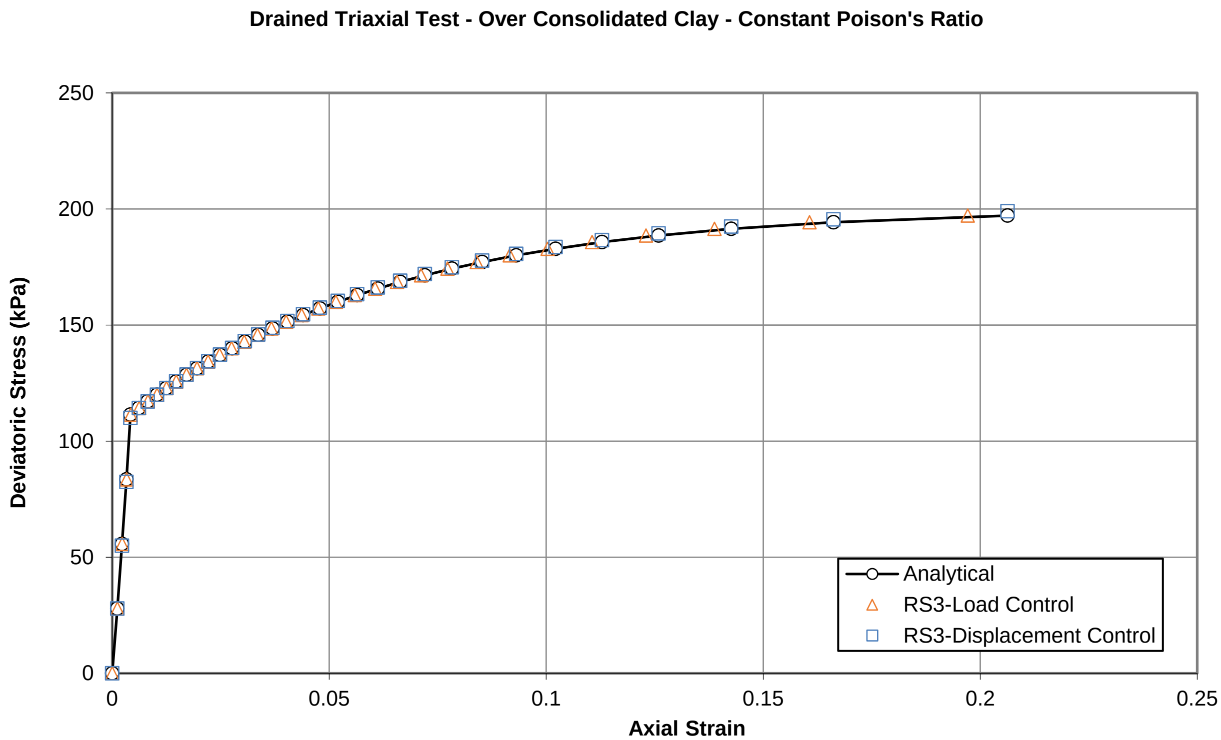

Figure 7.13: Variation of deviatoric stress with axial strain for Example 2 case of constant Poisson's ratio

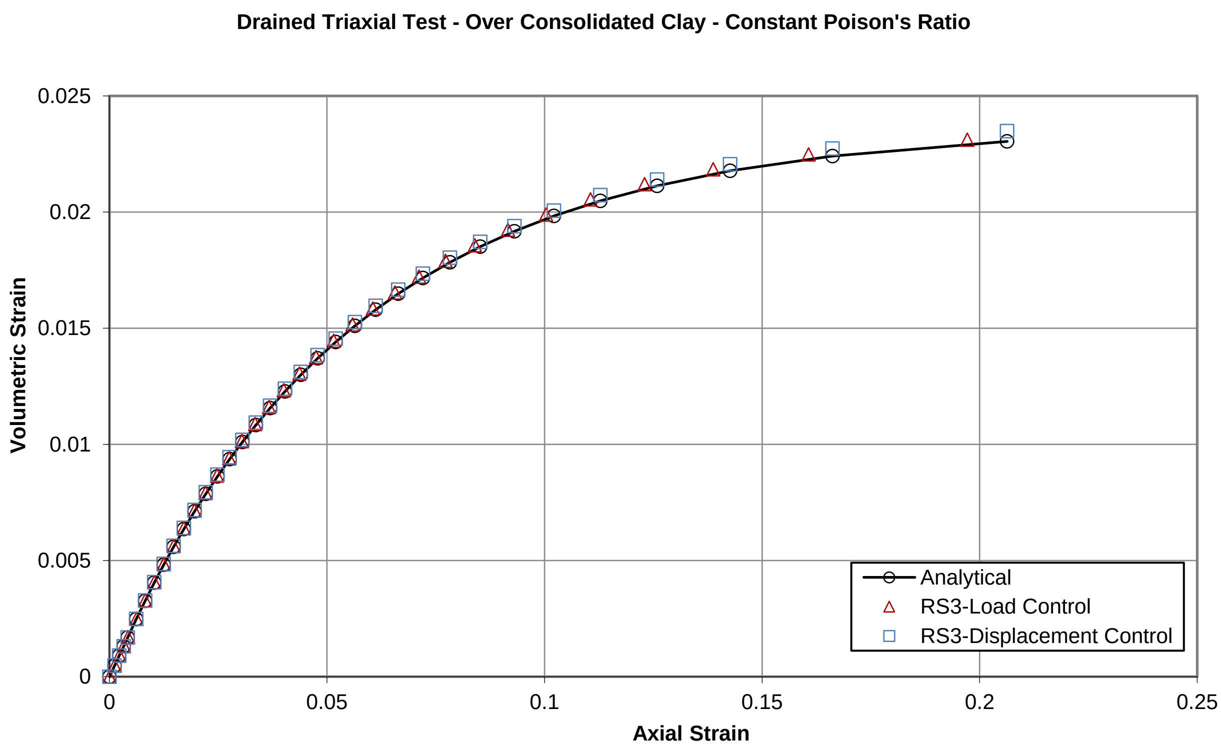

Figure 7.14: Variation of volumetric strain with axial strain for Example 2 case of constant Poisson's ratio

Table 7-6: Example 2, Triaxial test on a highly over consolidated clay sample; results for case of constant Poisson's ratio

	***RS3* Displacement-Control**			**Analytical Solution**		
No.	**q (kPa)**	**Axial strain, εa**	**Volumetric strain, εv**	**q (kPa)**	**Axial strain, εa**	**Volumetric strain, εv**
1	0.00	0.000000	0.000000	0.00	0.000000	0.000000
2	70.74	0.003029	0.001211	73.35	0.003029	0.001211
3	141.53	0.005518	0.002207	146.69	0.005518	0.002207
4	212.45	0.007634	0.003054	220.04	0.007634	0.003054
5	283.49	0.009474	0.003790	293.39	0.009474	0.003790
6	290.77	0.011149	0.003441	290.37	0.011149	0.003280
7	287.70	0.012888	0.002917	287.36	0.012888	0.002765
8	284.63	0.014695	0.002390	284.35	0.014695	0.002246
9	281.56	0.016576	0.001858	281.34	0.016576	0.001722
10	278.50	0.018536	0.001323	278.32	0.018536	0.001195
11	275.43	0.020581	0.000783	275.31	0.020581	0.000663
12	272.36	0.022719	0.000239	272.30	0.022719	0.000127
13	269.30	0.024957	-0.000310	269.29	0.024957	-0.000413
14	266.25	0.027304	-0.000862	266.27	0.027304	-0.000957
15	263.19	0.029771	-0.001419	263.26	0.029771	-0.001506
16	260.12	0.032369	-0.001981	260.25	0.032369	-0.002060
17	257.06	0.035111	-0.002547	257.24	0.035111	-0.002618
18	254.00	0.038014	-0.003117	254.22	0.038014	-0.003181
19	250.95	0.041095	-0.003692	251.21	0.041095	-0.003748
20	247.89	0.044377	-0.004272	248.20	0.044377	-0.004320
21	244.83	0.047885	-0.004856	245.19	0.047885	-0.004897
22	241.78	0.051650	-0.005445	242.17	0.051650	-0.005479
23	238.73	0.055711	-0.006038	239.16	0.055711	-0.006065
24	235.69	0.060115	-0.006636	236.15	0.060115	-0.006657
25	232.64	0.064921	-0.007239	233.14	0.064921	-0.007253
26	229.59	0.070206	-0.007847	230.12	0.070206	-0.007855

27	226.56	0.076072	-0.008458	227.11	0.076072	-0.008462
28	223.53	0.082655	-0.009073	224.10	0.082655	-0.009074
29	220.52	0.090148	-0.009690	221.09	0.090148	-0.009691
30	217.51	0.098830	-0.010313	218.07	0.098830	-0.010314
31	214.53	0.109138	-0.010935	215.06	0.109138	-0.010942
32	211.59	0.121802	-0.011556	212.05	0.121802	-0.011576
33	208.73	0.138189	-0.012168	209.04	0.138189	-0.012215
34	206.02	0.161369	-0.012744	206.02	0.161369	-0.012859
35	203.67	0.201143	-0.013260	203.01	0.201143	-0.013510

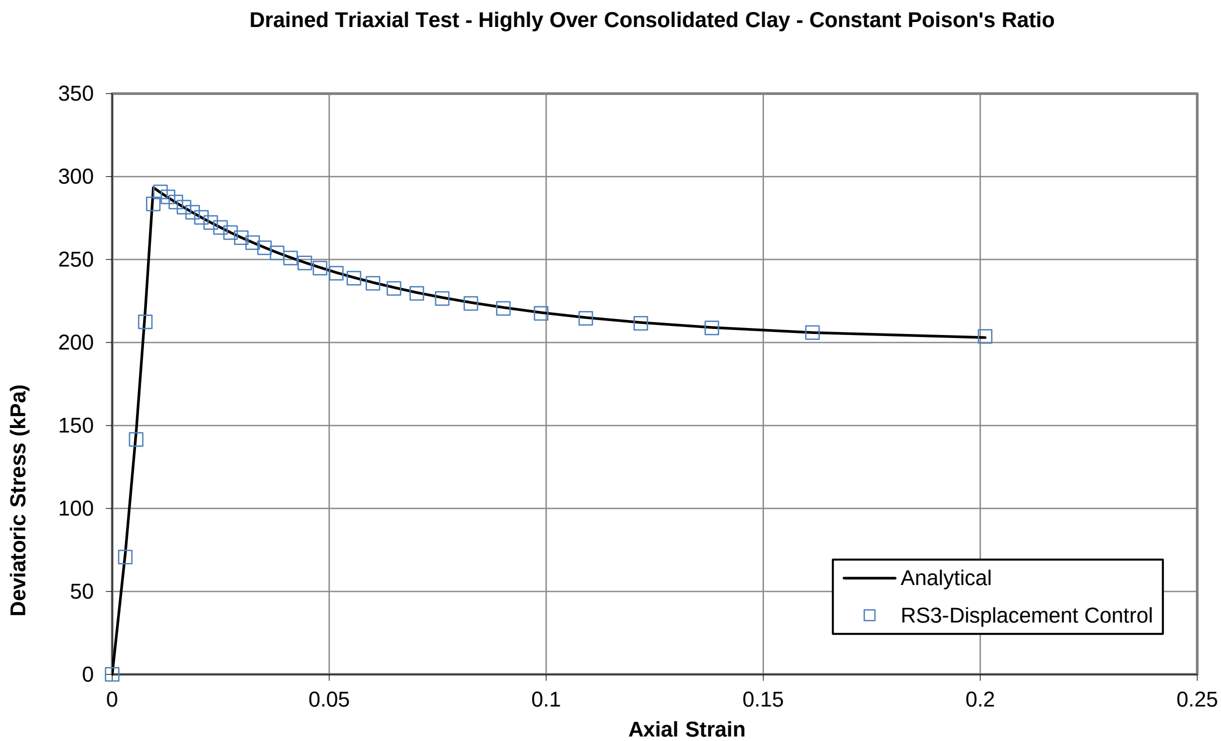

Figure 7.15: Variation of deviatoric stress with axial strain for Example 3 case of constant Poisson's ratio

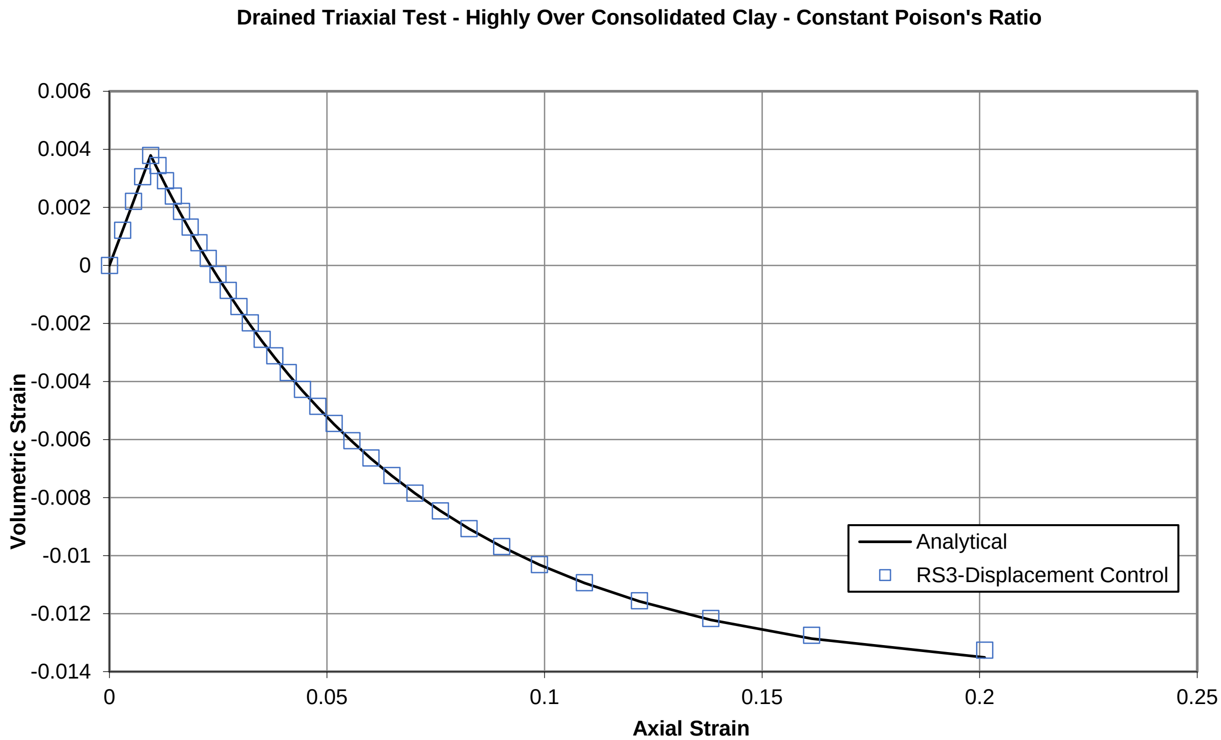

Figure 7.16: Variation of volumetric strain with axial strain for Example 3 case of constant Poisson's ratio

7.5. References

1. R.I. Borja (1991), Cam-Clay plasticity, Part II: Implicit integration of constitutive equation based on a nonlinear elastic stress predictor, Computer Methods in Applied Mechanics and Engineering, 88, 225-240.

2. D. Peric´ (2006), Analytical solutions for a three-invariant Cam clay model subjected to drained loading histories, Int. J. Numer. Anal. Meth. Geomech., 30, 363–387.

7.6. Data Files

The input data files for the drained triaxial compressive testing of Modified Cam Clay samples are:

File name	***Example No.***	***Assumption***	***Simulation type***	***Consolidation***
StressVerification-07 cnstG NC load.rs3v3	1	$G = const.$	Load Control	Normal
StressVerification-07 cnstv NC load.rs3v3	1	$\nu = const.$	Load Control	Normal
StressVerification-07 cnstG NC displ.rs3v3	1	$G = const.$	Displacement Control	Normal

StressVerification-07 cnstv NC displ.rs3v3	1	$\nu = const.$	Displacement Control	Normal
StressVerification-07 cnstG OC load.rs3v3	2	$G = const.$	Load Control	Over
StressVerification-07 cnstv OC load.rs3v3	2	$\nu = const.$	Load Control	Over
StressVerification-07 cnstG OC displ.rs3v3	2	$G = const.$	Displacement Control	Over
StressVerification-07 cnstv OC displ.rs3v3	2	$\nu = const.$	Displacement Control	Over
StressVerification-07 cnstv Highly OC displ.rs3v3	3	$\nu = const.$	Displacement Control	Highly Over

The input data files can be downloaded from the RS3 Online Help page. Microsoft Excel spreadsheet files are also included in the folder:

V07 (constant G) – NC Clay.xlsx

V07 (constant v) – NC Clay.xlsx

V07 (constant G) – OC Clay.xlsx

V07 (constant v) – OC Clay.xlsx

V07 (constant v) – Highly OC.xlsx

that implement the closed-form solutions for drained triaxial compressive testing for Modified Cam Clay soils.

8. Uniaxial Tests on a Mohr-Coulomb Material with Ubiquitous Joints

8.1. Problem Description

This problem verifies the uniaxial compressive strength of a Mohr-Coulomb material with varying sets of joints (Zienkiewicz & Pande, 1977). The material is isotropic (elastic-fully plastic) with the following properties:

Young's modulus = 20,000 kPa

Poisson's ratio = 0.3

Cohesion = 100 kPa

Friction angle = 35°

Dilation angle = 35°

The model was built in *RS3* and extruded to create a prismatic shape. The jointed rock mass is considered to be composed of an intact material that is intercepted by up to three sets of weak planes. The spacing of the weak planes is such that the overall effects of the sets can be smeared and averaged over the control volume of the material. Such a configuration with one, two or three sets of weak planes is illustrated in Figure 8.1 where the weak planes are oriented at an arbitrary angle θ_1, θ_2 and θ_3 in the rock mass.

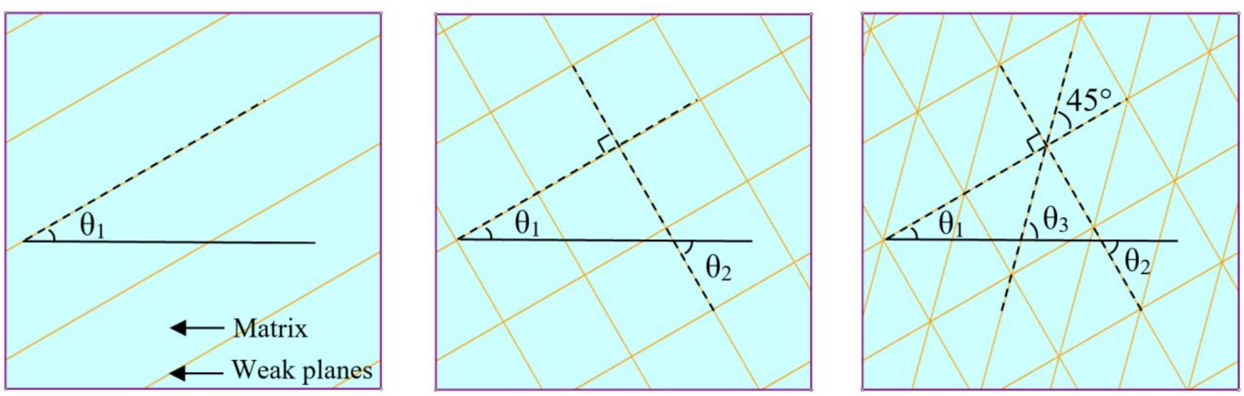

(a) (b) (c)

Figure 8.1: Typical material with (a) one set, (b) two sets and (c) three sets of weak planes with inclination angle θ_1, θ_2 and θ_3 respectively.

All joint sets are modeled as Mohr-Coulomb material with the following properties:

Cohesion = 40 kPa

Friction angle = 30°

Dilation angle = 30°

8.2. Analytical Solution

The analytical solution is taken from Pietruszczak who used a simple evaluation of failure functions for the weak planes and the matrix for different configurations of the model under uniaxial loading (Pietruszczak, 2010).

8.3. Model Properties

The model for this problem is built in *RS3* as a typical uniaxial compression test with a graded mesh of 10-noded tetrahedron elements as shown in Figure 8.2. A displacement is applied at the top and increases with each stage. The model has dimensions of 10 cm length, 10 cm width and 20 cm height. No in-situ field stress is applied to the model.

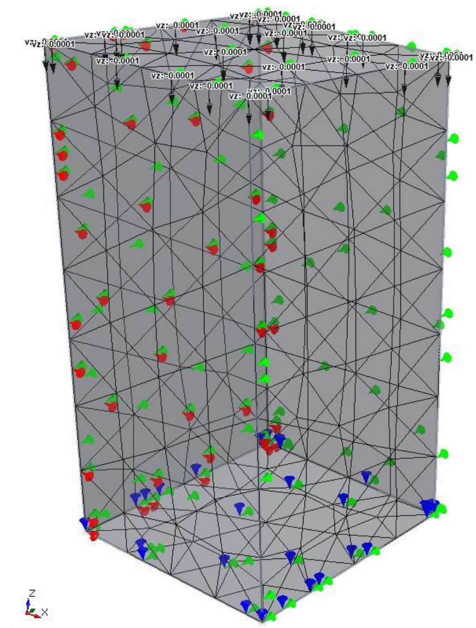

Figure 8.2: Model of uniaxial tests on a Mohr-Coulomb material with ubiquitous joints in *RS3*

8.4. Results and Discussions

Figure 8.3, Figure 8.4, and Figure 8.5 show the uniaxial compressive strength at different joint inclinations and varying number of joint sets. The *RS3* results are in very close agreement with the analytical solution.

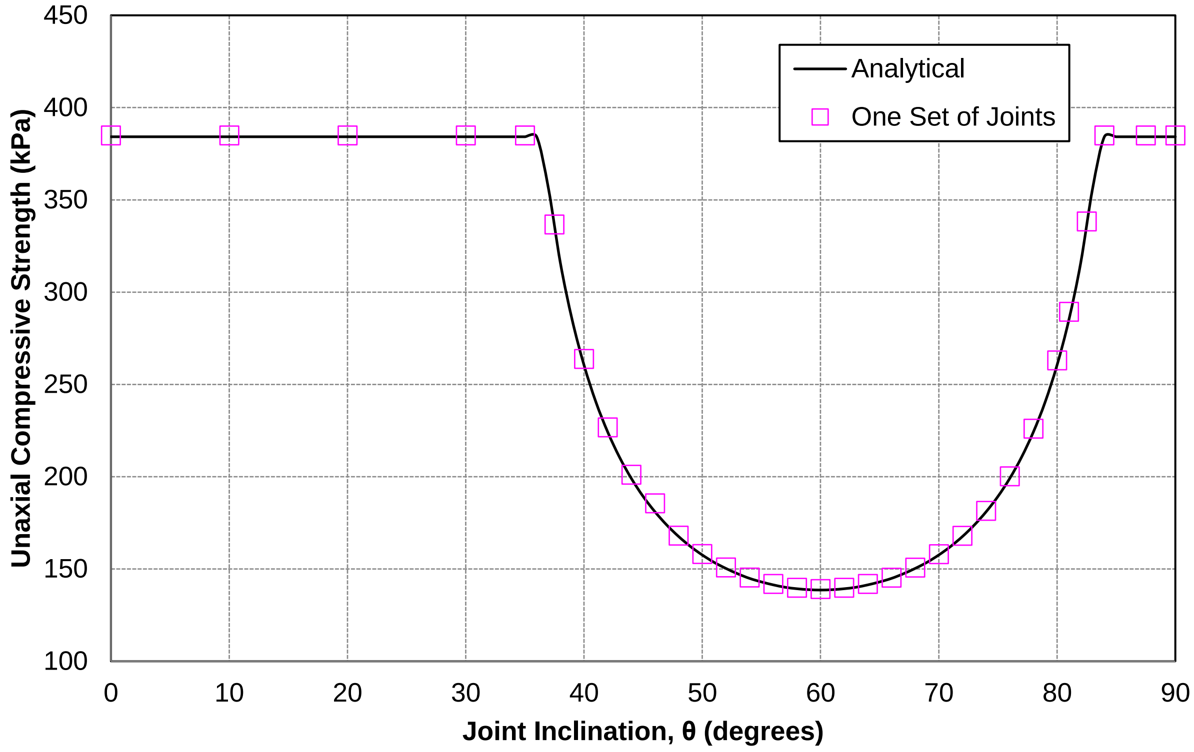

Figure 8.3: Variation of uniaxial compressive strength for one set of joints

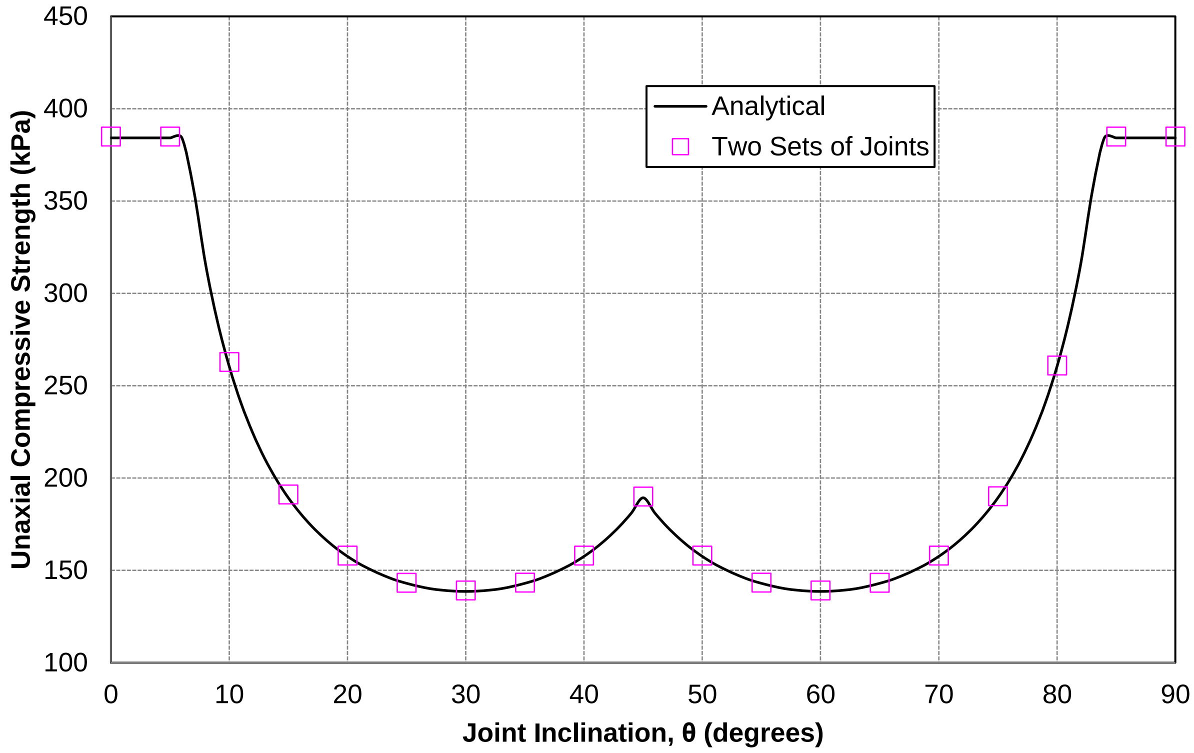

Figure 8.4: Variation of uniaxial compressive strength for two sets of joints

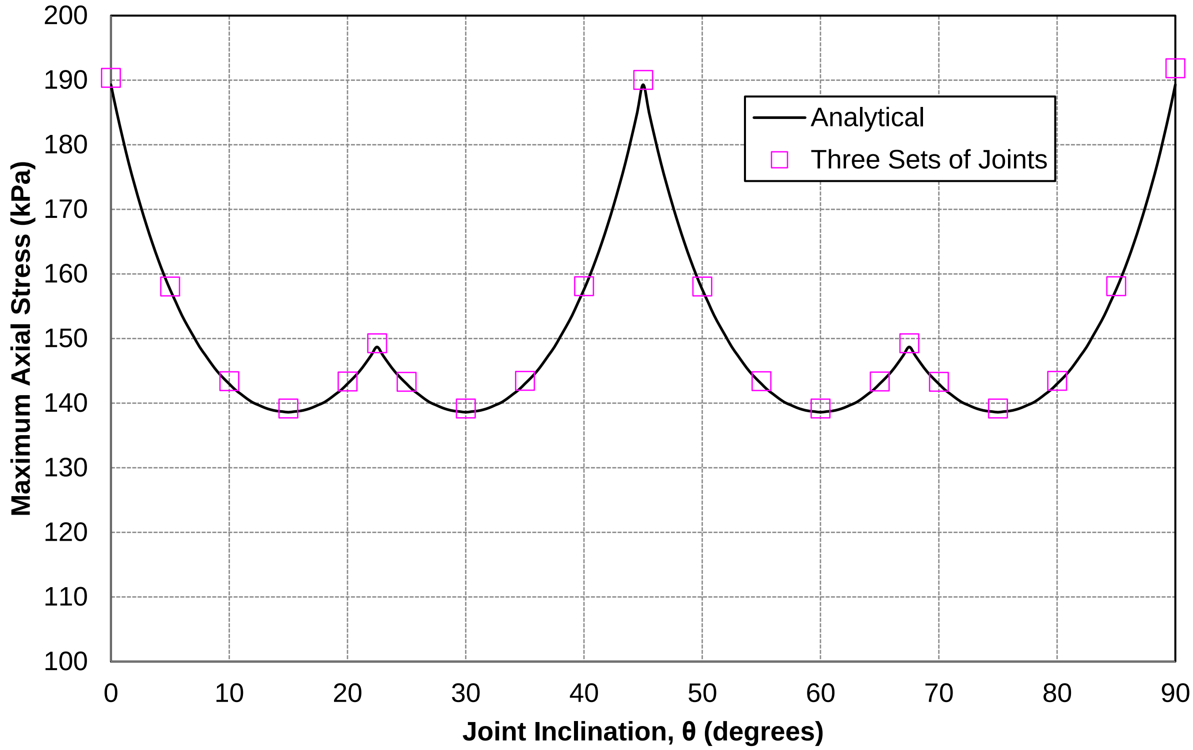

Figure 8.5: Variation of uniaxial compressive strength for three sets of joints

8.5. References

1. Pietruszczak, S. (2010). *Fundamentals of Plasticity in Geomechanics*. CRC Press/Balkema, The Netherlands.

2. Zienkiewicz, O.C. & Pande G.N. (1977). Time-dependent multilaminate model of rocks-A numerical study of deformation and failure of rock masses, *International Journal for Numerical and Analytical Methods in Geomechanics*, 1(3): 219–247.

8.6. Data Files

The following input data files can be downloaded from the RS3 Online Help page.

- **StressVerification-08**

9. Plane Strain and Axially Symmetric Consolidation of Clay Stratum (McNamee's Problem)

9.1. Problem Description

In this verification plane strain and axially symmetric consolidation of a clay stratum is analyzed. Two models are used for this verification:

1. The stratum is loaded by a uniform normal stress along a strip.
2. The stratum is loaded by a uniform normal stress over a circular area.

Two cases are considered for each model: with and without drainage at the surface.

9.2. Model Properties

The material is set to be "Mohr Coulomb" and the hydraulic behavior is "isotropic". Field stress is assigned in the form of gravity.

Strip Load Model:

The geometry of the strip model is shown in Figure 9.1. Figure 9.2 illustrates the boundary conditions and the mesh. The normal load is shown, and a refined mesh is applied near the applied load for better accuracy. The input parameters are listed in Table 9-1.

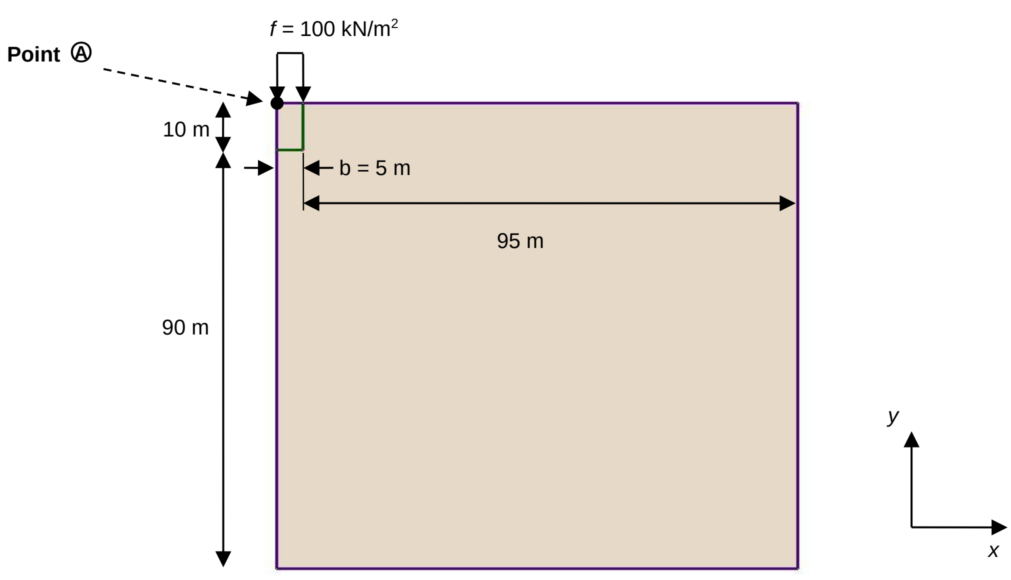

Figure 9.1: Geometry of the strip model

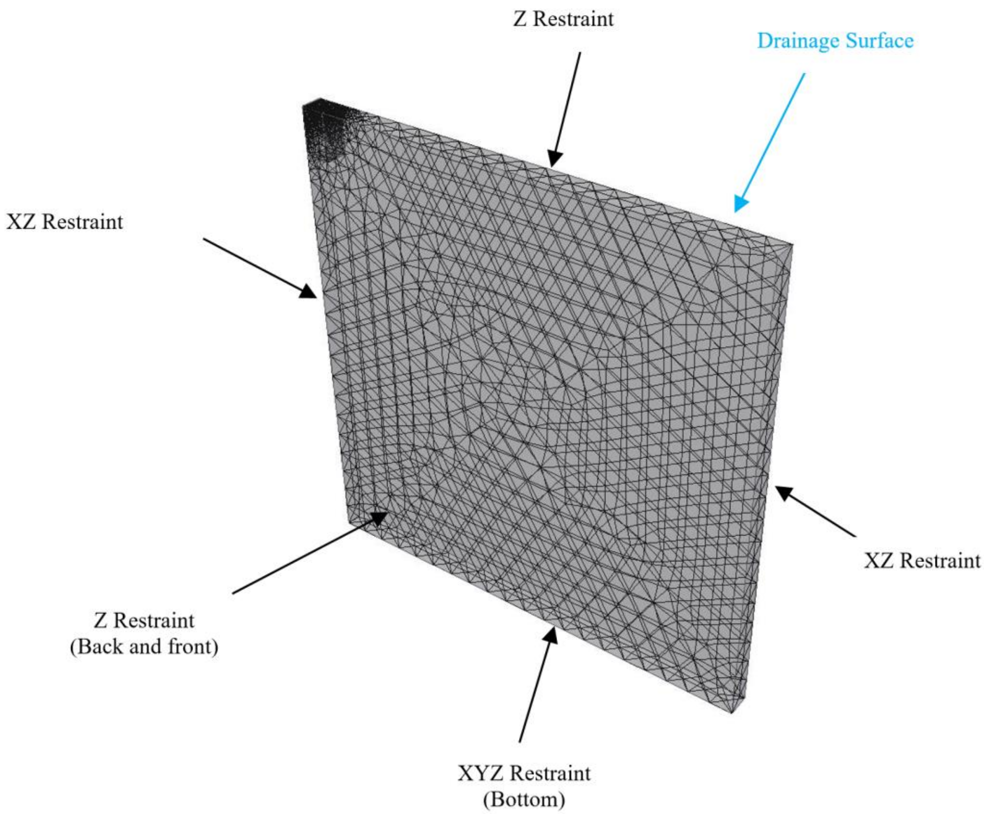

Figure 9.2 : Mesh and boundary conditions

Table 9-1: Table of input parameters for strip model

Parameter	***Value***
Young's Modulus (E)	40000 kPa
Shear Modulus (G)	20000 kPa
Poisson's Ratio (*v*)	0.0
Permeability (k)	9.81e-6 m/s
Initial Element Loading	None
Fluid Bulk Modulus	2200000 kPa

Circular Model:

The geometry of the circular model is shown in Figure 9.3. The mesh and boundary conditions are shown in Figure 9.4. Refined mesh is applied near the normal load. The model parameters are the same as parameters listed in Table 9-1.

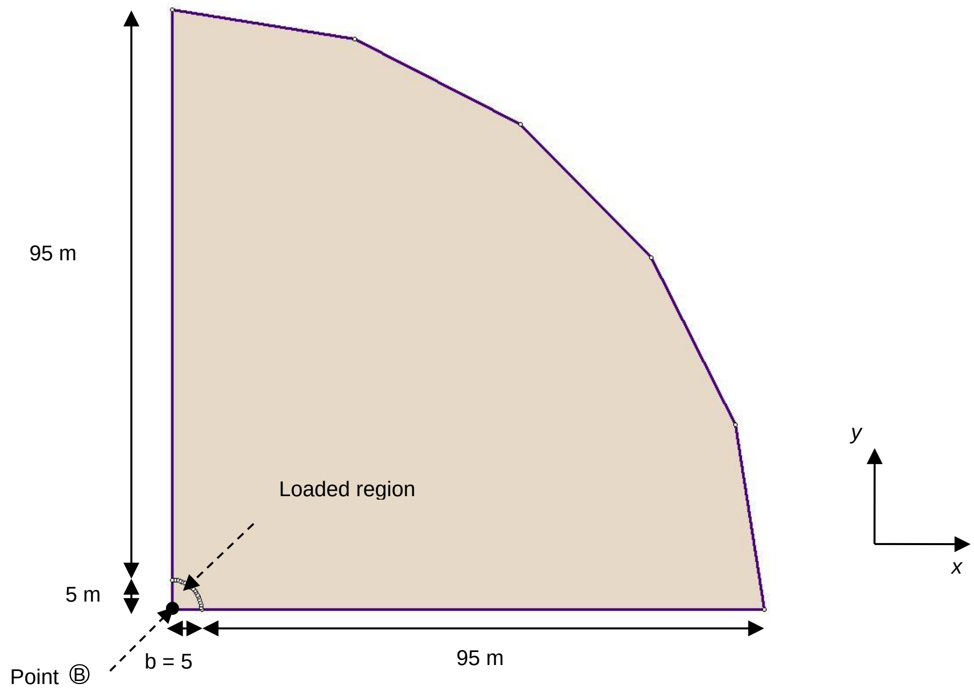

Figure 9.3: Geometry of the circular model

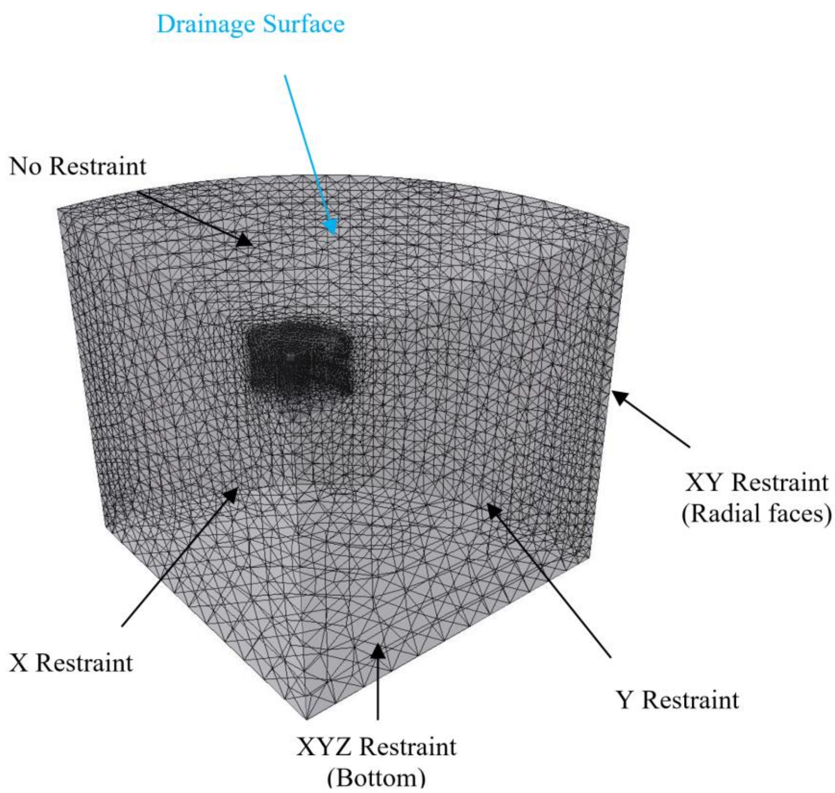

Figure 9.4: Mesh and boundary conditions

9.3. Results

Results for the strip model are shown in Figure 9.5 and Figure 9.6 and results for the circular model are shown in Figure 9.7 and Figure 9.8.

Figure 9.5 to Figure 9.8 show the relation between normalized settlement that is evaluated as $(\frac{2G}{fb}(\omega - \omega_{t=0})_{z=0})$ versus normalized time that is evaluated as $(\frac{dt}{b^2})$. *G* is the shear strength, *f* is the distributed normal load, *b* is the width of the section under normal load, ω is the displacement at time t, $\omega_{t=0}$ is the initial displacement, *d* is the coefficient of consolidation defined in Equation (9.1).

$$d = \frac{2Gk}{g} \qquad (9.1)$$

k is the coefficient of permeability and *g* is the gravity constant.

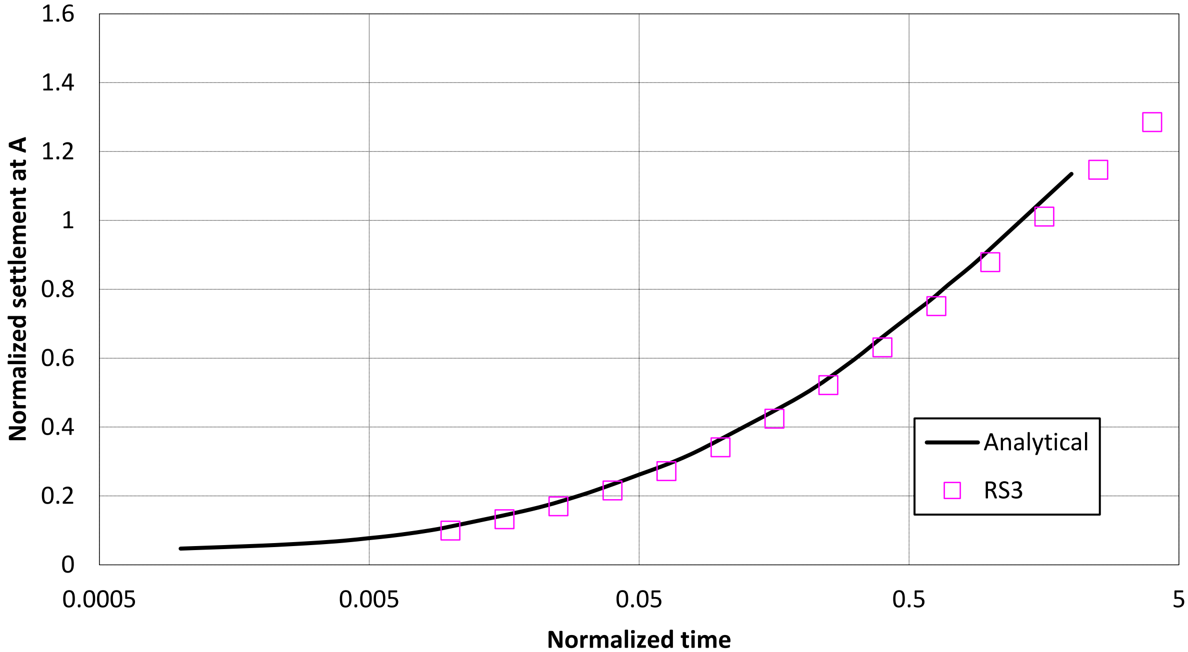

Figure 9.5 : Settlement at location point A (strip model) – with drainage

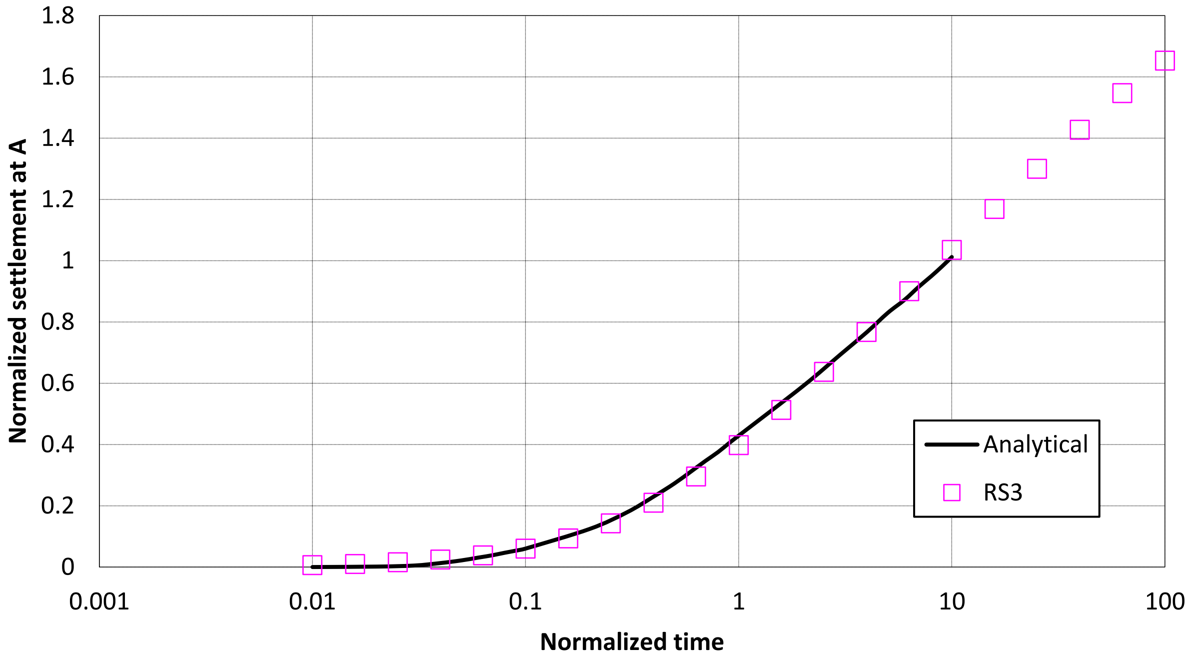

Figure 9.6 : Settlement at location point A (strip model) – without drainage

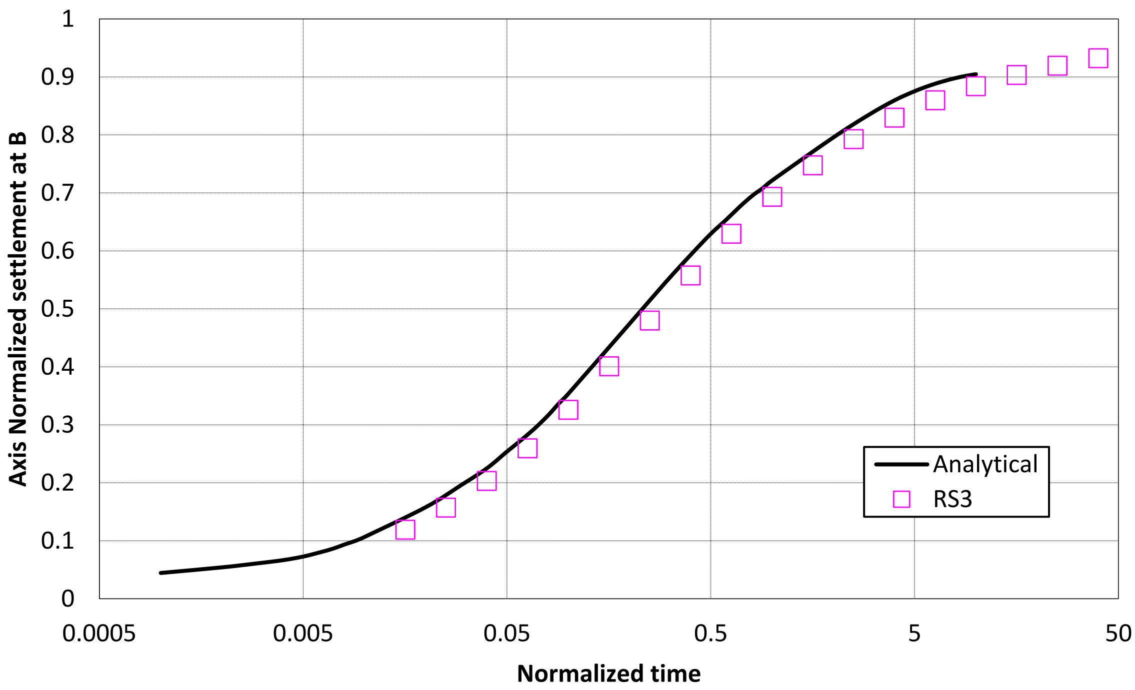

Figure 9.7 : Settlement at location point B (circular model) – with drainage

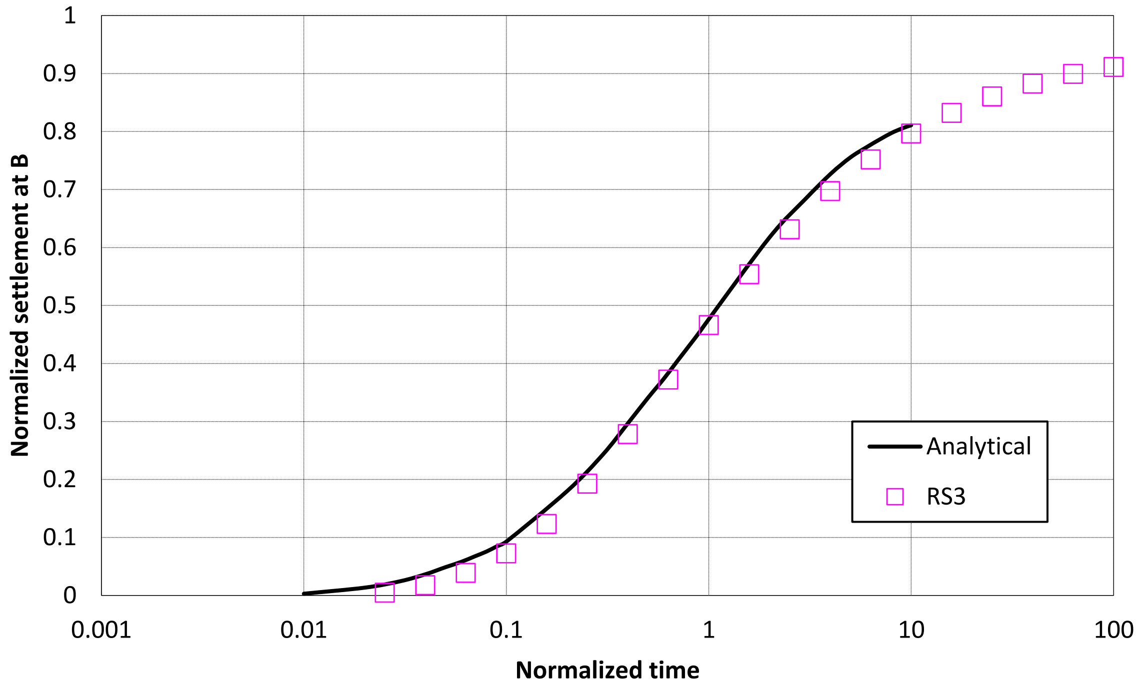

Figure 9.8 : Settlement at location point B (circular model) – without drainage

9.4. References

1. Mcnamee, J., & Gibson, R. E. (1960). Plane strain and axially symmetric problems of the consolidation of a semi-infinite clay stratum. *Quarterly Journal of Mechanics and Applied Mathematics*, 13(2), 210-227.

9.5. Data Files

The input data files can be downloaded from the RS3 Online Help page:

- **StressVerification-09(Circular, Drainage).rs3v3**
- **StressVerification-09 (Circular, No drainage).rs3v3**
- **StressVerification-09 (Strip-Drainage).rs3v3**
- **StressVerification-09 (Strip-No Drainage).rs3v3**

10. Non-Linear Analysis of Strip Footing in Sand

10.1. Problem Description

This problem considers a strip footing in sand subjected to an incrementally increasing load. The sand is assumed to exhibit non-linear elastic behavior according to the Duncan-Chang hyperbolic model. All parameters are drawn from Tomlinson's Foundation Design and Construction, which presents experimentally determined settlement result as well as the results of finite element analysis (Tomlinson, 2001). Figure 10.1 illustrates the problem as implemented in *RS3*. Dimensions are as indicated. Due to symmetry, only half of the footing is modeled.

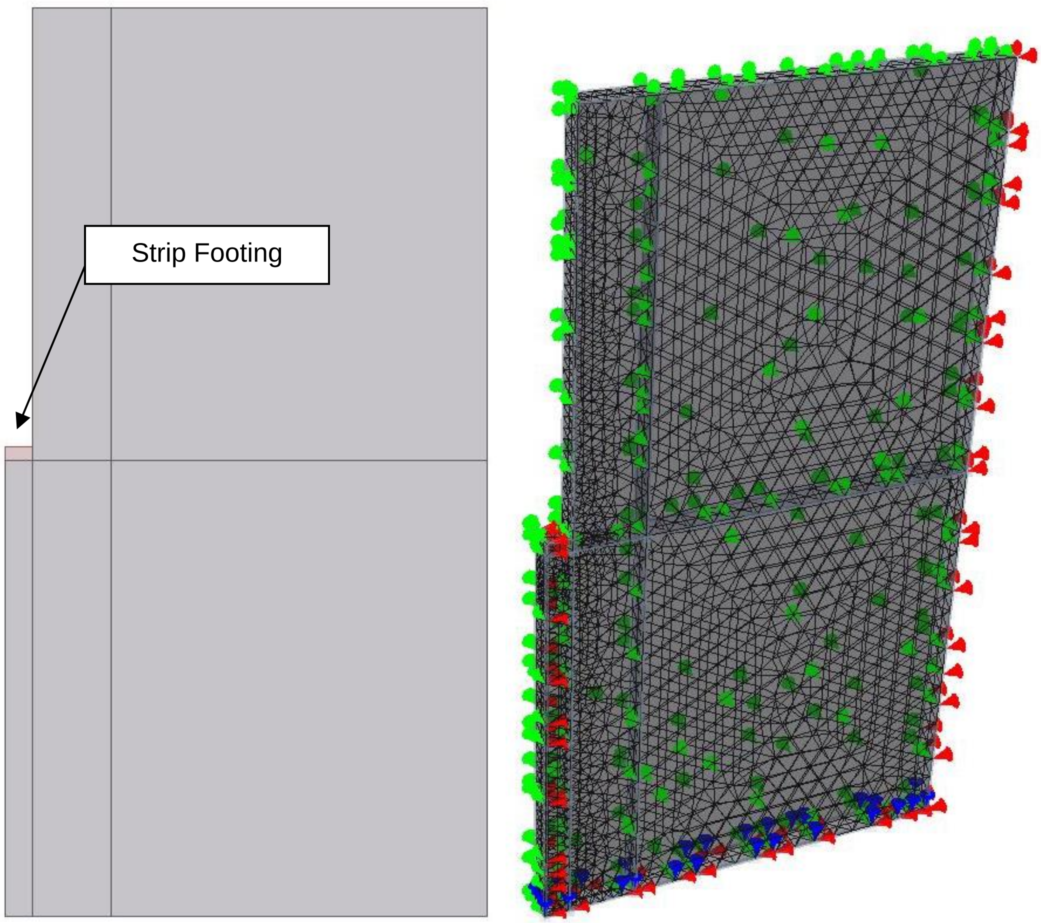

Figure 10.1: Strip footing in sand as constructed in *RS3*

The model shown in Figure 10.1 uses a graded mesh composed of 4-noded tetrahedron elements. Boundary conditions are as illustrated. A small region of stiff material is used to simulate the rigid footing.

Table 10-1 summarizes the model parameters used:

Table 10-1: Model parameters

Parameter	*Value*
Modulus number (K_E)	300
Modulus exponent (n)	0.55
Failure ratio (R_f)	0.83
Cohesion (c)	0 psf
Friction angle (ϕ)	35.5°
Unit weight (γ)	91 lb/ft3
Poisson's ratio (v)	0.35
Footing half-width ($b/2$)	1.22 in

10.2. Duncan-Chang Model

The Duncan-Chang Hyperbolic constitutive model is widely used for the modeling of soils with more generalized stress-strain behavior and is capable of modeling the stress-dependent strength and stiffness of soils. The Duncan-Chang Hyperbolic elasticity model can only be used in conjunction with the Mohr-Coulomb failure criterion in *RS3*. The following equations are derived, based on a hyperbolic stress-strain curve and stress-dependent material properties for the Duncan-Chang Hyperbolic model.

The tangential modulus, (E_t), is given by:

$$E_t = \mathrm{K_E} p_{atm} \left(\frac{\sigma_3}{p_{atm}}\right)^n \left[1 - \frac{R_f(1-\sin\emptyset)(\sigma_1-\sigma_3)}{2c\cos\emptyset + 2\sigma_3\sin\emptyset}\right]^2 \qquad (10.1)$$

where

p_{atm} = atmospheric pressure

σ_3 = minor principal stress

σ_1 = major principal stress

and other parameters are as identified in Table 10-1.

Tomlinson presents experimental load-settlement results in as well as the results of finite element analysis (Tomlinson, 2001). These are compared with *RS3* results in the next section.

10.3. Results

Figure 10.2 shows settlement as a function of increasing average footing pressure, as predicted by Tomlinson and *RS3* (Tomlinson, 2001). It can be seen that *RS3* is in good agreement with experimental results.

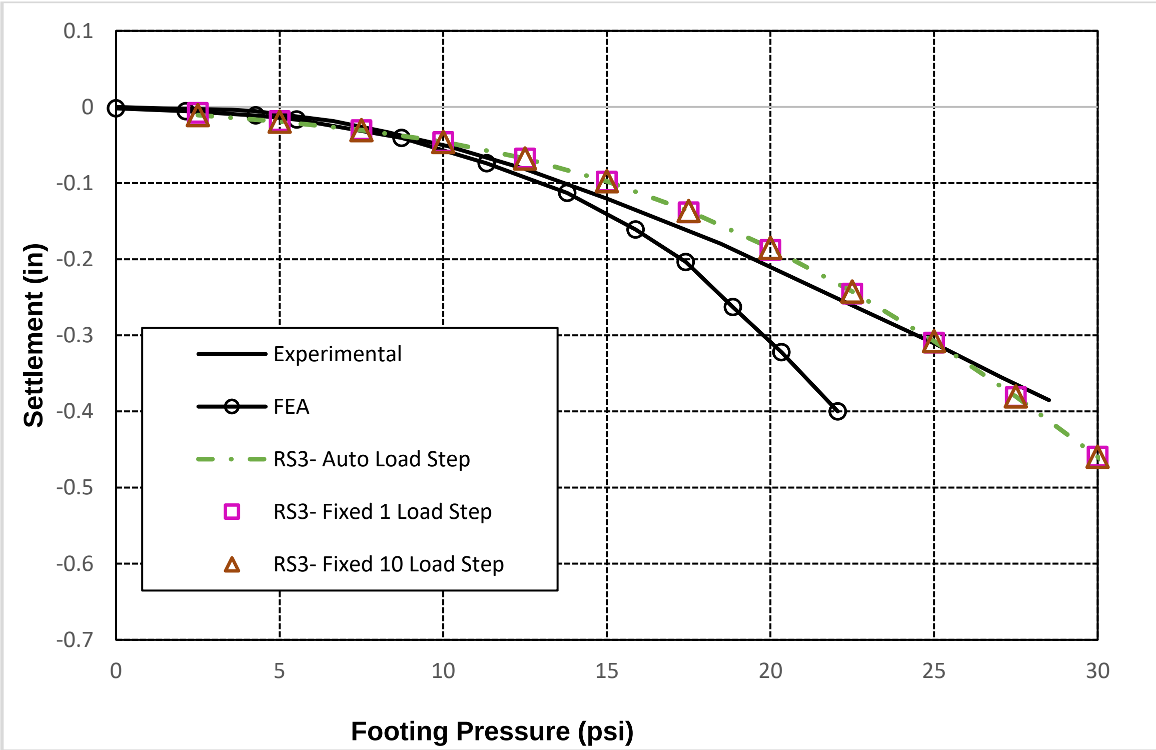

Figure 10.2: Settlement with increasing load as predicted by *RS3* (Tomlinson, 2001)(Duncan & Chang, 1970)

10.4. References

1. M. J. Tomlinson (2001), Foundation Design and Construction, 7th Ed., Upper Saddle River, NJ: Prentice Hall.

2. J. M. Duncan and C. Y. Chang (1970), “Nonlinear analysis of stress and strain in soils”, J. of Soil Mech. and Foundation Division, ASCE, 96 (SM5), pp. 1629-1653.

10.5. Data Files

The input data files can be downloaded from the RS3 Online Help page:

- **StressVerification-10-steps=1.rs3v3**
- **StressVerification-10-steps=10.rs3v3**
- **StressVerification-10-steps=Auto.rs3v3**

11. Non-Linear Behavior of Sand (Duncan-Chang Model)

11.1. Problem Description

This problem demonstrates the applicability of Duncan-Chang model in simulation of nonlinear behavior of soils. The nonlinear behavior of dense and loose Silica sand in triaxial tests is the focus of this example. The experimental results are taken from an article by Duncan and Chang (Duncan & Chang,1970). The stress paths of the experiments include loading, unloading and reloading of the samples. The Duncan-Chang model parameters for the dense and loose Silica sands are presented in Table 11-1.

Table 11-1 : Duncan Chang model parameters

Parameter	*Dense Silica Sand*	*Loose Silica Sand*
Modulus number (K_E)	2000	295
Unloading Modulus(K_{ur})	2120	1090
Modulus exponent (n)	0.54	0.65
Failure ratio (R_f)	0.91	0.90
Cohesion (c)	0 kPa	0 kPa
Friction angle (ϕ)	36.5°	30.4°
Poisson's ratio (v)	0.32	0.32

11.2. Model information

The drained compressive triaxial tests of the sample were modeled in *RS3* using 4-noded tetrahedral elements. The deviatoric stress is generated in the sample in a load-control process. The axial loading in the z direction increases in a number of stages, and automatic load stepping is considered in each stage. See Figure 11.1 for finite element mesh used in this simulation. See Figure 11.2 for the boundary conditions and an example of the axial and radial loads used.

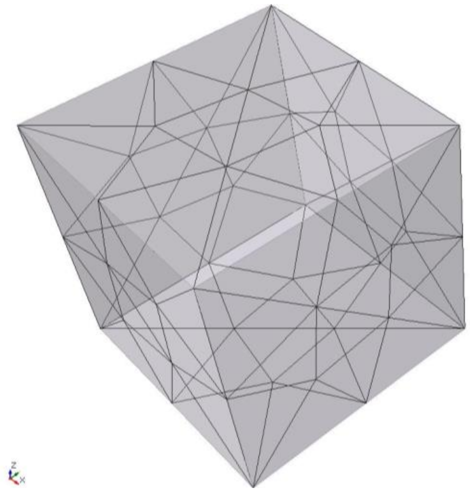

Figure 11.1 Mesh for axisymmetric *RS3* analysis

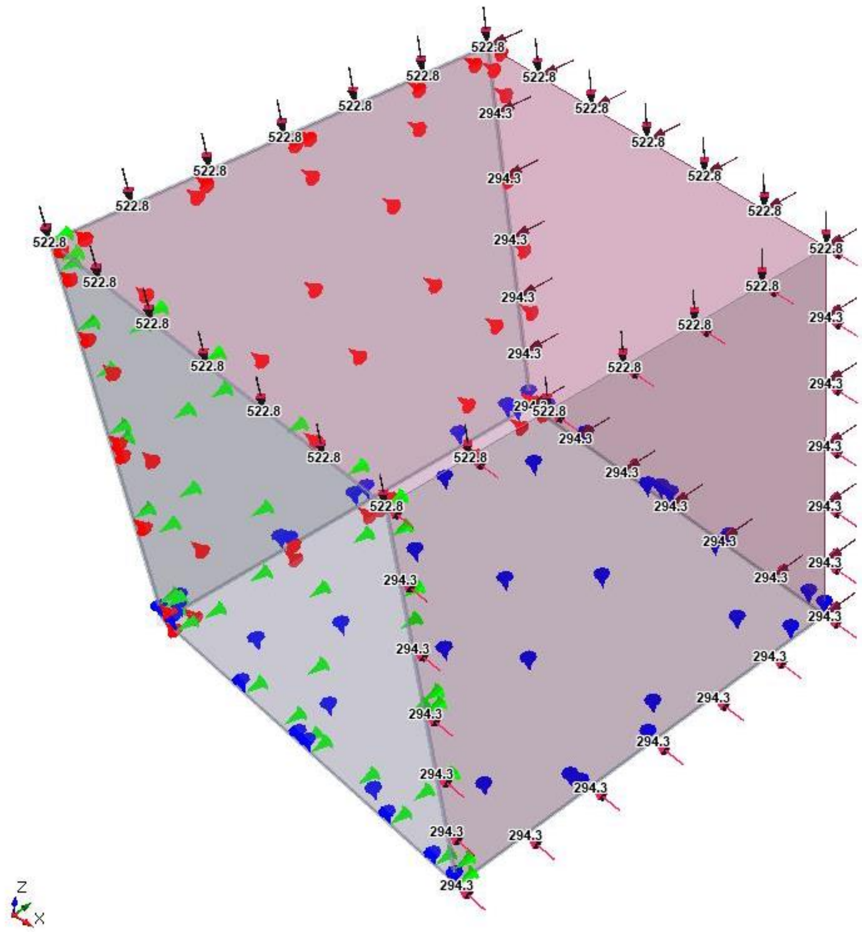

Figure 11.2 Boundary conditions and load for axisymmetric *RS3* analysis

11.3. Results

Figure 11.3 and Figure 11.4 show the plots of $\varepsilon_a - q$ obtained in numerical simulations using *RS3* in comparison with the observed behavior and the numerical results obtained by Duncan and Chang (Duncan & Chang,1970).

There is a good agreement between the experimental data and the numerical results. The difference between the numerical results of *RS3* and the ones presented by Duncan and Chang is because in *RS3* the elastic parameters, from load step *n* to *n+1*, are calculated based on the state of material at step *n* while in the latter they are averaged over the increment.

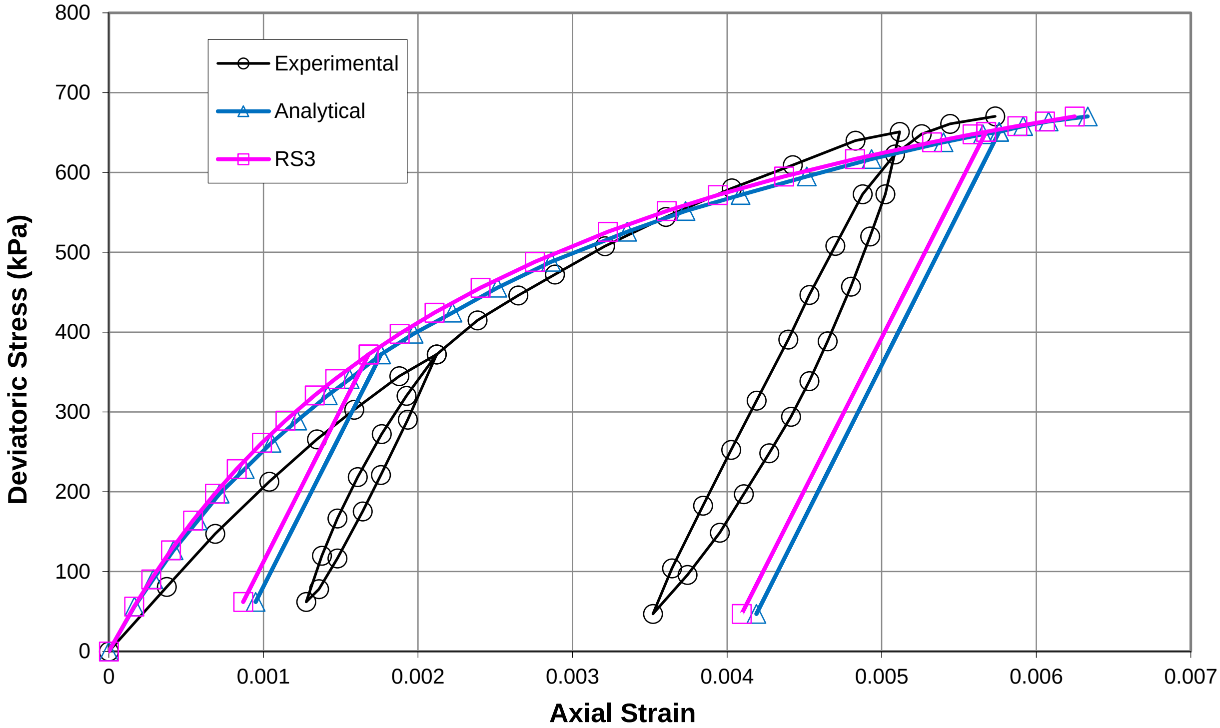

Figure 11.3: Triaxial test on dense Silica sand, variation of deviatoric stress with axial strain (Duncan & Chang,1970)

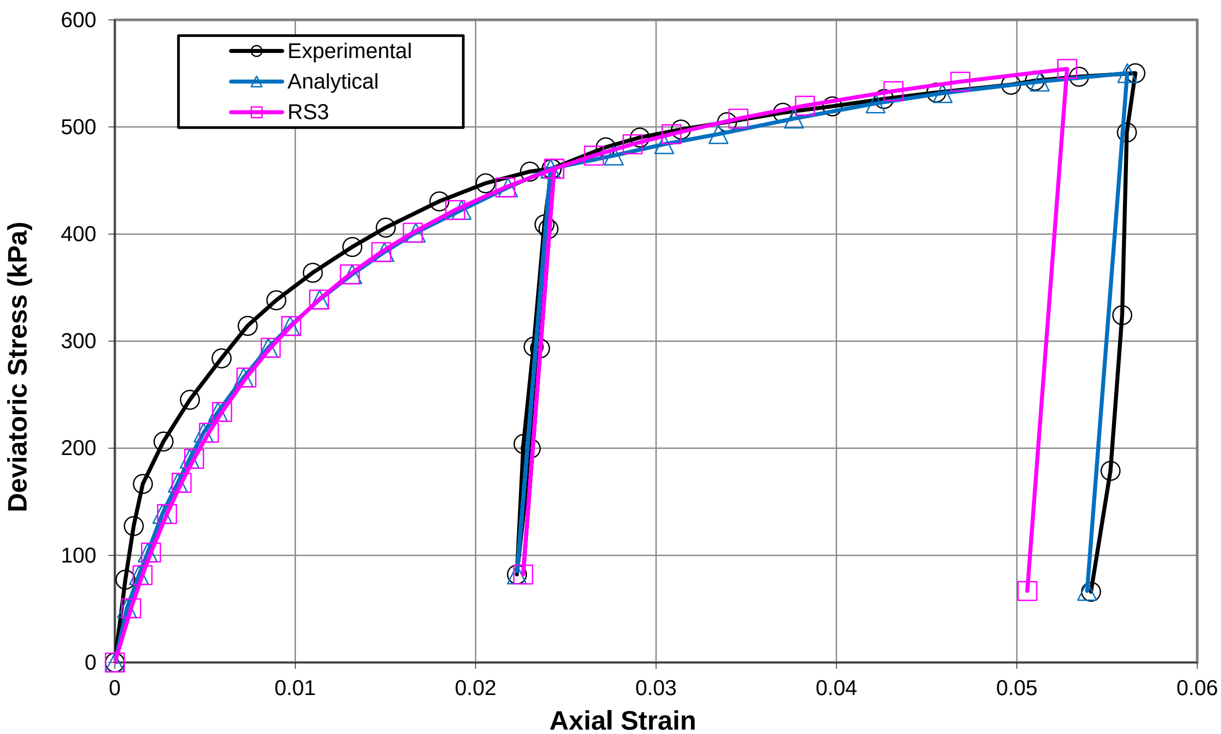

Figure 11.4 : Triaxial test on loose Silica sand, variation of deviatoric stress with axial strain (Duncan & Chang,1970)

11.4. References

1. J. M. Duncan and C. Y. Chang (1970), “Nonlinear analysis of stress and strain in soils”, J. of Soil Mech. and Foundation Division, ASCE, 96 (SM5), pp. 1629-1653.

11.5. Data Files

The input data files can be downloaded from the RS3 Online Help page:

- **StressVerification-11 (Dense).rs3v3**
- **StressVerification-11 (Loose).rs3v3**

12. Circular Tunnel Reinforced by Rock Bolts

12.1. Problem Description

This problem considers a circular tunnel in an elastic, isotropic rock mass reinforced with a circular array of rockbolts. Both end-anchored and grouted elastic rockbolts are considered; the former is assumed to interact with the rockmass only at the bolt ends and the latter is fully bonded to the rock along its entire length. The tunnel is exposed to an in-situ hydrostatic compression field of 10 MPa.

Figure 12.1 shows the problem as constructed in *RS3*. The model uses a graded mesh of 4-noded tetrahedral elements. Fixed boundary conditions are used on the outer boundary, which is located 20 m from the hole centre.

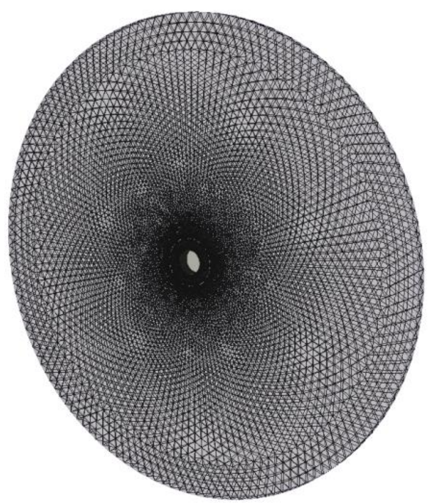

Figure 12.1: Tunnel in elastic medium supported by rockbolts as constructed in *RS3*

Table 12-1 and Table 12-2 summarize material and bolt properties.

Table 12-1: Model parameters

Parameter	***Value***
Tunnel radius (*a*)	1 m
In-situ stresses (σ_1, σ_2, σ_3)	10 MPa
Young's modulus (*E*)	250 MPa
Poisson's ratio (*v*)	0.3

Table 12-2: Bolt parameters

Parameter	Value
Diameter (d_b)	25 mm
Young's modulus (E_b)	116667 MPa
Length (L_b)	1 m
Number of bolts (N_b)	72
Bolt spacing along tunnel axis (D)	0.1 m

12.2. Analytical Solution

Carranza-Torres presents analytical stress and displacement distributions for both end-anchored and fully grouted rockbolts in an elastic medium (Carranza-Torres, 2022). This solution assumes that the effect of the support can be "smeared" circumferentially and along the tunnel axis to produce a single axisymmetric stress/displacement distribution. Figure 12.2 illustrates the tunnel schematically.

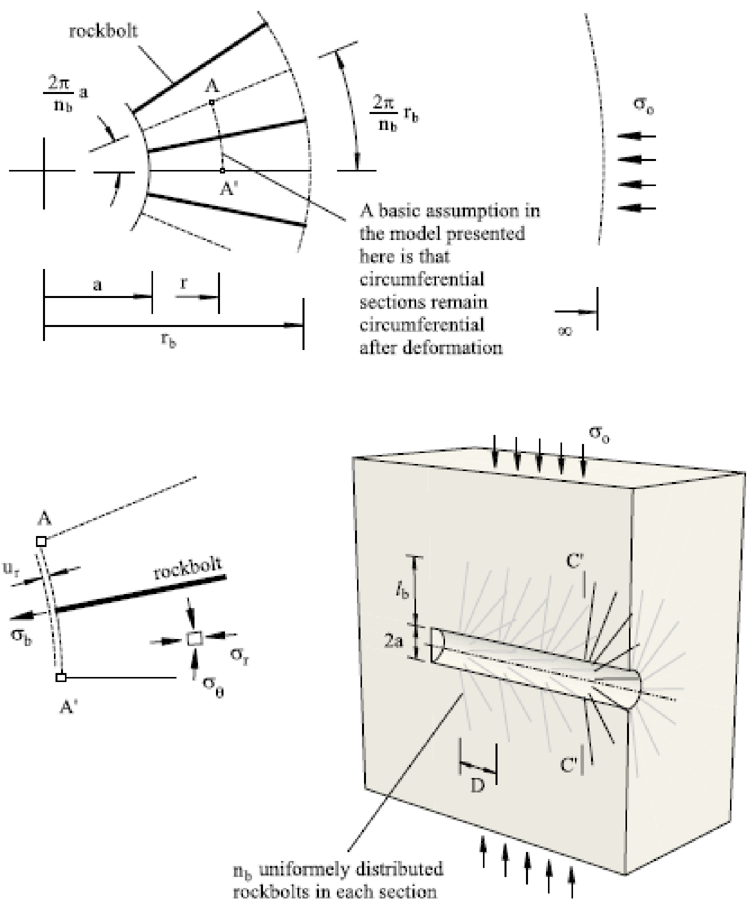

Figure 12.2: Reinforced circular tunnel (Carranza-Torres, 2022)

Dimensionless parameters β, α, μ, and ρ are defined as follows:

$$\alpha = \frac{N_b A_b}{2\pi a D} \tag{12.1}$$

$$\beta = \frac{\alpha E_b}{2G} \tag{12.2}$$

$$\rho = \frac{r}{a} \tag{12.3}$$

$$\mu = \frac{\nu}{1 - 2\nu} \tag{12.4}$$

where r is the radial distance from the centre of the tunnel and G is the shear modulus of the rockmass. At the ends of the rockbolts, i.e. $r = r_b$, the non-dimensional parameter ρ has the value:

$$\rho_b = \frac{r_b}{a} \tag{12.5}$$

For the end-anchored case, the radial stress ${\sigma_r}^b$ at $r = r_b$ is:

$$\frac{{\sigma_r}^b}{\sigma_0} = \frac{2(1 - {\rho_b}^2) + 2\mu(1 - \rho_b)(1 + \rho_b + \beta) + \beta\rho_b(1 - \rho_b)(3 + \rho_b)}{2 + \beta\rho_b(3 - \rho_b) + 2\mu(1 + \beta\rho_b - \beta\rho^2)} \tag{12.6}$$

For the fully grouted case, the radial stress ${\sigma_r}^b$ at $r = r_b$ is:

$$\frac{{\sigma_r}^b}{\sigma_0} = \frac{\beta N + (1 + \mu)(N_4 - N_3) - 2\beta\rho_b(N_2 - N_1) + 2(1 + \mu)(N_2 - N_1)\ln\left(\frac{1 + \mu + \beta\rho_b}{1 + \mu}\right)}{\beta N - N_3(1 + \mu) + 2\beta\rho_b N_1 - 2(1 + \mu)N_1\ln\left(\frac{1 + \mu + \beta\rho_b}{1 + \mu}\right)} \tag{12.7}$$

where, in the fully grouted case:

$$N = -2\beta(1-\rho_b)(1+2\mu)^2 + 2(1+\mu)(1+\beta+2\mu)(1+2\mu+\beta\rho_b)\ln\left(\frac{1+\mu+\beta}{1+\mu+\beta\rho_b}\right) \quad (12.8)$$

$$N_1 = \beta(1+2\mu+\beta) \quad (12.9)$$

$$N_2 = \beta(1+2\mu+\beta\rho_b) \quad (12.10)$$

$$N_3 = 2\beta^2\frac{1+2\mu}{1+\mu} - 2\beta(1+2\mu+\beta)\ln\left(\frac{1+\mu+\beta}{1+\mu}\right) \quad (12.11)$$

$$N_4 = 2\beta^2\rho_b\frac{1+2\mu}{1+\mu} - 2\beta(1+2\mu+\beta\rho_b)\ln\left(\frac{1+\mu+\beta\rho_b}{1+\mu}\right) \quad (12.12)$$

$$C_1 = -\frac{N_1\left(1-\frac{\sigma_r{}^b}{\sigma_0}\right)-N_2}{N} \quad (12.13)$$

$$C_2 = -\frac{N_3\left(1-\frac{\sigma_r{}^b}{\sigma_0}\right)-N_4}{N} \quad (12.14)$$

In the end-anchored case:

$$C_1 = \frac{(1-\rho_b)(1+\rho_b+\beta\rho_b)-(1+\beta\rho_b)\frac{\sigma_r{}^b}{\sigma_0}}{2\beta\rho_b(1+\mu)(1-\rho_b)+(1+2\mu)(1-\rho_b{}^2)} \quad (12.15)$$

$$C_2 = -\frac{\beta(1-\rho_b)-(1+2\mu+\beta)\frac{\sigma_r{}^b}{\sigma_0}}{2\beta\rho_b(1+\mu)(1-\rho_b)+(1+2\mu)(1-\rho_b{}^2)} \quad (12.16)$$

For both cases, the displacements (u_r) and stress (σ) in the unreinforced region $r \geq r_b$ are given by:

$$\frac{2Gu_r}{\sigma_0 a} = \left(1-\frac{\sigma_r{}^b}{\sigma_0}\right)\frac{\rho}{\rho_b{}^2} \quad (12.17)$$

$$\frac{\sigma_r}{\sigma_0} = 1-\left(1-\frac{\sigma_r{}^b}{\sigma_0}\right)\frac{\rho^2}{\rho_b{}^2} \quad (12.18)$$

$$\frac{\sigma_\theta}{\sigma_0} = 1+\left(1-\frac{\sigma_r{}^b}{\sigma_0}\right)\frac{\rho^2}{\rho_b{}^2} \quad (12.19)$$

In the reinforced region $r < r_b$, the solution for the end-anchored case is:

$$u_r = \frac{a\sigma_0}{2G}\left(\frac{C_1}{\rho} + C_2\rho\right) \quad (12.20)$$

$$\sigma_r = \sigma_0 + 2G\mu\rho\frac{u_r}{a} - 2G(1+\mu)\frac{\rho^2}{a}\frac{du_r}{d\rho} \quad (12.21)$$

$$\sigma_\theta = \sigma_0 + 2G(1+\mu)\rho\frac{u_r}{a} - 2G\mu\frac{\rho^2}{a}\frac{du_r}{d\rho} \quad (12.22)$$

$$\frac{du_r}{d\rho} = -\frac{a\sigma_0}{2G}\left(\frac{C_1}{\rho^2} - C_2\right) \quad (12.23)$$

The solution for the fully grouted case is:

$$\frac{2G}{\sigma_0}\frac{u_r}{a} = -C_2\frac{1}{\rho}\frac{1+\mu}{\beta} + 2C_1\left(1 - \frac{1}{\rho}\frac{1+\mu}{\beta}\ln\left(\frac{1+\mu+\beta\rho}{1+\mu}\right)\right) \quad (12.24)$$

$$\sigma_r = \sigma_0 + 2G\mu\rho\frac{u_r}{a} - 2G(1+\mu)\frac{\rho^2}{a}\frac{du_r}{d\rho} \quad (12.25)$$

$$\sigma_\theta = \sigma_0 + 2G(1+\mu)\rho\frac{u_r}{a} - 2G\mu\frac{\rho^2}{a}\frac{du_r}{d\rho} \quad (12.26)$$

$$\frac{du_r}{d\rho} = C_2\frac{1}{\rho^2}\frac{1+\mu}{\beta} - 2C_1\left(\frac{1+\mu}{\rho(1+\mu+\beta\rho)} - \frac{1}{\rho^2}\frac{1+\mu}{\beta}\ln\left(\frac{1+\mu+\beta\rho}{1+\mu}\right)\right) \quad (12.27)$$

12.3. Results

Figure 12.3 to Figure 12.6 shows the analytical stress and displacement distributions as determined analytically and using ***RS3***. Both sets of results are very similar.

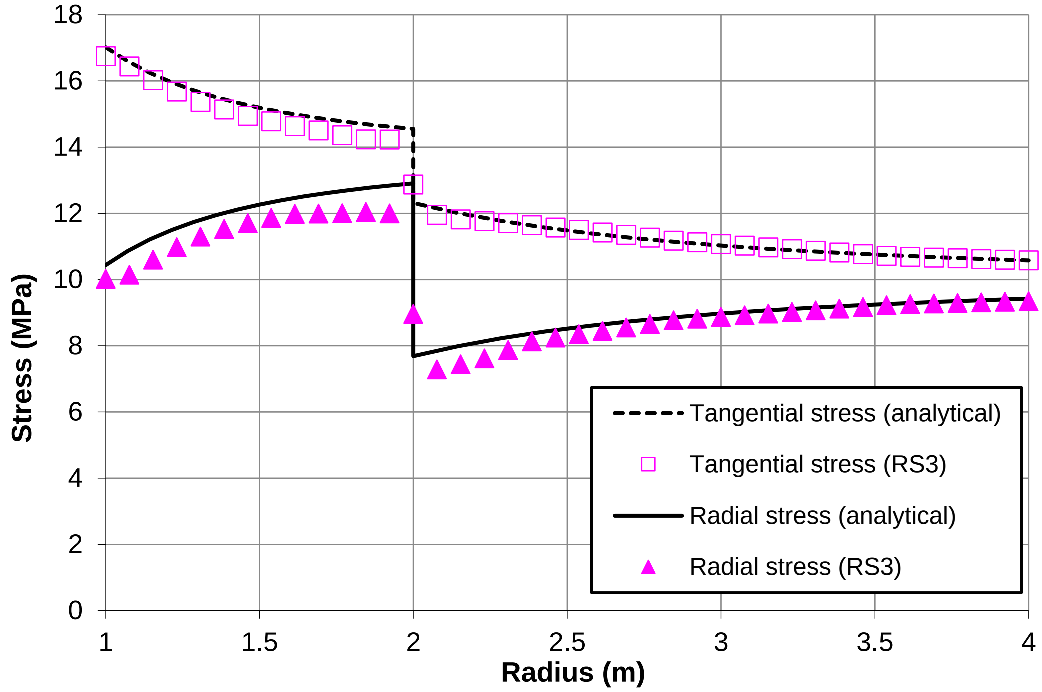

Figure 12.3: Radial and tangential stress distributions surrounding the tunnel reinforced with end-anchored bolts

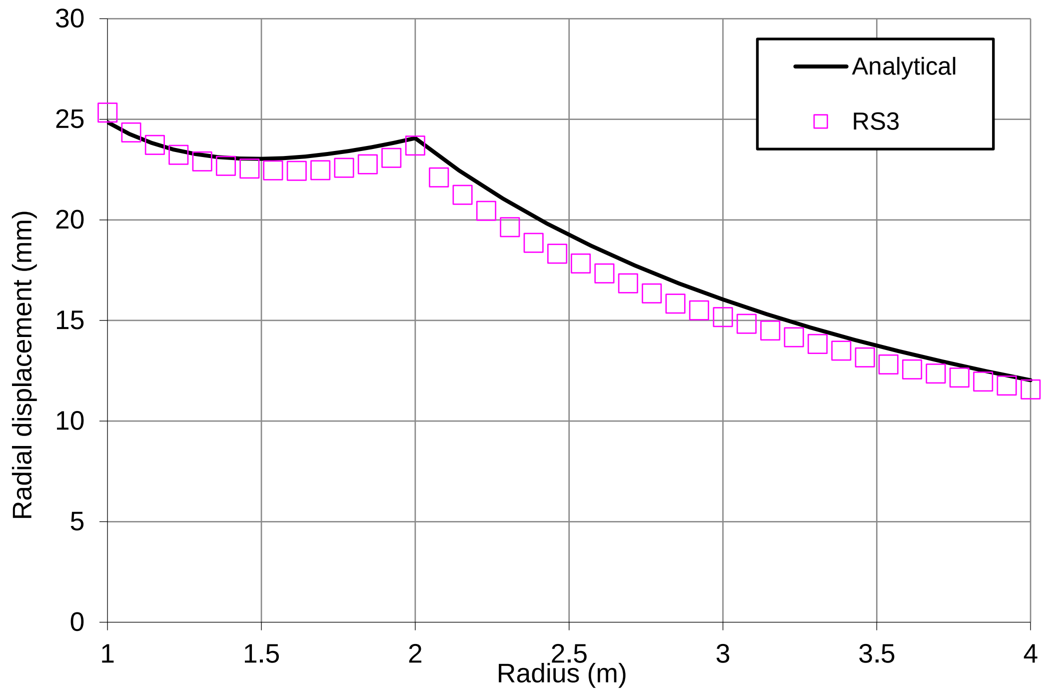

Figure 12.4: Radial displacement distributions surrounding the tunnel reinforced with end-anchored bolts

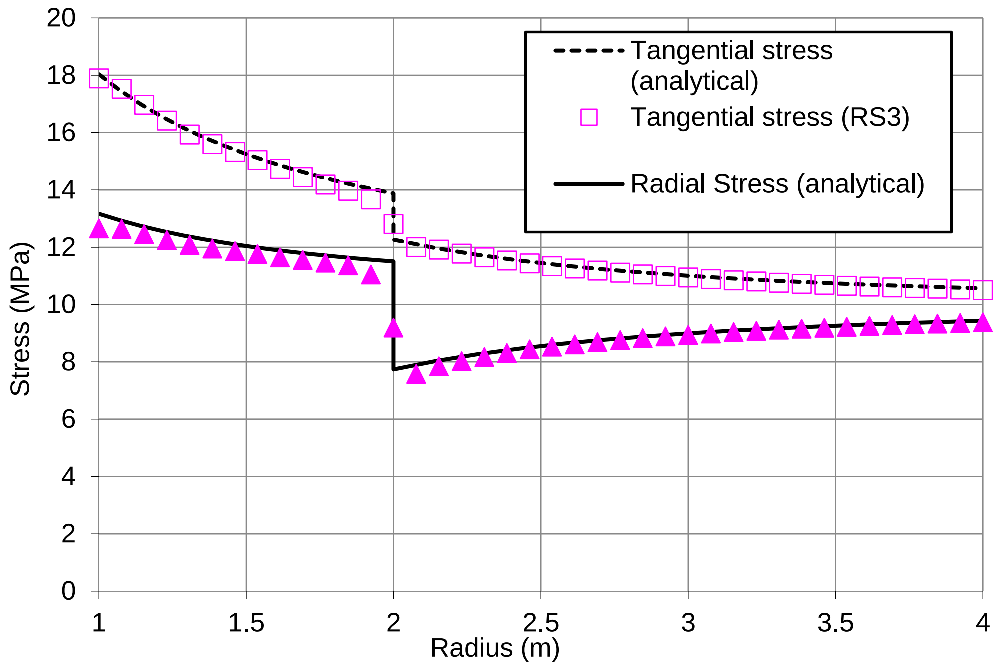

Figure 12.5: Radial and tangential stress distributions surrounding the tunnel reinforced with fully grouted bolts

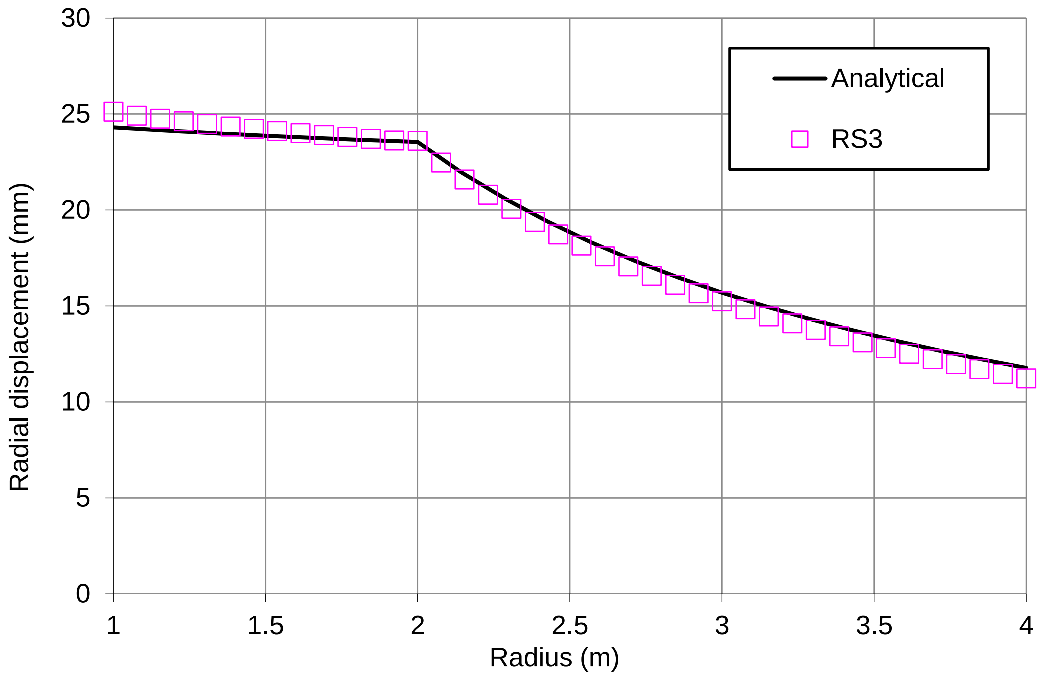

Figure 12.6: Radial displacement distributions surrounding the tunnel reinforced with fully grouted bolts

12.4. References

1. Carranza-Torres, C. (2002). “Elastic solution for the problem of excavating a circular tunnel reinforced by i) *anchored* or ii) *fully grouted* rockbolts in a medium subject to uniform far-fields stresses”. Note for the International Canada/US/Japan joint cooperation on rockbolt analysis.

12.5. Data Files

The input data file can be downloaded from the RS3 Online Help page:

- **StressVerification-012-End Anchored.rs3v3**
- **StressVerification-012-FullyBonded.rs3v3**

13. Stress Distribution Along a Grouted Rock Bolt

13.1. Problem Description

This problem examines the shear stress distribution along a thin annulus of grout around a grouted rock bolt subjected to an axial pull-out force. Figure 13.1 illustrates the situation and relevant parameters, while Figure 13.2 shows the problem as constructed in *RS3*.

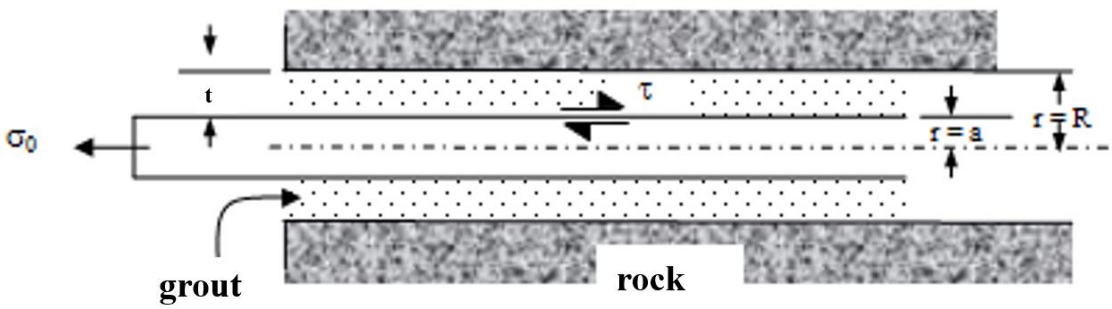

Figure 13.1: Fully grouted rockbolt in elastic rock mass

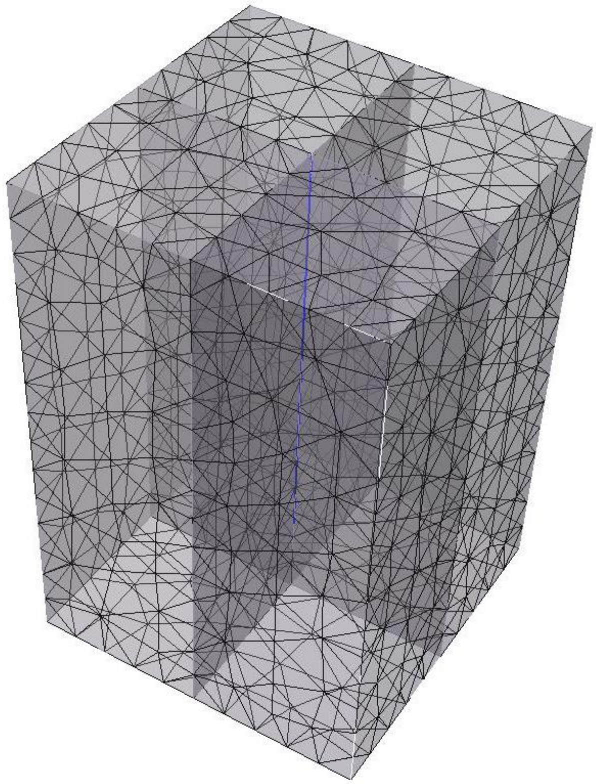

Figure 13.2: Fully grouted rockbolt as modeled in *RS3*

Table 13-1 and Table 13-2 summarize the material and rockbolt properties used.

Table 13-1: Model parameters

Parameter	***Value***
Young's modulus (*E*)	75000 MPa
Poisson's ratio (*v*)	0.25
Hole radius (*R*)	10.753 mm

Table 13-2: Bolt parameters

Parameter	***Value***
Tributary area	232.5 mm^2
Young's modulus (E_a)	98600 MPa
Bond shear stiffness	13882 MN/m
Grout shear modulus (G_g)	493 MPa
Bolt radius (*a*)	8.603 mm
Pull-out force	0.1 MN

13.2. Analytical Solution

According to Farmer, the shear stress distribution along a fully grouted rock bolt is given by (Farmer, 1975):

$$\frac{\tau_x}{\sigma_0} = 0.1exp\frac{-0.2x}{a} \quad (13.1)$$

Where τ_x is the shear stress in the grout, σ_0 is the applied pull-out stress, x is the distance from the head of the bolt and a is the bolt radius. Equation (13.1) is developed using the following assumptions:

1. The grout shear modulus $G_g = 0.005E_a$
2. The hole radius $R = 1.25a$, where a is the bolt radius

In order for the above assumptions to hold true, the grout shear modulus was set to 493 MPa. The grout shear stiffness was then calculated using the following equation (Itasca, 2004):

$$K_g = \frac{2\pi G_g}{\ln(1 + t/a)} \quad (13.2)$$

And here $t = R - a$, the thickness of the grout. The bolt tributary area was set to 232.5 mm^2, equivalent to a bolt having a radius a = 8.603 mm. By assumption 2 above, the radius of the hole R = 10.753 mm.

13.3. Results

The shear stress acting on the bolt can be calculated for two scenarios:

1. The shear stress acts at the boundary between the bolt and the grout. In this case, the shear stress is given by:

$$\tau = \frac{F_s}{2\pi a} \tag{13.3}$$

Where F_s is the interface shear force.

2. The shear stress acts at the boundary between the grout and the rock. In this case, the shear stress is given by:

$$\tau = \frac{F_s}{2\pi R} \tag{13.4}$$

Both of these cases are plotted in Figure 13.3, which shows the shear stress distribution along the bolt length. As can be seen, the two bracket the analytical solution.

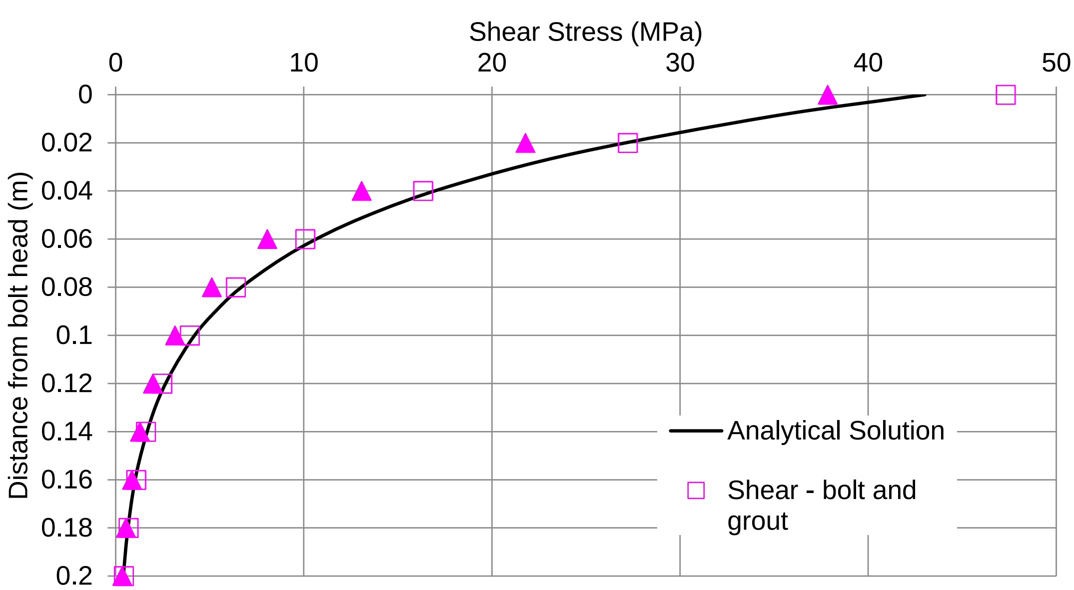

Figure 13.3: Shear stress distributions along bolt

13.4. References

1. Farmer, I.W., (1975), "Stress distribution along a resin grouted rock anchor", *Int. J. Rock Mech. Min. Sci. Geomech. Abstr*., 11, 347-351.

2. Itasca Consulting Group Inc., 2004. *FLAC v 5.0 User's Guide – Structural Elements*, Minneapolis, Minnesota, USA.

13.5. Data Files

The input data files can be downloaded from the RS3 Online Help page:

- **StressVerification-13.rs3v3**

14. Pull-Out Tests for Cable Bolt

14.1. Problem Description

This problem concerns the cable pull tests under constant radial stiffness. The results of field tests were performed in limestone. The pull-out strength of a bolt is function of both the frictional resistance by expansion of the bolt and the mechanical interlock between the bolt and asperities (extrusions) in the borehole. The pull-out force required can thus be expressed as:

$$F_{pull} = \min\,(R_f, S) \tag{14.1}$$

Where R_f is the total frictional resistance and S is the shear strength of all asperities in direct contact with the bolt. *RS3* does not make this distinction; the bolt-rock interface is assumed to have a single stiffness and pull-out strength. Refer to Hyett et al and Moosavi, 1996 on bond strength of cable bolts for more details on experimental data and numerical results for this study.

Figure 14.1 shows a rock mass with embedment length of cable 250 mm as modeled in *RS3*. The rock and bolt properties are summarized in

Table 14-1 and Table 14-2, respectively. The bolt is defined with joint shear under bolt model setting.

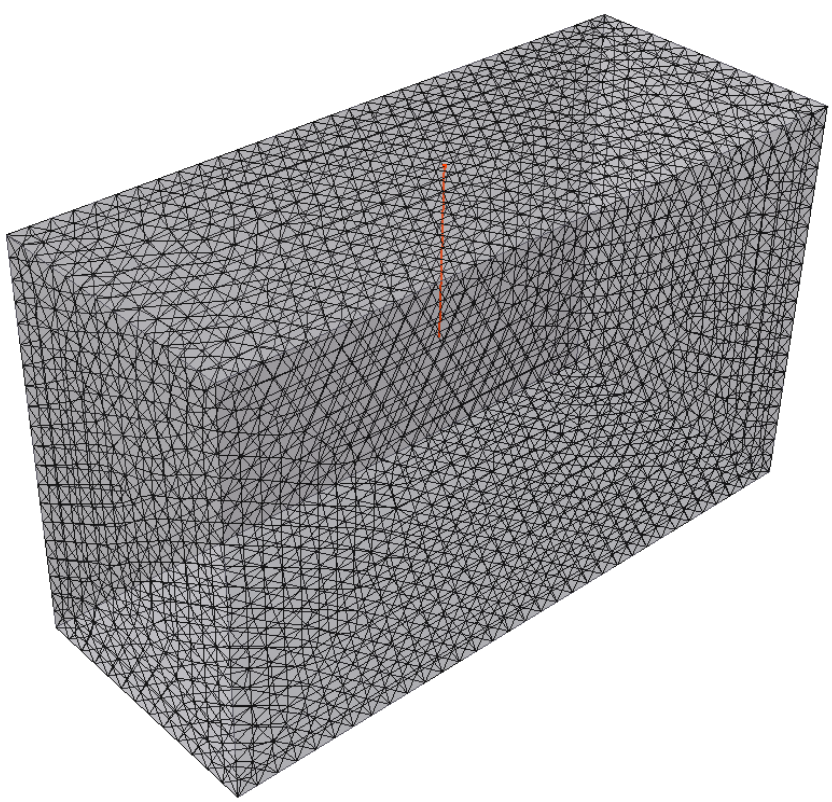

Figure 14.1: Plain strand cable rock bolt as modeled in *RS3*

Table 14-1 Limestone properties

Parameter	Value
Young's modulus (*E*)	23747 MPa
Poisson ratio	0.2
Friction angle	35
Cohesion strength	10.5 MPa

Table 14-2 Bolt Properties

Parameter	Value
Borehole Diameter	48 mm
Cable Diameter	19 mm
Cable Modulus (*E*)	98600 MPa
Cable Peak	100 MN
Water Cement Ratio	0.3
Residual Cable Peak	100 MN

The model shown in Figure 14.1 is made up of an elastic host material containing a 250 mm bolt, to which various pull-out forces (10 kN to 120 kN) were applied.

14.2. Results

Figure 14.2 shows the load displacement response for pull tests at three surface localities (Hyett et al and Moosavi, 1996). These experimental data points are labeled in the graphs as upper and lower bound to indicate the range of experimental results, where limestone is the confining medium. The model created by Moosavi and *RS3* results are also plotted to compare between obtained field results and the corresponding simulation for both of the models.

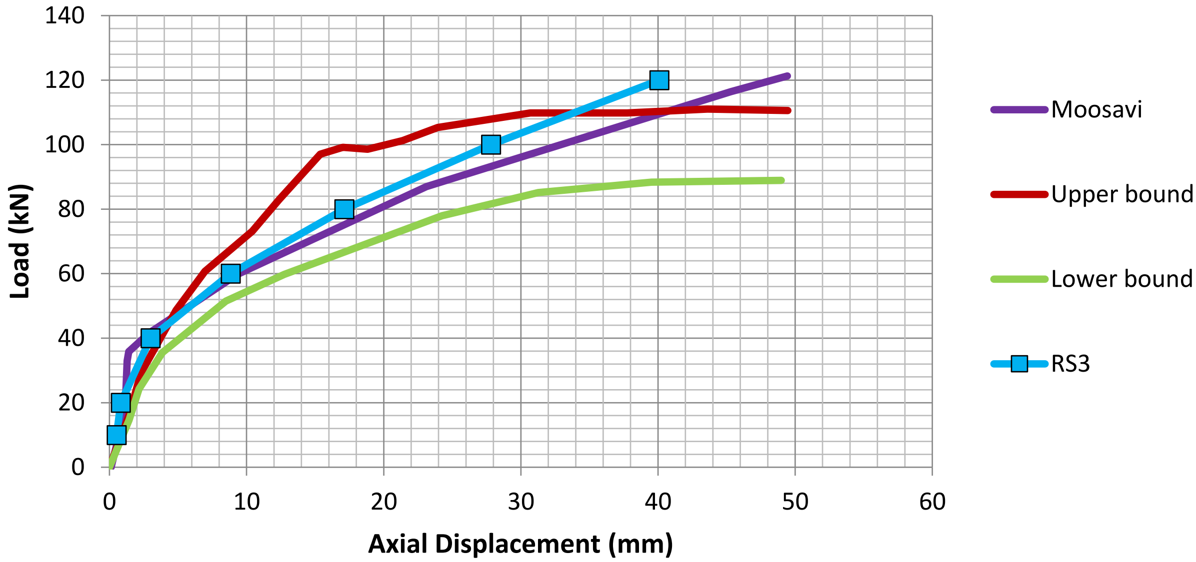

Figure 14.2: Elastic force-displacement behavior of single cable with limestone

Figure 14.2 show that *RS3* results are in close agreement with Moosavi simulation results.

14.3. References

1. Hyett et al. (1992) "The Effect of Rock Mass Confinement on the Bond Strength of Fully Grouted Cable Botls" *Int. J. Rock Mech. Min. Sci. & Geomech. Abstr,* vol 29. No.5. pp. 503-524, 1992.

2. Moosavi Mahdi. (1996) "Load Distribution Along Fully Grouted Cable Bolts based on Constitutive Models obtained from a Modified Hoek Cell" *Queen's University*, *Ontario.*

14.4. Data Files

The input data files can be downloaded from the RS3 Online Help page:

Table 14-3: Input data files for pull-out tests for cable bolts

File	*Pull-Out Forces*
StressVerification-14-10KN.rs3model	10 kN
StressVerification-14-20KN.rs3model	20 kN
StressVerification-14-40KN.rs3model	40 kN
StressVerification-14-80KN.rs3model	80 kN
StressVerification-14-100KN.rs3model	100 kN
StressVerification-14-120KN.rs3model	120 kN

15. Axially Loaded Piles in Cohesionless Soil

15.1. Problem Description

This problem examines two load transfer mechanisms in axially loaded piles: skin friction along the shaft, and end-bearing. The pile is first subjected to axial loads until failure resisted only by skin friction along the shaft. End-bearing effects are then included, and the simulation is repeated. The ultimate bearing capacity for both conditions are calculated and compared.

15.2. Analytical Solution

The following equations were taken from the FLAC3D - Structural Elements Manual (Itasca Consulting Group Inc., 2002). Cernica calculates the ultimate bearing capacity of a single pile in cohesionless soil from shaft resistance due to skin friction as (Cernica, 1995):

$$Q_s = \sum_i L_i (a_s)_i (s_s)_i \qquad (15.1)$$

where L_i = pile length at i increment

$(a_s)_i$ = area of pile surface per length in contact with soil at increment i

$(s_s)_i$ = unit shaft resistance at increment i

Equation (15.1) can be simplified assuming uniform soil material and constant pile cross section, a_s and s_s become constant:

$$Q_s = La_s s_s \qquad (15.2)$$

In free draining cohesionless soil, unit shaft resistance, s_s, is given by:

$$s_s = K_s \sigma_{avg} \tan \phi_s \qquad (15.3)$$

where K_s = average coefficient of earth pressure on the pile shaft

σ_{avg} = average effective overburden pressure along pile shaft

ϕ_s = angle of skin friction

The end-bearing capacity, Q_p, of a single pile in cohesionless soil is given by (Cernica, 1995):

$$Q_p = A_p \gamma L N_q \tag{15.4}$$

where A_p = cross sectional area of pile tip

γ = unit weight of soil

N_q = $\left(\frac{1+\sin\phi}{1-\sin\phi}\right)^2$, bearing capacity factor where ϕ is the soil friction angle

The total pile bearing capacity is simply the sum of skin resistance and end-bearing:

$$Q = Q_s + Q_p = La_s K_s \sigma_{avg} \tan\phi_s + A_p \gamma L \left(\frac{1+\sin\phi}{1-\sin\phi}\right)^2 \tag{15.5}$$

15.3. Model Information

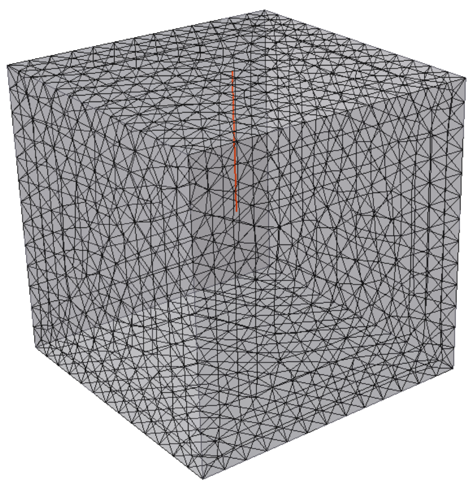

Figure 15.1: Plain strand cable rock bolt as modeled in *RS3*

Table 15-1 Soil Properties

Parameter	Value
Young's modulus (*E*)	2812.5 MPa
Unit weight	0.02 MN/m^3
Poisson's ratio	0.40625
Friction angle	10º
Cohesion strength	0 MPa
Average coefficient of earth pressure, (K_s)	1

Table 15-2 Pile Properties

Parameter	Value
Young's modulus (*E*)	80000 MPa
Poisson's ratio	0.3
Length	7 m
Diameter	1 m
Shear stiffness	2812.5 MPa/m
Normal stiffness	28125 MPa/m
Base normal stiffness	28125 MPa
Base force resistance	0.222 MN
Skin friction angle	10º
Skin cohesion	0 MPa

The model shown in Figure 15.1 is made up of an elastic material containing a 7 m pile to which various axial forces (10 kN to 500 kN) were applied.

15.4. Results

The graphs below show the load displacement response for axial load tests. Figure 15.2 shows the load-displacement response of piles considering only skin resistance. Figure 15.3 shows the load-displacement response after considering end-bearing effects. The graphs illustrate a clear plateau at the expected ultimate bearing capacity.

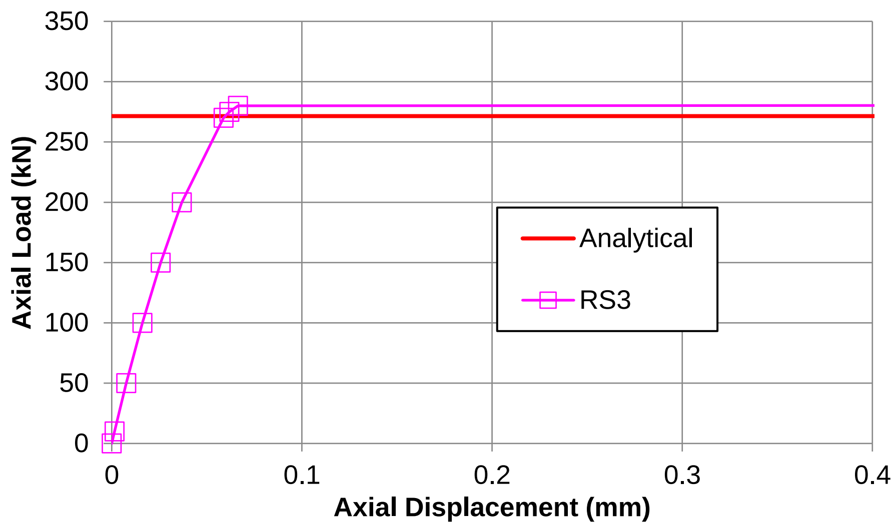

Figure 15.2: Load-displacement response of piles considering only skin resistance

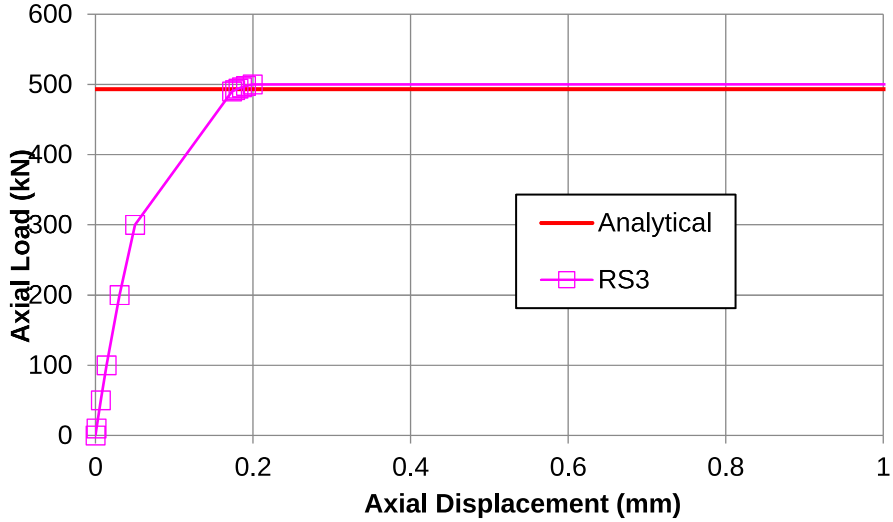

Figure 15.3: Load-displacement response of piles considering skin resistance and end-bearing effects

Table 15-3: Comparison of ultimate bearing capacity results

Effects considered	*RS3* Results	Analytical Solution
Skin resistance only	282 kN	271 kN
Skin resistance and end-bearing	502 kN	493 kN

The graphs and the table above show that *RS3* results are in close agreement with the analytical solution.

15.5. References

1. Cernica, J. N. (1995). *Geotechnical Engineering: Foundation Design,* New York: John Wiley & Sons,Inc.

2. Itasca Consulting Group Inc., 2004. *FLAC3D v 2.1 User's Guide - Structural Elements*, Minneapolis, Minnesota, USA.

15.6. Data Files

The input data files can be downloaded from the RS3 Online Help page:

- **StressVerification-15- EndBearing.rs3v3**
- **StressVerification-15- NoEndBearing.rs3v3**

16. Simply Supported Rectangular Plate

16.1. Problem Description

This verification example verifies the moment and the displacement of a rectangular plate under uniform pressure p = 100 MPa (Figure 16.1).

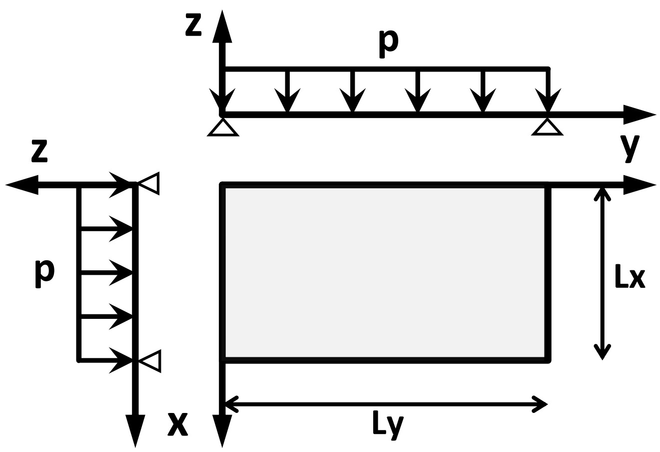

Figure 16.1: Simply supported rectangular plate under uniform pressure

The plate is isotropic and elastic with the following properties:

Young's modulus = 200 GPa

Poisson's ratio = 0.3

Lx = 10m

Ly = 10m

The results are compared to the analytical solution provided by Timoshenko and Woinowsky-Krieger (Timoshenko & Woinowsky-Krieger, 1959).

16.2. Closed Form Solution

The classical solution can be used to find the displacement and moment distribution at any point in the plate (Timoshenko & Woinowsky-Krieger, 1959).

The displacement *w* and the moment M_x and M_y at any point *(x,y)* are given by

$$w(x,y) = \frac{16p}{\pi^6 D} \sum_{m=1,3,5}^{\infty} \sum_{n=1,3,5}^{\infty} \frac{\sin\left(\frac{m\pi x}{L_x}\right) \sin\left(\frac{n\pi y}{L_y}\right)}{mn\left(\left(\frac{m}{L_x}\right)^2 + \left(\frac{n}{L_y}\right)^2\right)^2} \quad (16.1)$$

$$M_x(x,y) = \frac{16p}{\pi^4} \sum_{m=1,3,5}^{\infty} \sum_{n=1,3,5}^{\infty} \left(\left(\frac{m}{L_x}\right)^2 + \nu \left(\frac{n}{L_y}\right)^2 \right) \frac{\sin\left(\frac{m\pi x}{L_x}\right) \sin\left(\frac{n\pi y}{L_y}\right)}{mn\left(\left(\frac{m}{L_x}\right)^2 + \left(\frac{n}{L_y}\right)^2\right)^2} \quad (16.2)$$

$$M_y(x,y) = \frac{16p}{\pi^4} \sum_{m=1,3,5}^{\infty} \sum_{n=1,3,5}^{\infty} \left(\nu \left(\frac{m}{L_x}\right)^2 + \left(\frac{n}{L_y}\right)^2 \right) \frac{\sin\left(\frac{m\pi x}{L_x}\right) \sin\left(\frac{n\pi y}{L_y}\right)}{mn\left(\left(\frac{m}{L_x}\right)^2 + \left(\frac{n}{L_y}\right)^2\right)^2} \quad (16.3)$$

16.3. Model Information

The model is built in *RS3* with a uniform mesh of 10-noded tetrahedral. Figure 16.2Figure 16.2 shows two *RS3* models for a (a) non-rotated liner aligned with the global coordinate system and a (b) rotated liner. This was to ensure calculations were accurate for an arbitrary plate orientation. In the rotated case, a liner local coordinate system with local x axis oriented along the length of the liner was used to obtain results. The plate has a thickness of 0.1m. The model is restrained in all edges in x, y and z directions. The model geometry was devised to ensure there would be plate elements aligned along the major areas of interest for better comparison to the analytical solution. This does not cause plate elements to be disconnected at the plate boundaries as shown in the results.

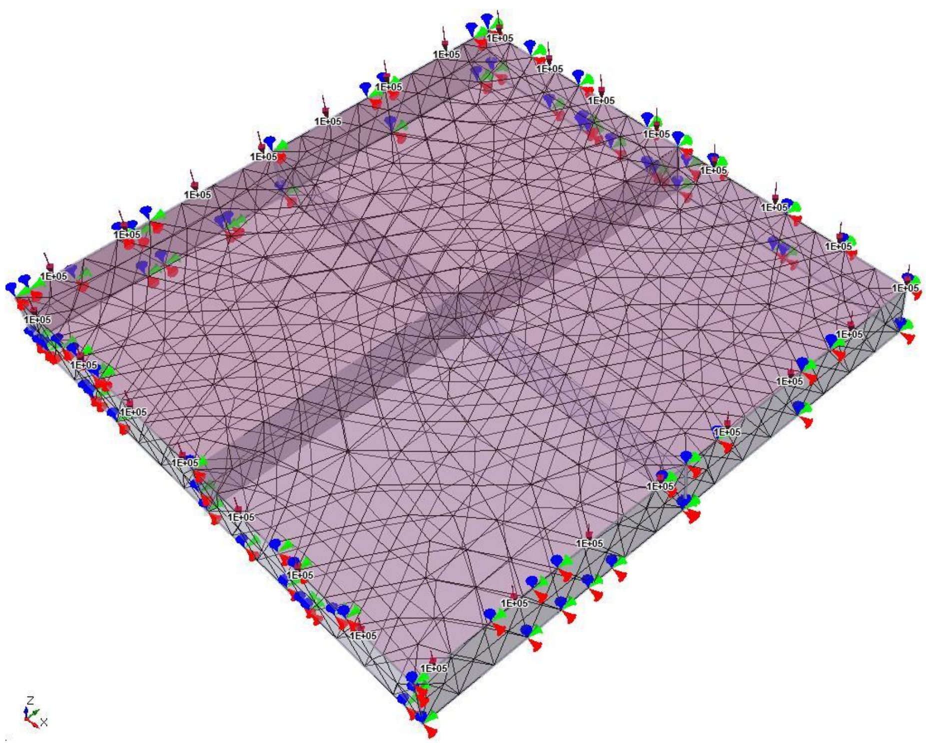

a) Non-rotated

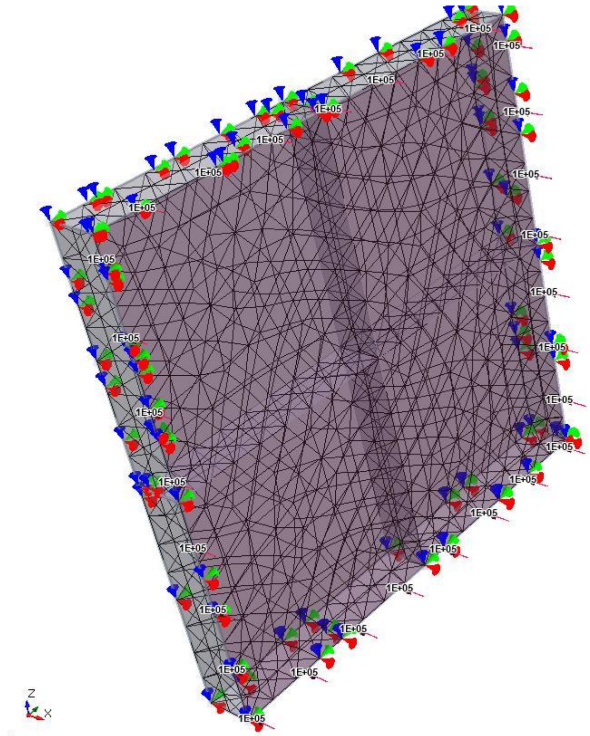

b) Rotated

Figure 16.2: Model of a simply supported rectangular plate under uniform pressure in RS3

16.4. Results and Discussions

Figure 16.3 and Figure 16.4 show the displacement and the moment distribution along a center line of the model (either the *x*- or *y*-axis). The *RS3* results are in very close agreement with the analytical solutions. A contour plot of the displacement is also and presented in Figure 16.5Figure 2.8.

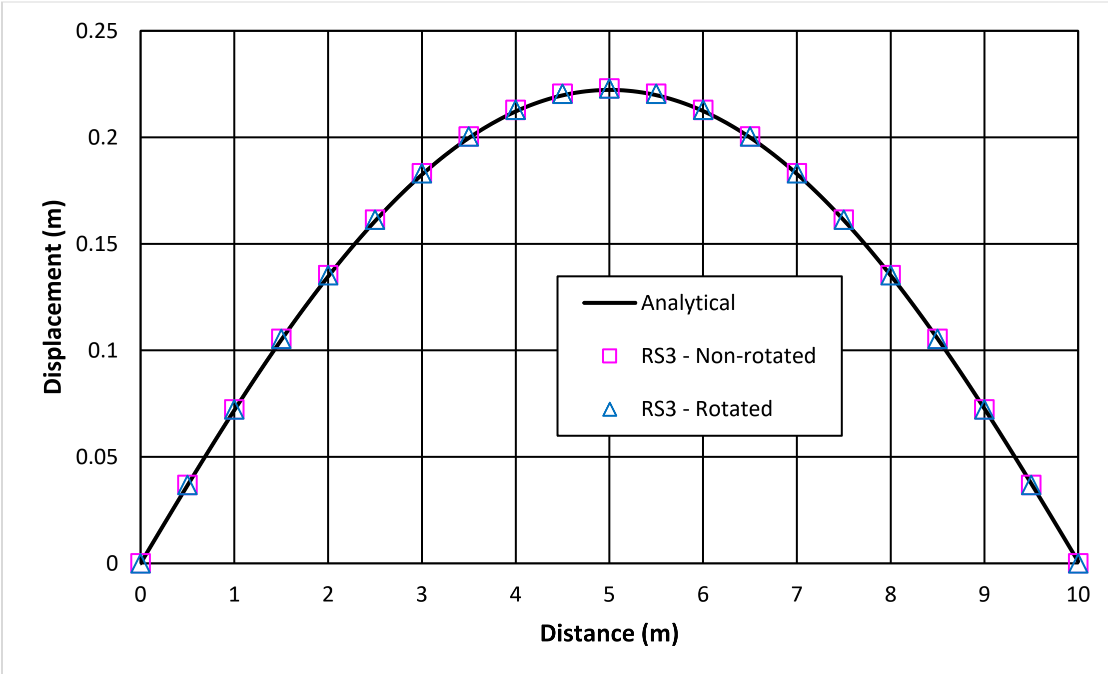

Figure 16.3: Comparison of displacement along the line x = 5m

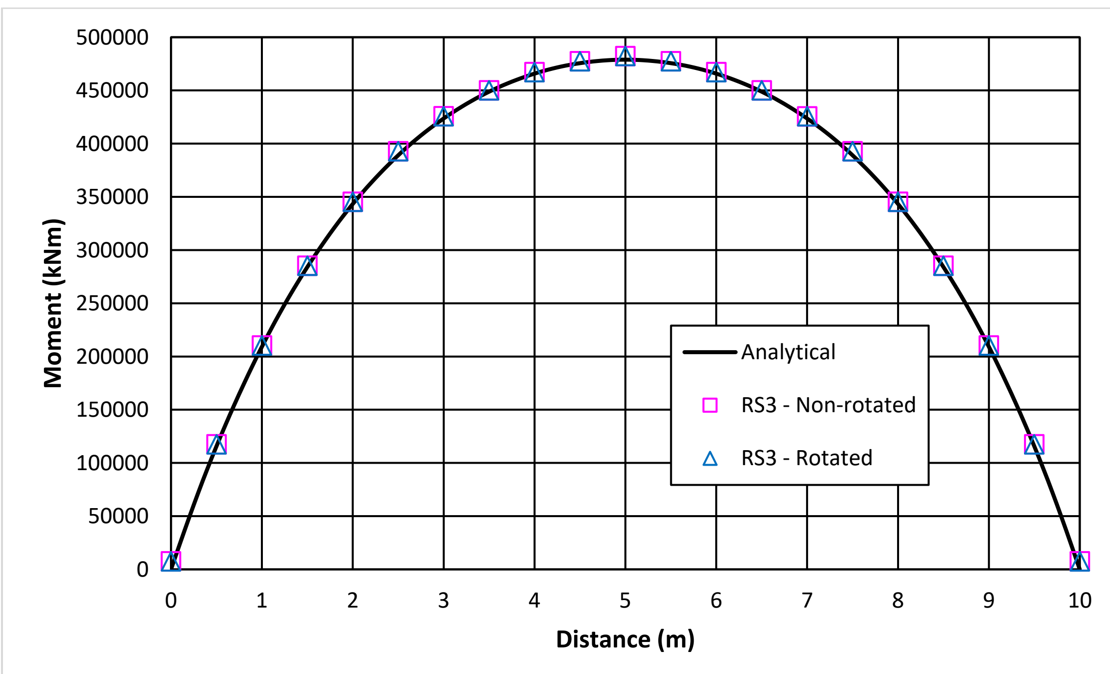

Figure 16.4: Comparison of moment along the line x = 5m

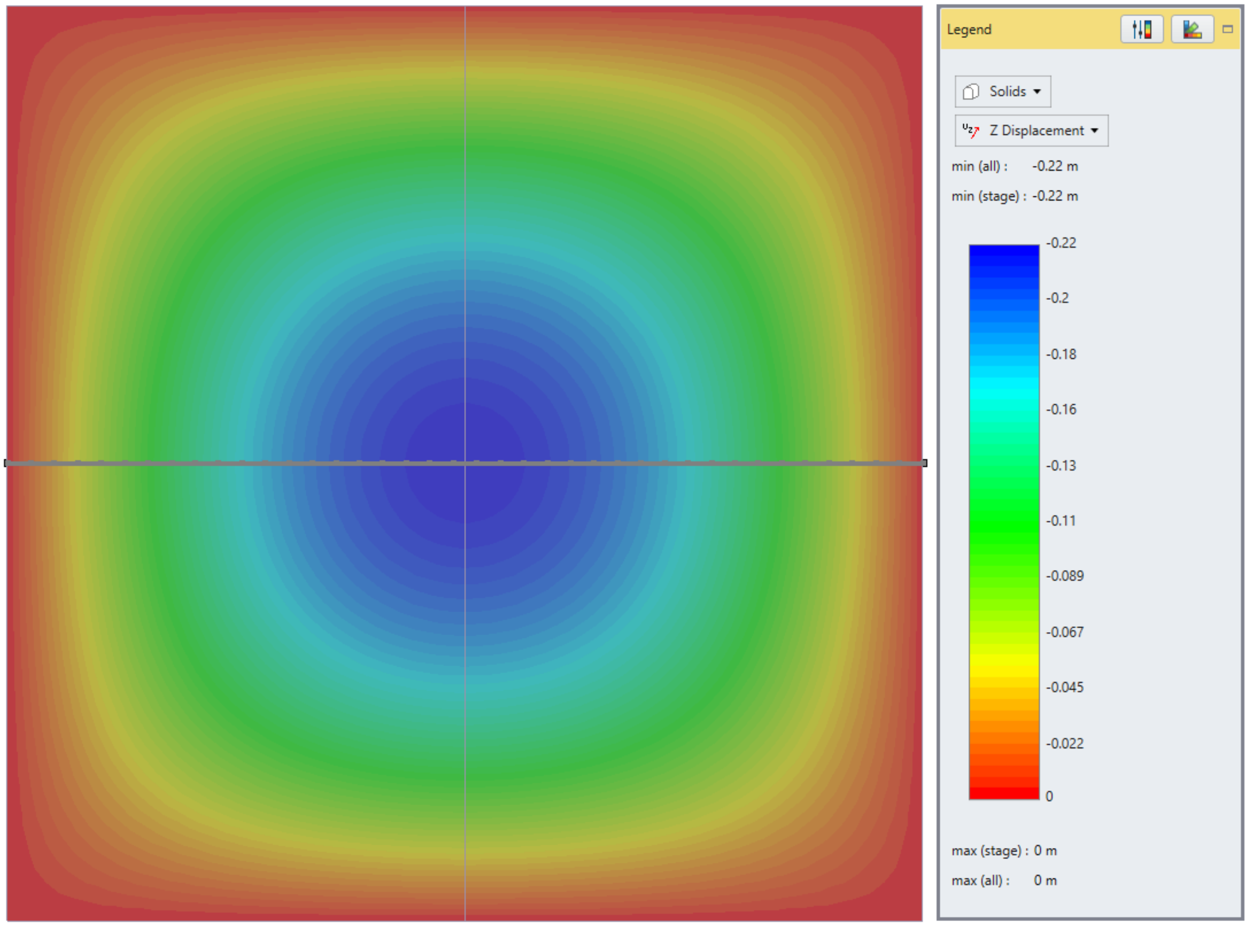

Figure 16.5 Vertical displacement distribution of *RS3* results

16.5. References

1. Timoshenko, S. and Woinowsky-Krieger, S. "Theory of plates and shells". McGraw–Hill New York, 1959.

16.6. Data Files

The input data files can be downloaded from the RS3 Online Help page:

- **StressVerification-16.rs3v3**
- **StressVerification-16-Rotated.rs3v3**